Random Environments and the Percolation Model

Non-dissipative Fluctuations of Random Walk Process on Finite Size Clusters

Yousof Mardoukhi

Kumulative Dissertation
zur Erlangung des akademischen Grades
"doctor rerum naturalium"
(Dr. rer. nat.)
in der Wissenschaftsdisziplin "Statistische Physik"

eingereicht an der
Mathematisch-Naturwissenschaftlichen Fakultät
Institut für Physik und Astronomie
der Universität Potsdam

Potsdam, den Juni 4, 2020

Hauptbetreuer (First Supervisor):
Professor Doctor Ralf Metzler
Faculty of Mathematics & Natural Sciences
Chair of the Theoretical Physics
Institute of Physics and Astronomy
Universität Potsdam
Germany

Betreuer (Second Supervisor):
Professor Doctor Arkady Pikovsky
Faculty of Mathematics & Natural Sciences
Institute of Physics and Astronomy
Universität Potsdam
Germany

Externer Gutachter (External Reviewer):
Professor Doctor Thomas Franosch
Faculty of Mathematics & Natural Sciences
Institute for Theoretical Physics
Universität Innsbruck
Austria

Published online in the
Institutional Repository of the University of Potsdam:
https://doi.org/10.25932/publishup-47276
https://nbn-resolving.org/urn:nbn:de:kobv:517-opus4-472762

Cordially dedicated to Stephan Foldes ...

Declaration

I hereby declare that except where specific reference is made to the work of others, the contents of this dissertation are original and have not been submitted in whole or in part for consideration for any other degree or qualification in this, or any other university. This dissertation is my own work and contains nothing which is the outcome of work done in collaboration with others, except as specified in the text and Acknowledgements.

Yousof Mardoukhi
Potsdam, den Juni 4, 2020

Acknowledgements

I would like to express my sincere gratitude to my supervisor Prof Ralf Metzler and his group who provided me with the chance to pursue my career as a PhD student at the Institute of Physics & Astronomy at the University of Potsdam. I take this opportunity to praise and appreciate the companionship and the collaboration of the then postdoc of Prof Ralf Metzler and the now assistant professor Jae-Hyung Jeon at Pohang University, with whom we laid the basis of this work. My utmost recognition goes to Prof Aleksei Chechkin whose insights and enthusiasm gave me the courage to further and nourish the earlier works. I would like to further acknowledge the fruitful collaboration I had with my brother Dr Ahmad Mardoukhi with whom we could apply the analytical results of my work to the experiments carried out in his laboratory at Tampere University of Technology. Moreover, I am thankful to his supervisors Prof Veli-Tapani Kuokkala and Prof Mikko Hokka who assisted us on this path. I further acknowledge the opportunity Prof Martin Wilkens provided me with to fulfil my PhD duties and enjoy exploring areas other than the topic of my PhD. I moreover acknowledge his family's hospitality. I highly appreciate the efforts Sarah A M Loos did put in to help me translating a thorough German script of the abstract of this dissertation. I would like to appreciate the support and love the Rafighi and Hertz family gave me during this strenuous period which was of great and heart-warming value to me. I am indebted to my friends Samudrajit Thapa, Vittoria Sposini and Vasundhara Shaw for their valuable friendship and support. In the end, and above all, I never forget the love my parents gave me and their unceasing emotional support which was my light during every step I took through my career and life.

The appendices A and B of this dissertation are reproduced from references [62, 63] with permission from the PCCP Owner Societies.

The appendix C of this dissertation is reproduced from the submitted manuscript to the New Journal of Physics with permission from the IOP Publishing. The accepted manuscript is now accessible via doi.org/10.1088/1367-2630/ab950b.

Abstract

Percolation process, which is intrinsically a phase transition process near the critical point, is ubiquitous in nature. Many of its applications embrace a wide spectrum of natural phenomena ranging from the forest fires, spread of contagious diseases, social behaviour dynamics to mathematical finance, formation of bedrocks and biological systems. The topology generated by the percolation process near the critical point is a random (stochastic) fractal. It is fundamental to the percolation theory that near the critical point, a unique infinite fractal structure, namely the infinite cluster, would emerge. As de Gennes suggested, the properties of the infinite cluster could be deduced by studying the dynamical behaviour of the random walk process taking place on it. He coined the term *the ant in the labyrinth*. The random walk process on such an infinite fractal cluster exhibits a subdiffusive dynamics in the sense that the mean squared displacement grows as $\sim t^{2/d_w}$, where d_w, called the fractal dimension of the random walk path, is greater than 2. Thus, the random walk process on the infinite cluster is classified as a process exhibiting the properties of anomalous diffusions. Yet near the critical point, the infinite cluster is not the sole emergent topology, but it coexists with other clusters whose size is finite. Though finite, on specific length scales these finite clusters exhibit fractal properties as well. In this work, it is assumed that the random walk process could take place on these finite size objects as well. Bearing this assumption in mind requires one address the non-equilibrium initial condition. Due to the lack of knowledge on the propagator of the random walk process in stochastic random environments, a phenomenological correspondence between the renowned Ornstein-Uhlenbeck process and the random walk process on finite size clusters is established. It is elucidated that when an ensemble of these finite size clusters and the infinite cluster is considered, the anisotropy and size of these finite clusters effects the mean squared displacement and its time averaged counterpart to grow in time as $\sim t^{(d+d_f(\tau-2))/d_w}$, where d is the embedding Euclidean dimension, d_f is the fractal dimension of the infinite cluster, and τ, called the *Fisher exponent*, is a critical exponent governing the power-law distribution of the finite size clusters. Moreover, it is demonstrated that, even though the random walk process on a specific finite size cluster is ergodic, it exhibits a persistent non-ergodic behaviour when an ensemble of finite size and the infinite clusters is considered.

Abstract

Der Perkolationprozess, der nahe dem kritischen Punkt von Natur aus ein Phasenübergangsprozess ist, ist allgegenwärtig in der Natur. Anwendungen dieses Prozesses umfassen ein breites Spektrum natürliche Phänomene von Waldbränden, der Ausbreitung von Infektionskrankenheiten, Dynamik des Sozialverhaltens bis hin zu der Finanzmathematik, der Bildung des von Gestein und biologische Systemen. Die durch der Perkolationprozess nahe dem kritischen Punkt generierte Topologie, ist ein zufälliges (stochastisches) Fraktal. Es ist eine fundamentale Aussage der Perkolationtheorie, dass nahe dem kritischen Punkt eine eindeutige unendliche fraktale Struktur, nämlich der unendliche Cluster, aufkommt. Wie de Gennes vorgeschlagen hat, können die Eigenschaften des unendliches Clusters durch die Dynamik der Irrfahrt, die auf dem Cluster stattfindet, abgeleitet werden. Er erfand den Ausdruck *the ant in the labyrinth*. Die Irrfahrt auf solchen unendlichen fraktalen Clustern weist eine subdiffusive Dynamik auf, in dem Sinne, dass ihre mittlere quadratische Verschiebung wie $\sim t^{d_w}$ skaliert, wobei d_w, genannt die fraktale Dimension der Zufallsbewegung, größer als 2 ist. Auf diese Weise wird die Irrfahrt auf dem unendlichen Cluster als ein Prozess, der die Eigenschaften von anomaler Diffusion aufweist, klassifiziert. Der unendliche Cluster ist allerdings nicht die einzige entstehende Topologie nahe dem kritischen Punkt. Tatsächlich, koexistiert er mit anderen Clustern deren Größe endlich ist. Obwohl sie endlich sind, weisen sie auf bestimmten Längenmaßen fraktale Eigenschaften auf. In dieser Arbeit wird angenommen, dass die Irrfahrt auch auf diesen Clustern stattfinden könnte. Diese Annahme verlangt, dass die Nichtgleichgewichts-Anfangsbedingung diskutiert wird. Aufgrund der mangelnden Kenntnisse über den Propagator der Irrfahrt in stochastischen Umgebungen, wird in diese Arbeit eine phänomenologische Übereinstimmung zwischen dem bekannten Ornstein-Uhlenbeck Prozess und der Irrfahrt auf dem endlichen Cluster hergestellt. Es wird erläutert, dass, wenn ein Ensemble von endlichen und unendlichen Clustern zusammen betrachtet wird, die Anisotropie und Größe der endlichen Cluster dazu führen, dass die mittlere quadratische Verschiebung und ihr zeitgemittlertes Gegenteil mit der Zeit wie $\sim t^{(d+d_f(\tau-2))/d_w}$ wachsen, wobei d die euklidische Einbettungsdimension ist, d_f die fraktale Dimension und τ, genannt der *Fisher Exponent*, ein kritischer Exponent ist, der die Power-Law Verteilung der Clustergröße angibt. Es wird außerdem dargestellt dass, obwohl die Irrfahrt auf einem bestimmten endlichen Cluster ergodisch ist, er dennoch ein unergodisches Verhalten aufweist, wenn ein Ensemble von endlichen und unendlichen Cluster betrachtet wird.

Preface

Percolation process and its geometrical beauty have been always intriguing subjects of studies ignited by the works of Flory and Stockmayer in the 1940s on a process called *gelation* where polymers by the means of cross-linking would bind to each other and form a larger molecule which could be infinitely large compared to the size of its polymer components. And the formation of this large molecule solely depends on the density of the polymers and their chemical energy with respect to the solvent. For an appropriate density of polymers and choice of a solvent, namely the *gelation point*, an incipient infinite molecule would emerge. At this point, the solution's liquid state would exhibit gel phase properties.

The beauty of this theory lies within its simple imposition and yet the complexity it bears within. After about seven decades and its mathematical formulation by the initiative of Broadbent and Hammersley, the problem still poses a challenge to the researchers to identify the gelation point, namely the *critical percolation density* and many of the theoretical aspects of the theory are open problems still. However, this did not impede the percolation of this theory into different branches of science and technology and it has been applied to different problems with different contexts ranging from stock, finance and sociology to physics and biology.

The inflexion point of the theory was in the 1970s when de Gennes proposed that the topological properties of media that are formed by the gelation process could be extracted by studying the statistical properties of the random walk process; he coined the term *Ant in Labyrinth* after his proposition. The commencement of this work presented here was due to a question addressing the diffusion process of proteins in lipid membranes. Lipid membranes, being porous media, are fine examples of a gelation process exhibiting a fractal geometry due to the existence of voids, and proteins' motion is an example of a random walk process in such environments to find their way to enter the membrane and exit from the other end of structure.

In the model considered here, not only the infinite void space was included, but also occasions where the protein could potentially get trapped in the lipid membrane due to the disconnectedness of the void spaces. The first attempts were to address this problem by

the means of the simulations and the results were interesting enough to make an attempt to formulate them mathematically to provide more insight into such ensembles.

Historically, in literature, the authors were mostly interested in the infinite structure formed by the gelation process and the amount of the literature on taking into account the coexistence of the finite and infinite structures simultaneously, barely contributes to the field. Therefore, en route, many of the attempts to quantify the statistical properties of the Ant in Labyrinth problem failed. It was at this point where a phenomenological approach was considered to compare the Ant in Labyrinth process with the well-known Ornstein-Uhlenbeck process.

The fruit of this approach is presented in this work after four years of challenges and my wish would be that the reader would find this dissertation useful for further studies on this topic and that the value of this work would bring the appreciation of the community. I hope I could have had the slightest contribution to the progress in this field and shed light on some of the not-yet-explored corners of the theory.

Yousof Mardoukhi
Potsdam January 29, 2020

Contents

List of Publications

1. Mardoukhi, Y., Jeon, J.H., Chechkin, A.V. and Metzler, R., 2018. *Fluctuations of random walks in critical random environments*. Physical Chemistry Chemical Physics, 20(31), pp.20427-20438.

2. Mardoukhi, Y., Jeon, J.H. and Metzler, R., 2015. *Geometry controlled anomalous diffusion in random fractal geometries: looking beyond the infinite cluster*. Physical Chemistry Chemical Physics, 17(44), pp.30134-30147.

3. Mardoukhi, Y., Chechkin, A.V. and Metzler R., (Submitted 2020, Editorial Assessment). *Spurious ergodicity breaking in normal and fractional Ornstein-Uhlenbeck process*. New Journal of Physics.

4. Cherstvy, A.G., Thapa, S., Mardoukhi, Y., Chechkin, A.V. and Metzler, R., 2018. *Time averaged and ergodic properties of the Ornstein-Uhlenbeck process: Particle starting distributions and relaxation to stationarity*. Physical Review E, 98, p.022134.

5. Mardoukhi, A., Mardoukhi, Y., Hokka, H. and Kuokkala, V.T., (Submitted 2019, Under Review). *Effects of test temperature and low temperature thermal cycling on the dynamic behavior of granitic rocks*. Rock Mechanics and Rock Engineering.

6. Mardoukhi, A., Mardoukhi, Y., Hokka, M. and Kuokkala, V.T., 2017. *Effects of heat shock on the dynamic tensile behavior of granitic rocks*. Rock Mechanics and Rock Engineering, 50(5), pp.1171-1182.

7. Mardoukhi, A., Mardoukhi, Y., Hokka, M. and Kuokkala, V.T., 2017. *Effects of strain rate and surface cracks on the mechanical behaviour of Balmoral Red granite*. Philosophical Transactions of the Royal Society A: Mathematical, Physical and Engineering Sciences, 375(2085), p.20160179.

Nomenclature

Roman Symbols

A	constant
$\mathcal{C}$	an open cluster generated by a percolation process
$\mathcal{D}$	dimensional constant
d	Euclidean dimension
d_f	fractal dimension
d_s	spectral or harmonic deminios
d_w	fractal dimension of a random walk path
$\mathbb{E}^2$	set of edges on the square lattice $\mathbb{Z}^2$
e	an edge in $\mathbb{E}^2$
EB	ergodicity breaking parameter
$\mathbb{E}$	expectation value
$\mathcal{F}$	σ-field of subsets on Ω generated by finite-dimensional cylinders
G	graph $G = (\mathbb{Z}^2, \mathbb{E}^2)$
h	dimensional constant
L	the length of an edge of a box in $\mathbb{Z}^2$
n	number of steps, summation dummy index
P	probability function

p	percolation density
p_c	critical percolation density
$\mathbb{R}^2$	embedding Euclidean support in two dimensions
$\mathbf{r}(t)$	spatial position of a random process at a given time t
R_g	radius of gyration
r_i	spatial position of a site in an open cluster indexed by i
R_∞	radius explored by a random walk process after taking infinitely many steps
s	site s in an open cluster
t	absolute time
w	stretched exponential exponent
ℓ_1	norm with $p = 1$ also Manhattan or Taxicab norm
$\mathbb{Z}^2$	simple square lattice with integral coordinates
z	coordination number of a site of a given lattice
$Z(s)$	number of open neighbours of site s

Greek Symbols

χ	characteristic time of an open cluster
Δ	lag time
δ	distance between two points in $\mathbb{Z}^2$, Dirac delta function, Kronecker delta
η	critical exponent of the connectivity probability
$\boldsymbol{\eta}$	Gaussion white noise in two dimensions
μ	Bernouli measure on the set $\{0, 1\}$
ν	critical exponent of the correlation length
Ω	sample space
ω	a configuration in a sample space

$\prod$ product

$\psi(p)$ probability measure of the existence of the infinite cluster

σ positive definite parameter

τ Fisher exponent, critical exponent of cluster size distribution near critical point

$\Theta(p)$ percolation probability at the percolation densitiy p

ξ correlation length

Ξ normalisation constante

Subscripts

eq equilibrium initial condition assumed

Other Symbols

$\otimes$ Cartesian product

Cov_X covariance function of an ensemble of the random process $X(t)$

μ_X mean value of an ensemble of the random process $X(t)$

$\left\langle r_{\mathcal{C}}^2(t)\right\rangle$ mean squared displacement on the open cluster $\mathcal{C}$

$\left\langle \mathbf{r}_{\mathrm{OU}}^2(t)\right\rangle$ mean squared displacement of an ensemble of the Ornstein-Uhlenbeck process

$*$ complex conjugate

$\left\langle \overline{\delta_{\mathcal{C}}^2(\Delta)}\right\rangle$ time averaged mean squared displacement on the open cluster $\mathcal{C}$

$\left\langle \overline{\delta_{\mathrm{OU}}^2(\Delta)}\right\rangle$ time averaged mean squared displacement of an ensemble of the Ornstein-Uhlenbeck process

$\overline{\mathrm{Cov}_X}$ covariance function of a single trajectory of a random process $X(t)$ with respect to time

$\overline{\mu_X}$ mean value of a single trajectory of a random process $X(t)$ with respect to time

Acronyms / Abbreviations

exp exponential function

MSD mean squared displacement

$\mathcal{N}(0, \rho^2)$ Normal distribution with zero mean and variance ρ^2

TAMSD time averaged mean squared displacement

Var variance

Chapter 1

Introduction

Consider a *Pólya's walk* (random walk) in one dimension [1]. The particle at every instance of time would take a step of unit length either to the left or to the right with equal probability $1/2$ independently of the previous step taken by the particle. The position of the particle is then given by a binomial distribution with zero mean and the variance n after taking n steps. It is well-known that according to the theorem of large numbers and the central limit theorem, when n tends to infinity, the distribution coincides with a normal distribution suggesting that every point lying on the axis of movement is visited with probability 1 infinitely many times [1, 2].

Now consider the same problem, yet this time, assign to every point on the axis equally the probability of $1/2$ to indicate the direction of the next step to be taken by the particle once visited. This process continues until the very moment when the two nearby points directing the particle oppositely. This is the *terminal position* of the process and contrarily to the previous case, the distribution of such points is not binomial. It is clear that in such a case as an instance of a *percolation process*, the motion of the particle is imposed by the medium only. This description should clearly draw a line, from which one can tell apart a percolation process from a diffusion process (refer to Fig. 1.1).

In their pre-eminent work, Broadbent and Hammersley devised the term *abstract crystal*, defined as a set of *atoms* (representing the nodes) and *bonds* (representing the edges), resembling a graph structure [3]. Each bond defines a connexion between two neighbouring atoms. The bonds represent a pipeline infrastructure distributing water in this abstract crystal. The sequel of blocking each bond randomly (or damming as referred by Broadbent and Hammersley), defines a structure called *random maze*. Once the fluid is supplied to the network, it can only flow through unblocked bonds.

Percolation theory concerns itself with the statistical distribution of the unblocked bonds. The very central and fundamental question in this theory is, under which circumstances

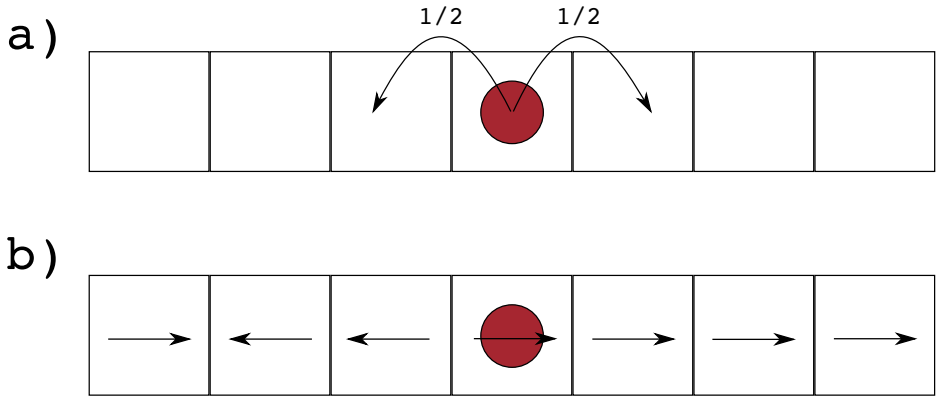

Figure 1.1 a) Pólya's walk where taking a step to the right or the left has the probability 1/2. b) Percolation process on a lattice where each site indicates the direction of the next steps to be taken. Each direction appears with the probability 1/2 and the position of the red disk is not distributed according to a binomial distribution. The red disk represents the Pólya's walker.

if a reservoir of fluid pumps the liquid into the structure, the liquid would wet infinitely many atoms (it is worth to remind the reader that a crystal mathematically is defined as an infinite set of points in space). It is also deduced immediately that the percolation problem for a Pólya's walk in a one dimensional random maze has a trivial solution as for any given probability of blocking the bonds which is larger than zero, there are at least two blocked bonds such that the pipeline would get clogged.

Amongst the many applications of the percolation theory, one could refer to some classical examples e.g. the spread of fire in a forest. In this scenario, trees represent the nodes. The process starts by setting a tree alight and in the next steps, nearby trees would catch fire if one of their neighbouring trees have already caught fire. Therefore, the density of the forest i.e. how densely the trees are covering the land, is the sole parameter which destines whether the whole forest would burn into ashes or the fire would eventually terminate due to the sparse population of the trees.

Another classic example of a percolation process is the spread of an epidemic in societies. In this scenario substitute the role of the trees with people and the fire with a contagious plague. Here, an individual represents a node and the social connexions it has with other individuals represent the bonds in the abstract crystal. For this scenario there is a real-life example in the history of mankind that was the most devastating epidemic the world had ever seen up to that time; the break out of the Black Death. Originated in China, it spread throughout Asia and Europe and took almost the life of approximately half of the population [4, 5]. Yet, the spread of the epidemic in Europe left behind an interesting observation. In some parts of Europe, indeed the epidemic spread out as a percolation

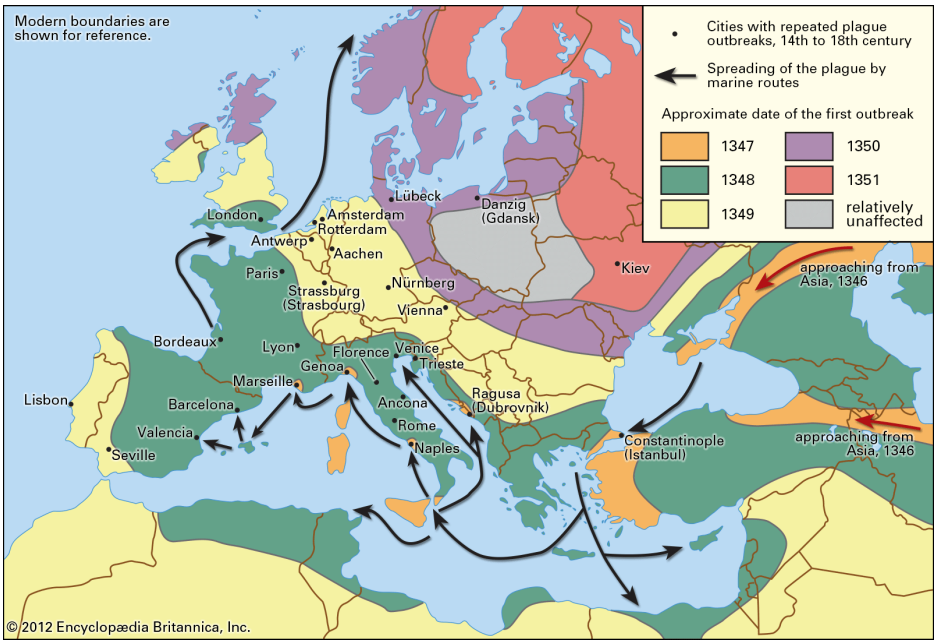

Figure 1.2 The waves of the Black Death in Europe between 1347 and 1351. Note that the majority of the Polish land and some parts of nowadays Belarus and Ukraine remained intact by the plague. Different arrival waves of the outbreak of the plague are shown in different colours indicated in the legend [6].

process, however, in nowadays Poland, the process terminated [6]. This is an example of a percolation process on an inhomogeneous graph where blocking the bonds has a different probability for different edges (see Fig. 1.2).

The reasons that are found in between the lines of history suggests that due to the fact that the land was largely covered by forest, which further implies that the land was sparsely populated, caused the plague not to transmit as frequently as in the other cities in Europe [7]. Moreover, this was not the sole reason that impeded the spread of the plague, but the precautionary measures the then King of Poland, Casimir the Great took to impose quarantine on the trade routes and securing the borders of Poland [7, 8]. This effectively secured the inland from being contaminated by the plague. This demonstrates that how a wise king as Solomon could spare a nation from being humiliated and wasted by one of the most destructive epidemic the world had ever seen till then. It is to be emphasised further that King Casimir the III was the only king of Poland whose name bears the title *the Great*.

Some of the consequences of Black Death were successive and frequent wars to secure more resources due to the lack of labourers and merchants which significantly affected the economy of many kingdoms in that era. Furthermore, due to the lack of labourer, new classes of societies and consequently professions were born. Such divisions and stratification in the

Figure 1.3 Geopolitical map of Poland during the reign of Casimir the Great between 1333 and 1370. The lighter shades of red depict the conquests of Casimir the Great during his reign. Compare this to the map of Black Death in Europe in Fig. 1.2. By imposing quarantine at the Polish boarders, he managed to deflect the progress of the plague into the Polish mainland [9].

casts of society and birth of new professions in the labour market are addressed in a recent publication by the means of the percolation model [10].

It is worthwhile to mention that in epidemic cases, like the Black Death where the scale of the displacement of individuals is much smaller than the geographical scale, for instance the distance between two cities, the spread of the disease emerges as a propagation of wavefronts as depicted in Fig. 1.2. On the contrary, in the modern days when the aviation is a part of daily life means of transportation, spread of a contagious disease is no longer bounded by the local interaction of individuals. In their model, Hufnagel *et. al.* accounted for a transition probability of a severe acute respiratory syndrome (SARS) not only between the local individuals but between the individuals belonging to different countries. By this means they could, to an astonishingly degree of accuracy, replicate the breakout of SARS between 2002 and 2003 [11].

Further application of the percolation theory can also be traced in the recent collaborative works of the author as an attempt to characterise the mechanical properties of brittle rocks based on the topological properties of the micro-cracks of the rock's surface under surface heat treatment [12, 13]. As the duration of the heat treatment increases, the propagation of the micro-cracks on the surface due to the expansion creates a backbone of connexions which once spanned the surface of the rock leads to a fracture in the rock under stress. The percolation process here is induced by the heat applied to the surface and causes the growth of the micro-crack structure of the surface; once reached a critical threshold, the rock is prone to break down by a significantly smaller applied pressure [14].

The reader must have noticed by now that in all the examples given above there is one essential measure that indicates whether a percolation process would thrive or would terminate at some point. That one essential measure is the density e.g. in the case of a forest fire is the density of the trees, in the case of an epidemic is the density of population or the number of bonds between each individual and in the last case, it is the bond between the micro-cracks. This density is the most essential quantity in the theory of percolation and it is specific to the underlying topological structure of the graph.

As a critical phenomenon and being inherently a phase transition process, most of the interests are attracted towards the critical density which once reached, implies that almost surely an infinite network of wet atoms would form. Thus, most of the studies are devoted to study these infinite objects. Despite of this fact, the aim in this dissertation is also to address the situation where the finite networks of wet atoms coexist with the finite ones near the critical density. In other words, central to this work, is to consider an ensemble which constitutes the infinite and finite networks of wet atoms at the same time near the critical density. The prime reason for this assumption is that in real world problems, finite networks

are more probable to emerge at the critical density rather than the infinite ones. Thus, it is more natural to consider an ensemble which encompasses both simultaneously. These finite networks exhibit a different behaviour than the infinite ones when dynamics of the wetting process is considered. On these finite networks, locally, for the length scales that are smaller than the effective radius of the network, the network exhibits the same structure as of infinite ones. Thus, for dynamical processes on these networks, where time is a relevant quantity, on time scales which mimic the length scales smaller than the effective radius of the network, the network would resemble the structure of an infinite structure near the critical density. Hence, depending on the time scale, the statistical properties of such ensembles could vary. This interconnection between the dynamical process and topological properties of the percolation process is central in this dissertation.

This dissertation is arranged and compiled in such a way that in the next chapter a formal mathematical definition of the percolation theory is provided to familiarise the reader with the essentials of the theory. Furthermore, it will be demonstrated how scaling arguments near the critical density could provide more insight into the behaviour of the percolation process. In the second chapter, the first steps are taken to approach the problem of taking into account the coexistence of infinite and finite networks of wet atoms and how the random walk process on these networks reveals the topological properties of the structure by analysing the behaviour of certain statistical quantities such as *mean squared displacement*. In the third chapter, the ergodic property of the random walk process on such networks is discussed. The fourth chapter is dedicated to the simulations that were carried out to justify the analytical results presented in this dissertation. And finally, conclusions are drawn to provide the reader with a clearer picture of the results yielded in this work.

Chapter 2

Mathematical Formulation of the Percolation Theory

To mathematically formulate the description of a percolation process in two dimensions, as the rest of this work is exclusively dedicated to the simple square lattice, consider $\mathbb{Z}^2$ to be the set of points on a Euclidean plane with integral coordinates. A bond is then a line connecting two adjacent points which have a distance 1. The distance between two points of x and y in $\mathbb{Z}^2$ is defined as

$$\delta(x, y) = \sum_{i=1}^{2} |x_i - y_i|. \tag{2.1}$$

Denote the set of the bonds with $\mathbb{E}^2$ then, $G = (\mathbb{Z}^2, \mathbb{E}^2)$ is a graph embedded in $\mathbb{R}^2$ which is referred to as an *abstract crystal*. Define a global value $0 \leq p \leq 1$ which is called *percolation density*. Refer to an edge $e \in \mathbb{E}^2$ unblocked with probability p or blocked otherwise with probability $1 - p$, independently of any other edges in $\mathbb{E}^2$. Consequently, the sample space is given by $\Omega = \otimes_{e \in \mathbb{E}^2}\{0, 1\}$, where for the edge e if $\omega(e) = 1$, it is understood as the edge is unblocked and if $\omega(e) = 0$ the edge is blocked. An instance of this sample space is a configuration denoted by $\omega = (\omega(e) : e \in \mathbb{E}^2)$. The very fact that each edge is either blocked or left unblocked independently of any other edges, naturally imposes a product measure $P_p = \prod_{e \in \mathbb{E}^2} \mu_e$ on the probability space $(\Omega, \mathcal{F}, P_p)$, where $\mu_e(\omega(e) = 1) = p$ is the Bernoulli measure on the set $\{0, 1\}$, and $\mathcal{F}$ is the σ- field of subsets of Ω generated by finite-dimensional cylinders.

A configuration ω is a percolation process on G and it is referred to as *bond-percolation* model compared to the *site- percolation* model where instead of dealing with edges, one associate the state of being blocked and unblocked to the sites of $\mathbb{Z}^2$. The neighbourhood relation

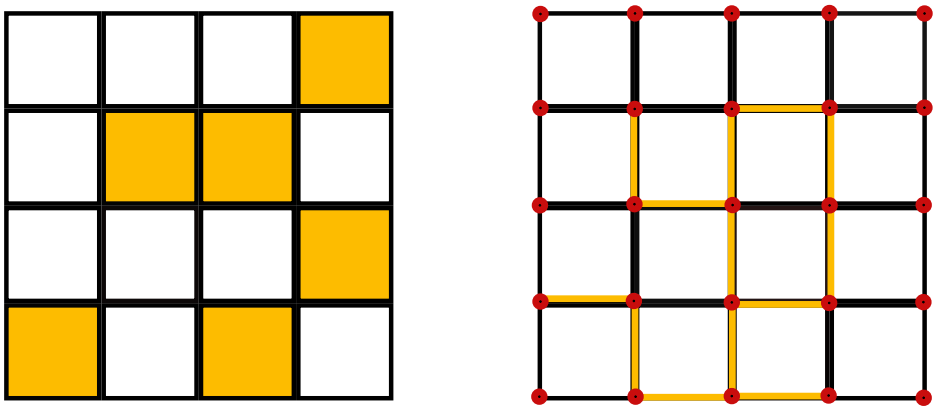

Figure 2.1 Site-percolation on the left hand side versus the bond-percolation on the right hand side. Every bond-percolation model has a site-percolation representation but not vice versa. The yellow colour depicts the open sites or bonds. The red dots depict the nodes of the lattice. Note that the depiction on the right site does not represent the site-percolation example on the left side.

between the sites is then identified by a given rule e.g. von Neumann neighbourhood [15]. It has been proven that every bond-percolation model has an equivalent site-percolation representation [16–18]. This map is injective meaning that not every site-percolation model has an equivalent bond-percolation representation. Hence, site-percolation models describe a more general class of percolation processes which will be the focus of this work as well (see Fig. 2.1). The set of unblocked sites that are connected through a specified neighbourhood relation (e.g. von Neumann) form an *open cluster*. It is clear that the larger the p is, the appearance of such open clusters becomes more probable. The prime quantity in the percolation theory is the percolation probability $\theta(p)$ of a site belonging to an infinite open cluster. Since a lattice is an infinite set of sites, it is immediately followed that it remains invariant under translational maps. Therefore, the quantity θ for a specific site can be translated into the percolation probability of the centre of the lattice belonging to an infinite open cluster. Note that θ for $p = 1$ is identically 1 and for $p = 0$ is admittedly 0. It is intuitive that if one gradually increases p from 0 to 1, isolated islands of open clusters form on the lattice until a critical value of p, denoted by p_c, is reached when for the first time these isolated islands become interconnected and an infinite open cluster spans the underlying lattice.

Denote the open cluster to which the centre of the lattice belongs by $\mathcal{C}$ and the number of the open sites belonging to such a cluster with $||\mathcal{C}||$. By definition $\theta(p)$ is given by

$$\theta(p) = P_p(||\mathcal{C}|| = \infty), \tag{2.2}$$

and with respect to p it behaves as

$$\theta(p) \begin{cases} = 0 & p < p_c, \\ > 0 & p > p_c \end{cases} . \tag{2.3}$$

The threshold value p_c is called the *critical percolation density* and for any embedding Euclidean dimension d of the lattice is defined as

$$p_c(d) = \sup\{p : \theta(p) = 0\}. \tag{2.4}$$

The critical percolation density p_c as a function of the embedding Euclidean dimension d is a *strictly* decreasing function. This is observed by referring to the coordination number of each site; as d increases, the coordination number increases subsequently. Thus, with even a smaller number of open sites one could form an interconnected path of open sites.

The existence of such a threshold implies that there are two phases for a percolation process. This is true only when $d \geq 2$, as it has been shown previously that for the case of $d = 1$, p_c is 1 trivially. Hence, for any $d \geq 2$, for $p < p_c$, the percolation process is called to be in the *subcritical* phase and for $p > p_c$, in the *supercritical* phase. In the subcritical phase, all the open clusters have a finite size almost surely. On the other hand, in the supercritical phase, the probability of any site of the lattice belonging to an open cluster of infinite size is strictly larger than 0. For the proof on the existence of p_c as a critical phenomenon refer to [18]. This leads naturally to define another probability measure $\psi(p)$ which addresses the existence of an infinite open cluster which satisfies the following

$$\psi(p) = \begin{cases} 0 & if \quad p < p_c, \\ 1 & if \quad p > p_c \end{cases} . \tag{2.5}$$

Note that this probability measure only speaks of the existence of an infinite open cluster in the supercritical phase, and does not guarantee the uniqueness of the infinite open cluster. Furthermore, it does not provide any information regarding the fact that an infinite open cluster exists at the critical probability p_c or not. It is known that for $d = 2$, there is no such cluster at p_c, but it is left as an open question for $d \geq 3$. But there is a proof that the infinite open cluster , if exists, is unique [18]. Moreover, proven by Kesten [19] by letting p to be slightly different than p_c one can speak of an incipient infinite cluster instead of the infinite cluster strictly. The value of p_c for some of the generic lattices in two and three dimensions is given in Table 2.1.

Lattice	Site-percolation	Bond-percolation
Honeycomb	0.6962	0.65271
Square	0.592746	0.50000
Triangular	0.500000	0.34729
Diamond	0.43	0.388
Simple cubic	0.3116	0.2488
BCC	0.246	0.1803
FCC	0.198	0.119
d = 4 hypercubic	0.197	0.1601
d = 5 hypercubic	0.141	0.1182
d = 6 hypercubic	0.107	0.0942
d = 7 hypercubic	0.089	0.0787

Table 2.1 Table of critical percolation densities p_c for some two-dimensional and three-dimensional lattices [20]. Note that as d increases, p_c decreases subsequently.

2.1 Scaling Theory

Hitherto, the formal definitions were provided to make the reader familiar with the essentials of the percolation process. As this dissertation is dedicated to the study of the percolation process near the critical point p_c, the focus henceforth is drawn towards the *scaling theory* which is tightly related to the physical theory of the phase transition. It must be very clear to the reader that for $p \sim p_c$, a phase transition occurs from the subcritical phase were all the open clusters are finite in size and isolated, to the supercritical phase where almost surely there exists an infinite cluster. The percolation probability $\theta(p)$ then clearly behaves as the order parameter of this phase transition. It is essential to bear in mind that the behaviour of the macroscopic quantities suggested by the scaling theory are not yielded via rigorous mathematical deductions. On the other hand, they are interpreted by empirical observations, whether this observation be through a physical experiment carried in the laboratory or a computer simulation. Thus, one should not seek a rigorous proof for them but to receive them as conjectures.

2.1.1 Critical Exponents: Correlation Length, Fractal Dimension and the Fisher Exponent

At the core of the scaling theory, lies the most essential macroscopic quantity called the correlation length. Denoted by ξ, it is related to the concept of the probability that the origin of the lattice and any other randomly chosen site of the lattice at distance n from the origin,

Exponent	Estimated	Literature
d_f	1.9 ± 0.1	$91/48$
τ	2.03 ± 0.01	$187/91$
d_w	2.7 ± 0.1	2.87

Table 2.2 Table of critical exponents estimated at $p = 0.6$ (middle column) and near p_c (rightmost column) for the square lattice [20]. In chapter 5 it will be delineated how these exponents are extracted by the means of simulation.

belong to the same open cluster. This probability is called the *connectivity probability* and it is believed that near p_c it scales as $n^{2-d-\eta}$ for some given η and any p other than $0, 1$ and p_c. The connectivity probability scales as $e^{-n/\xi(p)}$, where $\xi(p)$ diverges when $p \sim p_c$, since the probability of the origin and any site of the lattice belonging to the infinite cluster is non-zero [18]. It is fundamental to the scaling theory that irrespective of whether p approaches p_c from above or beneath, for an exponent $\nu > 0$, $\xi(p)$ scales as

$$\xi(p) \approx |p - p_c|^{-\nu}. \tag{2.6}$$

The importance of $\xi(p)$ lies within the fact that it imposes naturally a length scale such that for any length scales larger than the correlation length, the cluster which encompasses the origin appears to be homogeneous. For any length scales smaller than $\xi(p)$, the topological properties of the cluster differ from the topological properties of the cluster for length scales larger than the correlation length.

Another quantity central to the scaling theory is the probability of the appearance of the cluster $\mathcal{C}$ with size $||\mathcal{C}||$. The *average cluster size* defined as $\sum_n n P_{p_c}(||\mathcal{C}|| = n)$ at p_c diverges as the percolation theory suggests that the probability of the appearance of the infinite cluster $\sim p_c$ is 1. The divergence of the average cluster size hence suggests that $P_{p_c}(||\mathcal{C}|| = n) \approx n^{-\tau}$ for some exponent $\tau > 0$ called the *Fisher exponent* after the Fisher droplet model [20, 21].

The last but not least of the parameters that concerns with the topological properties of the open clusters is the *fractal dimension* [22]. Without getting deeper into how the fractal dimension is mathematically defined which is out of the scope of this dissertation [23, 24], the shortest distance between two sites belonging to the same open cluster is not the shortest distance according to the ℓ_1 norm defined by Eq. (2.1). To elaborate this further, without loss of generality, consider a square lattice and choose a box of size L. The hypervolume of such a box is L^2. Assume that the lattice unit length to be unity, mesh the box and then observe that with L^2 boxes one can carpet the hypervolume of this box. Now consider a percolation

process within this box, and let the edges of this box tend to infinity. Obviously, close to p_c, the infinite cluster emerges and the number of the tiles needed to cover the hypervolume of the infinite cluster no longer scales as L^2 but scales as L^{d_f}, where in two dimensions $1 < d_f < 2$ [20, 24]. The exponent d_f is called the fractal dimension. The algorithm utilised to estimate the fractal dimension is one of the widely used ones called the *Box counting* method. The dimension yielded by this method is often referred to as the *box-counting dimension* or *Minkowski–Bouligand dimension* [25]. The estimated value of d_f, d_w (which will be introduced in the next section) and τ for this work and their theoretical value are provided in Table 2.2 (it will be elaborated in chapter 4 how the corresponding values of the aforementioned exponents are extracted numerically).

2.2 Dynamical Scaling Theory

2.2.1 Ant in a Labyrinth

Another approach to extract the topological properties of the open clusters is based on the statistical behaviour of the random walk process on such clusters known as the *dynamical scaling theory* [26]. De Gennes in his seminal work suggested that asymptotic properties of the random walk process on infinite open clusters at the percolation threshold reveal the geometry of such clusters [27]. Since near p_c the infinite cluster exhibits a fractal nature, he devised the term *ant in labyrinth*[1]. There are two canonical modes of walks when the ant explores an open cluster. Assuming a lattice with co-ordination number z, one denotes the number of nearest open neighbours of the site s by $Z(s)$. Upon the arrival of a *myopic ant* at the site s, the ant identifies the nearest open sites and in the next step, it chooses one of them with probability $1/Z(s)$. This mode of walk corresponds to the classical *Pólya walk*; sometimes referred to as *Pólya ant* as well [29, 30]. Contrarily, the *blind ant*, since it is blind, upon its arrival at the site s, chooses one of the nearest neighbour with probability $1/z$ for its next step, and if that neighbouring site the ant is about to move to is occupied, it stays at the site which it currently resides at with probability $[z - Z(s)]/z$ [31].

The equilibrium probability distribution is reached differently for these two modes of walk. For the blind ant, denoting the probability of the ant to be at site s by $P(s|s_0)$ given that it started initially at site s_0, and the number of sites of the open cluster by $||\mathcal{C}||$. The probability distribution function after taking n steps would be given by

$$P(s|s_0) = 1/||\mathcal{C}||, \tag{2.7}$$

[1]The labyrinth is a well-known fractal structure due to its scale-free geometry [28]

for all n after reaching equilibrium state. Meanwhile, for the myopic ant, this probability can depend on whether the number it has taken is even or odd; it also depends on the initial site s_0 of the ant [26, 32]. If the underlying lattice is bipartite, then one can deterministically identify on which sub-lattice the ant is, given that the number of the steps the ant has already taken is even or odd.

The distinction becomes apparent once matrix transfer formalism is exploited to analyse the eigenvalue spectrum of the matrix associated with the distribution of the obstacles on a given lattice [32]. By decomposing the eigenvalue of the matrix, three different classes of eigenvalues may appear, positive, negative and complex. Since the matrix is real, the complex eigenvalues must appear in pair conjugates. Moreover, for the blind ant, since the matrix is symmetric all the eigenvalues and their corresponding eigenvectors must be real. For the myopic ant, conversely, the transfer matrix is not symmetric, nonetheless, it was proven that there exists a transformation such that the transfer matrix for the myopic ant could be converted into a symmetrical one [32] (Jacobs cited a private communication he had with N. Fuchs). Hence, the same statement regarding the existence of the complex eigenvalues extends to the myopic ant. As previously mentioned, if in an occasion in which the underlying lattice is bipartite, the coexistence of negative and positive eigenvalues for the myopic ant indicates consecutive jumps from one sub-lattice to the other, corresponding to the odd or even steps taken by the ant. Yet for blind ant, as well as for myopic ant on a non-bipartite lattice, all the eigenvalues are positive, since one cannot deterministically identify whether the ant is taking its odd or even step. By comparing the differences between these two modes of the walk, quoting Hughes, apparently many authors have claimed that blind ant mode is more natural to study the random walk process in randomly obstructed environments([26] p. 438). Therefore, the mode chosen here, as well, is the blind ant and what is presented henceforth, discusses the scaling behaviour of this mode of walk on open clusters appearing near critical percolation density p_c.

2.2.2 Mean Squared Displacement

One of the statistical quantities of interest for the random walk process is the mean squared displacement. Abbreviated as MSD, for an ensemble of random walk processes on a given open cluster $\mathcal{C}$ it is defined as

$$\left\langle r_{\mathcal{C}}^2(t)\right\rangle = \left\langle \left|\mathbf{r}(t)-\mathbf{r}(0)\right|^2 \right\rangle, \tag{2.8}$$

where $\mathbf{r}(t)$ denotes the spatial position of the random walk process at time t. For a random walk process after taking t steps on an incipient infinite cluster MSD scales as t^{2/d_w}, where

d_w is called the fractal dimension of the random walk path [26, 33]. For the Bernoulli percolation model used in this work, $d_w > 2$ which further implies that the exponent of t is smaller than unity. This suggests that the random walk process in such random environments are subdiffusive [34]. Nevertheless, there are other measures than the Bernoulli probability measure or other types of dynamical interaction between the random walk process and the random environment which could lead to superdiffusive dynamics where the exponent of t is larger than unity [35]. Moreover, it is noteworthy to mention that the random walk process in random environments is not the only model of anomalous diffusion. Others such as *diffusing diffusivity, random walk in heterogenous media, continuous random walk (CTRW)* and *fractional Brownian motion* are a few to name which reproduce subdiffusive or superdiffusive dynamics [36–39]. Another quantity of interest is the number of distinct visited sites which after t steps, on statistical average, scales as $t^{d_s/2}$ where d_s is called the *spectral dimension* (also *harmonic dimension*) [26, 33]. The fractal dimension of the open cluster, the fractal dimension of the random walk path and the spectral dimension are related through the following

$$d_s = 2d_f/d_w, \tag{2.9}$$

known as Alexander-Orbach scaling law [40]. As mentioned earlier, the intention of this work is not to only study the topological properties of the incipient infinite clusters, but to take into account the contribution of all possible realisations of the open clusters with different sizes. Dynamical scaling theory provides one with the essential means for relating the statistical properties of the random walk process averaged on all open clusters with different sizes to the geometrical exponents of the infinite cluster near the critical point. The main driver for this intention is that in experimental setups, all the open clusters are finite in size. Yet, concerning the time scale of the experiment, the open clusters may appear as an incipient infinite cluster. To elaborate this further, consider a realisation of a percolation process on a two-dimensional square lattice. Assume that the centre of the lattice belongs to an open cluster $\mathcal{C}$ and that the cluster is finite in size. Consider a random walk process on this open cluster; the MSD of such a process scales as

$$\left\langle r_{\mathcal{C}}^2(t)\right\rangle \sim t^{2/d_w}, \tag{2.10}$$

for time scales that are firstly, sufficiently smaller compared to the size of the cluster, such that the random walk process would not reach the boundary of the cluster and secondly, mimic length scales for which the cluster appears to be homogeneous. Nonetheless, it is evident that as t grows, the random walk process would eventually sample all the accessible

open sites within the cluster and MSD would reach its terminal value. Denote this terminal value by R^2_∞, where the subscript denotes the radius explored by the random walk process after taking infinitely many steps. It is held such that [26]

$$\frac{R^2_\infty - \left\langle r^2_{\mathcal{C}}(t)\right\rangle}{R^2_\infty} \sim \exp\left(-\left[\frac{t}{\chi}\right]^w\right), \tag{2.11}$$

where χ is the characteristic time required for the random walk process to reach the boundary of the open cluster. Obviously, this characteristic time solely depends on the size of the open cluster, namely $||\mathcal{C}||$. The exponent w is smaller than unity and determines how fast the MSD of the random walk process reaches its terminal value. A glance reveals that for time scales $t \ll \chi$, MSD should monotonically increase as the dynamical scaling theory predicts. Thus, it is evident that w is indeed $2/d_w$. This has been also proven by the means of numerical simulations and further was justified by the means of the matrix transfer formalism that $w = 2/d_w$. But historically, w was assigned to unity which by the means of numerical simulations was defied [41–43].

For a given open cluster $\mathcal{C}$ and an ensemble of random walk processes, the equilibrium initial condition is fulfilled if the ant parachutes randomly with the equal probability $1/||\mathcal{C}||$ on each site of the open cluster. Recall that this is the probability distribution of the ant being at a specific site after reaching the stationary state. Thence follows immediately that R^2_∞ is nothing but twice the second power of the radius of gyration of the cluster $\mathcal{C}$. To arrive at this conclusion, assume the equilibrium initial condition and let the ant takes infinitely many steps on this very open cluster. After certain elapse of time which is comparable to χ, all the sites of the open cluster will be visited equally with the probability $1/||\mathcal{C}||$. This is identified as the stationary state of the random walk process. Whence, it is a simple exercise to prove that for the ensemble of random walk processes, MSD is nothing but $2R^2_g$, where R_g is the radius of gyration of cluster $\mathcal{C}$ which is defined as

$$R^2_g = \frac{1}{2||\mathcal{C}||^2}\sum_{i,j}|\mathbf{r}_i - \mathbf{r}_j|^2, \tag{2.12}$$

where r_i and r_j are the vectors pointing to the position of the sites of cluster $\mathcal{C}$ indexed by i and j respectively. An instance of such an open cluster with size $||\mathcal{C}|| = 793$ is demonstrated in Fig 2.2 alongside with its radius of gyration and the centre of mass. Recall the definition of MSD which is given by $\left\langle|\mathbf{r}(t) - \mathbf{r}(0)|^2\right\rangle$. When $t \to \infty$, $\mathbf{r}(t)$ could be any of the sites lying within the cluster $\mathcal{C}$ with the probability $1/||\mathcal{C}||$. Furthermore, assume the equilibrium initial condition which implies that $\mathbf{r}(0)$ could also be any of the sites within the cluster $\mathcal{C}$ with probability $1/||\mathcal{C}||$. Therefore,

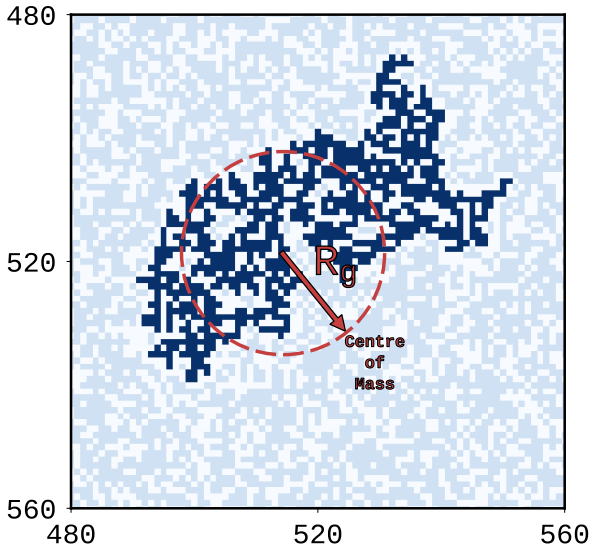

Figure 2.2 An instance of a finite size open cluster with size 793 near the critical point. The cluster is identified by its Oxford blue colour. The sky blue represents other vacant sites which do not belong to the concerned open cluster. The white-off powder blue sites are blocked. The radius of the gyration is depicted by the red arrow and the corresponding circle is depicted with red dashed-line whose centre is the centre of mass of the open cluster.

$$\lim_{t\to\infty}\left\langle r_{\mathcal{C}}^2(t)\right\rangle = \lim_{t\to\infty}\left\langle \left|\mathbf{r}(t)-\mathbf{r}(0)\right|^2\right\rangle$$
$$= \sum_{i,j}\left|\frac{\mathbf{r}_i}{||\mathcal{C}||}-\frac{\mathbf{r}_j}{||\mathcal{C}||}\right|^2 = \frac{1}{||\mathcal{C}||^2}\sum_{i,j}|\mathbf{r}_i-\mathbf{r}_j|^2 = 2R_g^2.$$

Thus, through Eq.(2.11), MSD will be identified to be

$$\left\langle r_{\mathcal{C}}^2(t)\right\rangle_{\text{eq}} = 2R_g^2\left(1-\exp\left[-\left(\frac{t}{\chi}\right)^{2/d_w}\right]\right), \tag{2.13}$$

where the subscript 'eq' indicates that the equilibrium initial condition is asserted.

In the expression above, R_g and χ can be expressed in term of the cluster size $||\mathcal{C}||$ by exploiting the scaling theory and the dynamical scaling theory respectively. Recall that in dynamical scaling theory the number of distinct visited sites by a random walk process on an incipient infinite cluster with respect to time scales as $S(t)\sim t^{d_f/d_w}$. Thus, the time required by the ant to visit all the sites within the open cluster is given by $||\mathcal{C}||^{d_w/d_f}$. To relate R_g to the size of the cluster, assume a circle with radius R. If one tiles the area of this very circle with squares of unit area, then the number of tiles encircled by the perimeter is proportional to R^2, where the exponent is the Euclidean dimension of the disk. For a finite size open cluster, since it exhibits fractal nature, the relevant topological dimension would be d_f. Thus

the number of sites included within the radius of gyration of the cluster scales as $||\mathcal{C}||^{2/d_f}$. Subsequently, Eq. (2.13) can be rewritten as

$$\left\langle r_{\mathcal{C}}^2(t)\right\rangle_{\text{eq}} = 2h^2||\mathcal{C}||^{2/d_f}\left(1-\exp\left[-\frac{\mathcal{D}t^{2/d_w}}{||\mathcal{C}||^{2/d_f}}\right]\right), \tag{2.14}$$

where h and $\mathcal{D}$ are dimensional constants defined through $R_g^{d_f} = h^{d_f}||\mathcal{C}||$ and $\chi^{2/d_w} = \mathcal{D}||\mathcal{C}||^{2/d_f}$ respectively.

Nonetheless, this very expression is not pertinent to the main objective of this work. As it will be delineated in the following chapters, the procedure chosen here to simulate such an ensemble is to force the ant to parachute always at the centre of the lattice. This is to due to some practical limitations imposed by the complexity of the percolation process. Specifically, fulfilling the equilibrium initial condition for significantly large clusters is computationally an exhaustive task. Furthermore, for many experimental set-ups in laboratories, it is more natural to fix spatially the initial condition. Thus, the initial condition of the random walk processes is always affixed to the centre of the lattice which would negate the assumption of the equilibrium initial condition. Consequently, one has to seek an expression for MSD when the constraint of the equilibrium initial condition is lifted. Notwithstanding, this is proved to be non-trivial. The reason that the deduction of such an expression is laborious lies within the fact that, contrary to many other random walk or stochastic processes, the probability density function of the random walk process in random environments, due to the complexity of the topology of the support, remains unknown [44, 45]. Despite this fact, the random walk process on deterministic fractals has exact solutions [46, 47]. To rephrase it, no systematic way, such as solving the *stochastic differential equation* of the random walk process on incipient infinite clusters has been developed. In this regard, here, a phenomenological approach is suggested to overcome this difficulty and by claiming a conjecture, an expression is deduced such that it could arguably describe the behaviour of MSD in the absence of the criterion of equilibrium initial condition for the problem of the *Ant in the Labyrinth*.

2.3 Ornstein-Uhlenbeck Processes and Ant in Labyrinth: Phenomenological Approach

A closer look at Eq. (2.11) draws one's attention towards the similarity between the random walk process on finite size open clusters and the renowned *Ornstein-Uhlenbeck process* [48]. Simply substitute the exponent w by 1 and then one immediately recovers the MSD for the Ornstein-Uhlenbeck process with the equilibrium initial condition asserted [49].

The Ornstein-Uhlenbeck process belongs to the class of the *Gauss-Markov processes*, which implies that it is simultaneously identified as a Gaussian and a Markov process [48]. The fact that it is a Gaussian process, implies that the covariance function of the process fully defines the process if the mean is assumed to be zero [50]. Furthermore, the process has a unique strong stationary solution.

Although the two processes have different supports - infinite for the Ornstein-Uhlenbeck process and finite for the random walk process on finite-size open clusters - both processes are Markovian ([26] p.438) with finite first and second moments of statistics. Another difference between the two cases is that the metric imposed by the geometry in the case of the Ornstein-Uhlenbeck process is Euclidean while for the latter, it is dictated by the Hausdorff measure. That being said, it seems that a rescaling relation could be made between the two by facilitating the scaling and dynamical scaling theory. To demonstrate this further, recall that the stochastic differential equation for the Ornstein-Uhlenbeck process in two dimensions is given by

$$\frac{d\mathbf{r}}{dt} = -\frac{\mathbf{r}}{\chi} + \sigma\boldsymbol{\eta}(t), \tag{2.15}$$

where $\mathbf{r} = (r_x, r_y)$, and χ and σ are positive definite parameters. The stochastic function $\boldsymbol{\eta}(t)$ is the Gaussian white noise with zero-mean and the correlation function satisfying

$$\left\langle \eta_i(t_1)\eta_j(t_2)\right\rangle = \delta_{ij}\delta(t_1 - t_2); \quad i, j \in \{x, y\},$$

where δ_{ij} is the Kronecker delta and $\delta(x)$ is the Dirac delta function. The solution of the differential Eq. (2.15) is found to be

$$\mathbf{r}(t) = e^{-t/\chi}\left(\mathbf{r}_0 + \sigma\int_0^t e^{s/\chi}\boldsymbol{\eta}(s)ds\right), \tag{2.16}$$

where $\mathbf{r}_0$ is the initial condition of the process. From the equation above one deduces that the mean and the position autocorrelation function of the process are given by

$$\langle r_i(t)\rangle = \left\langle r_0^i\right\rangle e^{-t/\chi} \tag{2.17}$$

$$\langle r_i(t_1)r_i(t_2)\rangle = \left(\left\langle r_0^{i\,2}\right\rangle - \frac{\chi\sigma^2}{2}\right)e^{-(t_1+t_2)/\chi} + \frac{\chi\sigma^2}{2}e^{-|t_1-t_2|/\chi}, \tag{2.18}$$

where $i \in \{x, y\}$. Thus, one arrives at the following expression for the MSD of the process

$$\begin{aligned}\left\langle \mathbf{r}^2(t)_{\mathrm{OU}} \right\rangle &= \left\langle \left| \mathbf{r}(t) - \mathbf{r}(0) \right|^2 \right\rangle \\ &= \left\langle \mathbf{r}_0^2 \right\rangle \left(1 - \exp\left[-\left(\frac{t}{\chi} \right) \right] \right)^2 + \chi\sigma^2 \left(1 - \exp\left[-2\left(\frac{t}{\chi} \right) \right] \right). \end{aligned} \tag{2.19}$$

The equilibrium initial condition for $\mathbf{r}_0$ is a is a normal distribution $\mathcal{N}(0, \rho^2)$, where the variance is simply concluded to be $\chi\sigma^2$ by recalling Eq. (2.16) and infer that,

$$\begin{aligned} r_0^i &= \sigma \int_{-\infty}^{0} e^{s/\chi} \eta_i(s) ds, \\ \left\langle r_0^{i\,2} \right\rangle &= \sigma^2 \int_{-\infty}^{0} e^{2s/\chi} ds = \frac{\sigma^2 \chi}{2}. \end{aligned}$$

Readily, Eq. (2.19), once equilibrium initial condition is assumed, would simplify to the following expression

$$\left\langle \mathbf{r}^2(t)_{\mathrm{OU}} \right\rangle_{\mathrm{eq}} = 2\chi\sigma^2 \left(1 - \exp\left[-\left(\frac{t}{\chi} \right) \right] \right). \tag{2.20}$$

Now compare the equation above with Eq. (2.13) and identify the exponent w is unity for the Ornstein-Uhlenbeck process and $2/d_w$ for the random walk process on finite size open clusters. The base of this work for further analyses is founded upon the following conjecture after the observation of the similarity between the Ornstein-Uhlenbeck process and the random walk process on finite size open clusters.

Conjecture: Random walk process on a finite size open cluster $\mathcal{C}$ is analogous to Ornstein-Uhlenbeck process with the positive definite parameters χ and σ where R_g is the radius of gyration of the cluster $\mathcal{C}$ satisfying $R_g^2 = \chi\sigma^2$, and the time t is rescaled as t^{2/d_w}.

The conjecture above paves the way to adopt Eq. (2.19) and transform it accordingly by scaling the time, to identify an expression for MSD of random walk process on finite size open clusters when the equilibrium initial condition is not fulfilled. Therefore, MSD for an ensemble of random walk processes on a finite size open cluster is concluded to be

$$\begin{aligned}\left\langle r_{\mathcal{C}}^2(t) \right\rangle = \left\langle \mathbf{r}_0^2 \right\rangle &\left(1 - \exp\left[-\frac{\mathcal{D}t^{2/d_w}}{||\mathcal{C}||^{2/d_f}} \right] \right)^2 \\ &+ 2h^2 ||\mathcal{C}||^{2/d_f} \left(1 - \exp\left[-\frac{2\mathcal{D}t^{2/d_w}}{||\mathcal{C}||^{2/d_f}} \right] \right). \end{aligned} \tag{2.21}$$

Note that R_g and χ are written in term of the size of the cluster $\mathcal{C}$. It is worthy to mention that $\mathbf{r}_0$ is given in the reference frame of centre of mass coordinate of the open cluster. As mentioned earlier, when the equilibrium initial condition is met - when the ant could parachute on any open site of the cluster $\mathcal{C}$ - $\langle \mathbf{r}_0^2 \rangle$ is simply $2R_g^2$ and the equation above reduces to Eq. (2.13) subsequently.

This conjecture should conclude this chapter by providing the means to establish an analogy between the well-known stochastic process of Ornstein-Uhlenbeck process and the random walk process on finite size open cluster. In the following chapter, this would provide a firm ground to address the ergodic property of an ensemble of random walk processes in an ensemble of open clusters near the critical point p_c.

Chapter 3

Ergodic Property of the Random Walk Process near the Critical Point

As discussed earlier, the random walk process on finite size open clusters near the critical point p_c has a stationary state after sufficient elapse of time which is dictated by the size of the cluster. The statistical properties of the stationary process remain invariant under time shifts. Therefore, ensemble averaged quantities and their equivalent time averaged quantities are statistically equivalent [51]. This implies that the process is *ergodic* in the sense that the statistical properties of an ensemble of random processes can be inferred by having an instance of them which is sufficiently long. For further clarification, assume a stationary random process $X(t)$ and identify the mean and the autocovariance of the process as

$$\begin{aligned} \mu_X(t) &= \langle X(t) \rangle , \\ \mathrm{Cov}_X(\Delta) &= \langle (X(t+\Delta) - \mu_X(t+\Delta))(X(t) - \mu_X(t)) \rangle . \end{aligned}$$

Then the process is *mean* and *autocovariance ergodic* if it holds such that

$$\begin{aligned} \overline{\mu_X} &= \frac{1}{T}\int_0^T X(t)dt = \mu_X(t), \\ \overline{\mathrm{Cov}_X(\Delta)} &= \frac{1}{T-\Delta}\int_0^{T-\Delta} [X(t+\Delta) - \mu_X(t+\Delta)][X(t) - \mu_X(t)]dt = \mathrm{Cov}_X(\Delta) \end{aligned}$$

where the overline indicates the time average, T is the measurement time and Δ is called the *lag time*.

The equivalency between the ensemble averages and time averages is essential in single particle tracking as it is not always possible to repeat an experiment due to laboratorial

limitations. Thus, the only possible solution is to have a sufficiently long trajectory and infer the statistical properties of the process with a single trajectory in hand.

3.1 Time Averaged Mean Squared Displacement

Time averaged mean squared displacement, abbreviated as TAMSD, is one of such quantities from which one can deduce statistical properties of a certain process from a sufficiently long trajectory [52, 53]. It is defined as

$$\left\langle \overline{\delta^2_{\mathcal{C}}(\Delta)} \right\rangle = \frac{1}{T-\Delta} \int_0^{T-\Delta} \left\langle \left| \mathbf{r}(t+\Delta) - \mathbf{r}(t) \right|^2 \right\rangle dt, \tag{3.1}$$

where T is the length of the trajectory and Δ is called the lag time which indicates the time difference between two spatial points visited during the course of the process. Assuming the equilibrium initial condition, the process would be stationary for all $t \geq 0$ and it immediately follows from the equivalency between MSD and TAMSD that[1]

$$\left\langle \overline{\delta^2_{\mathcal{C}}(\Delta)} \right\rangle = 2h^2 ||\mathcal{C}||^{2/d_f} \left(1 - \exp\left[-\frac{\mathcal{D}\Delta^{2/d_w}}{||\mathcal{C}||^{2/d_f}} \right] \right). \tag{3.2}$$

Yet, the initial position of the random walk process is attached to the centre of the lattice and is fixed. For this case where the equilibrium initial condition is not met, the process is not stationary and thus, one should seek a suitable expression for TAMSD. Once more, by assuming the validity of the conjecture, one could solve TAMSD for the Ornstein-Uhlenbeck process for the case of the non-equilibrium initial condition and rescale time to arrive at an expression for the TAMSD of random walk process on finite size open clusters. Solving TAMSD for the Ornstein-Uhlenbeck process yields

$$\begin{aligned} \left\langle \overline{\delta^2_{\mathrm{OU}}(\Delta)} \right\rangle = {} & 2\chi\sigma^2 \left(1 - \exp\left[-\left(\frac{\Delta}{\chi} \right) \right] \right) \\ & + \left(\langle \mathbf{r}_0^2 \rangle - \chi\sigma^2 \right) \left(1 - \exp\left[-\left(\frac{\Delta}{\chi} \right) \right] \right)^2 \left(\frac{1 - \exp\left[-2\left(\frac{T-\Delta}{\chi} \right) \right]}{2\left(\frac{T-\Delta}{\chi} \right)} \right). \end{aligned} \tag{3.3}$$

[1] This statement holds true for the Markovian processes only. For the significance of the initial condition in non-Markovian processes refer to [54].

Once the equilibrium initial condition is asserted, implying that $\langle \mathbf{r}_0^2 \rangle = \chi\sigma^2$, one recovers the stationary Ornstein-Uhlenbeck process and TAMSD would be deduced to be

$$\left\langle \overline{\delta^2_{\mathrm{OU}}(\Delta)} \right\rangle_{\mathrm{eq}} = 2\chi\sigma^2 \left(1 - \exp\left[-\left(\frac{\Delta}{\chi}\right)\right]\right). \tag{3.4}$$

Compare to the Eq. (2.20) and observe that they are equivalent, which affirms the earlier statement that the Ornstein-Uhlenbeck process is ergodic and stationary. This also can be inferred solely by perceiving the fact that if the equilibrium initial condition is satisfied, the position autocorrelation function of Eq. (2.18) is reduced to

$$\langle \mathbf{r}(t_1) \cdot \mathbf{r}(t_2) \rangle = \chi\sigma^2 e^{|t_1 - t_2|/\chi}, \tag{3.5}$$

where $\cdot$ is the inner product defined as $\mathbf{a} \cdot \mathbf{b} = \sum_i a_i b_j^*$, where $\mathbf{a}$ and $\mathbf{b}$ are vectors, $i \in \{x, y\}$ and $*$ is the complex conjugate. Note that, since the correlation between the positions depends solely on the time difference, the process is ergodic and stationary.

Now by invoking the earlier conjecture, one arrives at

$$\begin{aligned}\left\langle \overline{\delta^2_{\mathcal{C}}(\Delta)} \right\rangle =& 2h^2 ||\mathcal{C}||^{2/d_f} \left(1 - \exp\left[-\frac{\mathcal{D}\Delta^{2/d_w}}{||\mathcal{C}||^{2/d_f}}\right]\right) + \left(\langle \mathbf{r}_0^2 \rangle - 2h^2 ||\mathcal{C}||^{2/d_f}\right) \\ &\times \left(1 - \exp\left[-\frac{\mathcal{D}\Delta^{2/d_w}}{||\mathcal{C}||^{2/d_f}}\right]\right)^2 \left(\frac{1 - \exp\left[-\frac{2\mathcal{D}(T-\Delta)^{2/d_w}}{||\mathcal{C}||^{2/d_f}}\right]}{\frac{2\mathcal{D}(T-\Delta)^{2/d_w}}{||\mathcal{C}||^{2/d_f}}}\right).\end{aligned} \tag{3.6}$$

For the random walk process on finite size open clusters, some subtleties should be addressed regarding the asymptotes of Eq. (2.21) and Eq. (3.6) once the process reaches its stationary state. The stationary state for both MSD and TAMSD is attained when $t \to \infty$ and $T \to \infty$ respectively. In those limits

$$\lim_{t\to\infty} \left\langle r_{\mathcal{C}}^2(t) \right\rangle = \langle \mathbf{r}_0^2 \rangle + R_g^2, \tag{3.7}$$

$$\lim_{T\to\infty} \left\langle \overline{\delta^2_{\mathcal{C}}(\Delta)} \right\rangle = \begin{cases} 2R_g^2 & \text{if} \quad \chi < \Delta \ll T \\ \langle \mathbf{r}_0^2 \rangle + R_g^2 & \text{if} \quad \Delta \to T \end{cases}. \tag{3.8}$$

Note that, when equilibrium initial condition is fulfilled, regardless of the time scale of Δ, MSD and TAMSD approach the same asymptote namely $2R_g^2$. Yet, if the equilibrium initial condition is not asserted, there is a gap of magnitude $|R_g^2 - \langle \mathbf{r}_0^2 \rangle|$ between MSD and TAMSD when $\chi < \Delta \ll T$. This is due to the intrinsic way MSD and TAMSD are defined. A closer look reveals that, MSD is a measure which quantifies the dispersal of an ensemble of a

stochastic process till time t. On the other hand, TAMSD is a measure which quantifies the growth of the increments of the process that are apart from each other by the time difference Δ. These are generic definitions of the two aforementioned quantities and it is evident that they are not compatible. An attempt to define a set of generalised definitions for MSD and TAMSD is addressed in [54] which is out of the scope of this work. The caveat here is that the apparent gap between MSD and TAMSD when the equilibrium initial condition is not asserted should not be interpreted as a non-ergodic property of the random walk process on finite size open clusters. As mentioned earlier, it is crystal clear that such a process has a stationary state once all the open sites of the open cluster are visited by the ant. The same discrepancy also applies to the case of the Ornstein-Uhlenbeck process, and the gap is still observable if the equilibrium initial condition is not assumed, although, it is known that the Ornstein-Uhlenbeck process is stationary and ergodic and the appearance of this gap between MSD and TAMSD is solely the consequence of their incompatible definitions.

Now that a plausible expression for TAMSD has been concluded, time is ripe to address the ergodic property of single particle trajectories in an ensemble of finite size open clusters near the critical point. This paves the way to further study how asymptotically the random walk process in an ensemble of finite size open clusters reach the ergodic limit.

3.2 Disorder Average: Anisotropy and Cluster Size Averages

It was mentioned earlier, and it will be elaborated in the following chapter, that the ensemble of concern here does not only consist of samples of the random walk process on a specific cluster but also clusters with different sizes. In other words, each random walk process takes place on different open clusters which are different in shape and size, which subsequently implies that their geometrical properties vary case to case. Open clusters of the same size could have different shapes. For instance, a cluster of size three could be a straight line or could have a bend. This demonstrates that the clusters are anisotropic with respect to the centre of the lattice. And obviously, clusters have different sizes which as it was addressed in the earlier chapter, near the critical point, the distribution of the clusters concerning their size follows a power-law distribution. Therefore, averaging over the ensemble of clusters consists of two steps; first averaging over the clusters which have the same size but obviously possess different shapes and, the second step is averaging over the size of the clusters. The former one is referred to as *anisotropy average* and the latter one is called *cluster size average*. The procedure of taking the two averages consecutively is called *disorder average*.

3.2.1 Anisotropy Average

Clusters having the same size are different in shapes. Open sites could be symmetrically distributed around the centre of the lattice or could be asymmetrical. Therefore, it is necessary to take this into account when the ensemble average is taken over the set of clusters. Anisotropy average yields an interesting result which is equivalent to asserting equilibrium initial condition. To prove this, first, recall Eq. (3.6) and bear in mind that $\langle \mathbf{r}_0^2 \rangle$ is given in the reference frame of the centre of mass coordinate. Consider the set of all clusters with size three which are depicted in Fig. 3.1. There are two classes of such clusters, one that constitutes clusters of straight line, which is denoted by $[-]$ and is depicted in the first row of Fig. 3.1, and one that consists of clusters with a sharp corner, which are depicted in the lower row of the same figure and the class is denoted by $[\llcorner]$. The rest of the clusters are identified by applying the symmetry groups of the square lattice. The clusters are shown with green borders and the centre of the lattice is distinguished by the red colour. Each one of these clusters is equally probable to appear as the percolation model considered here is the Bernoulli percolation model. Recall that the ant always parachutes at the centre of the lattice. The only parameter that varies in these different realisations, is the centre of the mass of these clusters; it shifts case to case. Hence, one can assume the centre of mass can be chosen randomly to be any of the open sites of these clusters depicted in Fig. 3.1. Therefore $\langle \mathbf{r}_0^2 \rangle = \langle |\mathbf{r}(0) - \mathbf{r}_{\rm cm}|^2 \rangle$ is identified to be nothing but the radius of gyration of that specific class of clusters once averaged over the anisotropy. This can also be shown by a simple calculation. Consider the first row of Fig. 3.1 and find out that

$$
\begin{cases} \mathbf{r}_0^2 = (0-1)^2 = 1 \\ R_g^2 = \frac{1}{3}\left[(0-1)^2 + (1-1)^2 + (2-1)^2\right] = \frac{2}{3} \end{cases} \quad \text{(Leftmost)}
$$

$$
\begin{cases} \mathbf{r}_0^2 = (0-0)^2 = 0 \\ R_g^2 = \frac{1}{3}\left[(-1-0)^2 + (0-0)^2 + (1-0)^2\right] = \frac{2}{3} \end{cases} \quad \text{(Middle)}
$$

$$
\begin{cases} \mathbf{r}_0^2 = (-1-0)^2 = 1 \\ R_g^2 = \frac{1}{3}\left[(-2+1)^2 + (-1+1)^2 + (0+1)^2\right] = \frac{2}{3} \end{cases} \quad \text{(Rightmost).}
$$

Now average over $\mathbf{r}_0^2$ and deduce that anisotropy average yields $\langle \mathbf{r}_0^2 \rangle = \frac{2}{3} = R_g^2$. This at the first glance my seem surprising, but bear in mind that since lattices remain invariant under translational transformation along the lattice primitive vectors. Thus, anisotropy average is equivalent to let the ant parachute with equal probability $1/||\mathcal{C}||$ on each open site of the cluster $\mathcal{C}$. The only difference here is that the role of $\mathbf{r}(0)$ and $\mathbf{r}_{\rm cm}$ is exchanged. Basically,

instead of letting the ant parachute randomly on each open site of the cluster, shift the underlying lattice and observe that the centre of the lattice is now associated with another open site of the cluster which consequently represents another possible configuration with a displaced centre of mass of the same cluster. Thus, taking anisotropy average over TAMSD for the set of clusters of size $||\mathcal{C}||$, yields

$$\left\langle \overline{\delta^2_{\mathcal{C}^*}(\Delta)} \right\rangle = 2h^2 ||\mathcal{C}||^{2/d_f} \left(1 - \exp\left[-\frac{\mathcal{D}\Delta^{2/d_w}}{||\mathcal{C}||^{2/d_f}} \right] \right), \tag{3.9}$$

which is indeed the expression for TAMSD when equilibrium initial condition is asserted (refer to Eq. (3.2)). The subscript $\mathcal{C}^*$ indicates that anisotropy average has been taken into account for clusters having size $||\mathcal{C}||$. This result is of utmost importance in the sense that it reveals how the concept of topology and time are intertwined. It is noteworthy to mention that averaging over the anisotropy of the clusters with the same size yields essentially a geometry which is homogeneous and isotropic and its effective radius is identified by R_g. Further, one should bear in mind that recovering the stationary solution of TAMSD is the antecedent of the translational invariance of the lattice structure.

It is also of importance to mention that sampling all the possible configurations of the clusters with the same size is of practical impossibility, due to the computational limitations. For instance, the number of the total possible configurations for the clusters with size 24 is of the order of 10^3 [55]. Then it is evident that the realisation of all possible configurations of clusters with size 100 and above is almost impossible in a given finite amount of time.

It should be emphasised also that $\left\langle \overline{\delta^2_{\mathcal{C}^*}(\Delta)} \right\rangle$, viewed as a set of random variables, obeys a power law distribution. The distribution can be inferred by exploiting the conservation law of probability between the cluster size distribution and the probability distribution of the TAMSDs after the anisotropy average being taken. This yields the following

$$P\left(\left\langle \overline{\delta^2_{\mathcal{C}^*}(\Delta)} \right\rangle \right) \sim ||\mathcal{C}||^{2-2/df-\tau}. \tag{3.10}$$

Instances of TAMSDs for open clusters with different sizes are depicted in Fig 3.2. Observe that although on finite size open clusters the TAMSD saturates, the disorder averaged TAMSD (which will be discussed in the following section) is monotonically and linearly increasing in the logarithmic scales.

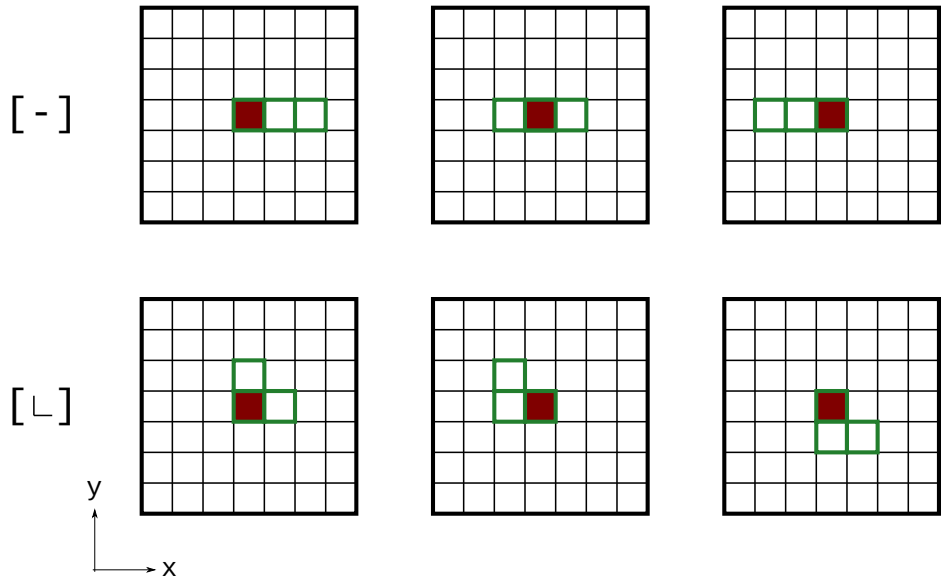

Figure 3.1 Demonstration of the two classes of clusters of size 3. The upper row depicts the clusters that are straight with respect to the horizontal line. The lower row depicts the clusters that have a sharp corner. The other configurations of the clusters with size 3 are attained by applying the symmetry groups of the square lattice. The clusters are shown with green edges and the centre of the lattice is shown by red colour.

3.2.2 Cluster Size Average

After taking the anisotropy average over clusters with the same size, define the cluster size average for the set of an ensemble of isotropic and homogeneous clusters denoted by $\{\mathcal{C}^*\}$ as

$$\widetilde{\left\langle \overline{\delta^2_{\mathcal{C}}(\Delta)} \right\rangle} = \sum_{\{\mathcal{C}^*\}} \mathcal{P}\left(||\mathcal{C}||\right) \left\langle \overline{\delta^2_{\mathcal{C}^*}(\Delta)} \right\rangle, \tag{3.11}$$

where $\mathcal{P}\left(||\mathcal{C}||\right)$ is the probability of the ant to land on a cluster with size $||\mathcal{C}||$. Near the critical point p_c according to the scaling theory, it is known that the probability of a cluster with size $||\mathcal{C}||$ to appear at the centre follows a power law distribution and it scales as $||\mathcal{C}||^{-\tau}$, where the exponent τ as mentioned earlier is called the Fisher exponent. But this is only the probability of the appearance of such a cluster at the centre. Also, one has to take into account the probability of the ant to parachute on such a cluster at the centre which is proportional to the size of the cluster. Thus, the probability $\mathcal{P}\left(||\mathcal{C}||\right)$ is found to scale as $||\mathcal{C}||^{1-\tau}$. Consequently, the equation above can be identified as

$$\widetilde{\left\langle \overline{\delta^2_{\mathcal{C}}(\Delta)} \right\rangle} = \Xi \sum_{||\mathcal{C}||=1}^{\infty} \left\langle \overline{\delta^2_{\mathcal{C}^*}(\Delta)} \right\rangle ||\mathcal{C}||^{1-\tau}, \tag{3.12}$$

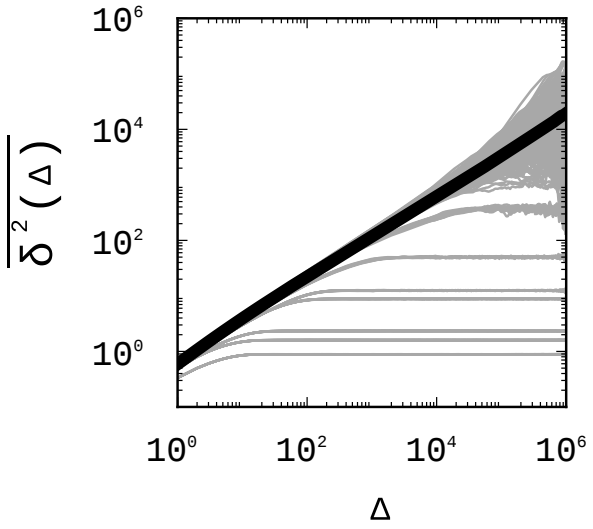

Figure 3.2 Individual TAMSDs (grey lines) versus lag time Δ at $p_c = 0.6$. in logarithmic scale. Note that TAMSDs due to finite support saturate where the level of the saturation is imposed by the size of the cluster. The disorder average of the TAMSDs (thick black line) on the contrary increases monotonically.

where Ξ is a normalisation constant and bear in mind that the summation starts from the smallest possible cluster size which in discrete lattice space is unity. It is worth mentioning that, summation (integration) over power-law distributions diverges unless a minimum lower cut-off is assumed for the distribution. The lower cut off is naturally introduced by noticing that the probability space is devoid of clusters with size zero. By taking the continuum limit of Eq. (3.12) and by substituting $\left\langle\overline{\delta^2_{\mathcal{C}^*}(\Delta)}\right\rangle$ with the expression given in Eq. (3.9), one arrives at the following integral

$$\left\langle\widetilde{\overline{\delta^2_{\mathcal{C}}(\Delta)}}\right\rangle = \Xi \int_{||\mathfrak{c}||}^{\infty} 2h^2 \left(1-\exp\left[-\frac{\mathcal{D}\Delta^{2/d_w}}{||\mathcal{C}||^{2/d_f}}\right]\right) ||\mathcal{C}||^{2/d_f+1-\tau} d\,||\mathcal{C}||, \tag{3.13}$$

where $||\mathfrak{c}||$ is the smallest cluster size in $\{\mathcal{C}^*\}$ in the continuum limit. Furthermore, $\Xi \int_{||\mathfrak{c}||}^{\infty} ||\mathcal{C}||^{1-\tau} = 1$, which yields $\Xi = (\tau-2)||\mathfrak{c}||^{\tau-2}$. Subsequently, the integral above yields the following result for the *disorder averaged* TAMSD;

$$\begin{aligned}\left\langle\widetilde{\overline{\delta^2_{\mathcal{C}}(\Delta)}}\right\rangle =& (\tau-2)||\mathfrak{c}||^{\tau-2}\Bigg\{-\frac{2d_f h^2}{2+d_f(2-\tau)}||\mathfrak{c}||^{2d_f+2-\tau} \\ & - d_f h^2 \mathcal{D}^{1+\frac{d_f}{2}(2-\tau)} \gamma\left(-1-\frac{d_f}{2}(2-\tau), \frac{\mathcal{D}\Delta^{2/d_w}}{||\mathfrak{c}||^{2/d_f}}\right)\Delta^{\frac{2+d_f(2-\tau)}{d_w}}\Bigg\}.\end{aligned} \tag{3.14}$$

The expression above is the chief result describing the behaviour of an ensemble of random walk processes in an ensemble of open clusters near the critical point. A closer look at the equation above reveals some interesting observations. There is a natural time scale emerging for the set of all clusters which is given by $||\mathfrak{c}||^{2/d_f}/\mathcal{D}$. For any Δ^{2/d_w} significantly larger than this scale, disorder averaged TAMSD scales as a power of Δ, where the power is identified to be $\frac{2+d_f(2-\tau)}{d_w}$. Moreover, for time scales smaller than the aforementioned natural time scale, disorder averaged TAMSD has a lower bound (the first term in the curly bracket) whose value is identified by only knowing the geometrical properties of the smallest cluster $||\mathfrak{c}||$. Not surprisingly, thanks to the anisotropy average, disorder averaged TAMSD is independent of the measurement time T. In other words, one can compensate for the limitations in laboratories for generating long trajectories by sampling more percolation processes (sampling more random clusters).

The result above could be further simplified when the embedding Euclidean dimension is 2. This follows after exploiting the *hyperscaling* relation implied by the scaling theory. Hyperscaling relations are those that connect the critical exponents through the embedding Euclidean dimension d. One of such relations establishes an identity between the fractal dimension d_f and the Fisher exponent τ and is given by $\tau = d/d_f + 1$. By substituting this in Eq. (3.14) and recalling that $d_s/2 = d_f/d_w$, one arrives at the following

$$\widetilde{\left\langle \overline{\delta^2_{\mathcal{C}}(\Delta)} \right\rangle} = (\tau-2)||\mathfrak{c}||^{\tau-2}\Bigg\{-2h^2||\mathfrak{c}||^{2d_f+2-\tau} - d_f h^2 \mathcal{D}^{\frac{d_f}{2}} \gamma\left(-\frac{d_f}{2}, \frac{\mathcal{D}\Delta^{2/d_w}}{||\mathfrak{c}||^{2/d_f}}\right)\Delta^{\frac{d_s}{2}}\Bigg\}. \tag{3.15}$$

This result holds true if and only if $d = 2$ and imposes that, regardless of the underlying lattice structure, in two dimensions, disorder averaged TAMSD for large lag times grows as $\Delta^{d_s/2}$ since d_s, the spectral dimension, is the same for all two dimensional lattices [26, 40][2].

3.3 Normalised Variance of Disorder Averaged TAMSDs

One interesting measure to quantify how each anisotropy averaged TAMSDs are scattered around the mean is the *normalised variance*. It is tightly related to the *ergodicity breaking parameter* addressed and introduced in [52, 56–58] to measure the tendency of a stochastic process to its ergodic behaviour. For the sake of consistency and simplicity and to avoid

[2]This may hold true for the homogeneous class of fractals. Random fractals that are generated by the means of a Bernoulli percolation process belong to such a class. Sierpinski lattice (not to be confused with Sierpinski gasket) is a counter example of homogeneous fractals.

possible ambiguities, henceforth *normalised variance* is referred to as *ergodicity breaking parameter*. Denoted by EB it is defined as

$$\mathrm{EB}(\Delta, T) = \frac{\mathrm{Var}[X]}{\mathbb{E}[X]^2}, \tag{3.16}$$

where $\mathbb{E}[.]$ denotes the expectation value and Var[.] denotes the variance. The time dependent random variable X depends on Δ and T. Albeit it is historically defined for TAMSD, any variable X could be substituted in the equation above. To perceive better what does EB measure, consider the normal Brownian motion in two dimensions for which $\mathrm{EB} = \frac{4\Delta}{3T}$. This indicates that after sufficiently large measurement time T, EB asymptotically approaches zero; an indication that fluctuations due to finite measurement time T would vanish as T becomes larger and larger and ensemble averaged quantities coincide with their time averaged counterparts (this is the consequence of the fact that Brownian motion has stationary increments).

To quantify how scattered are the anisotropy averaged TAMSDs with respect to the cluster size distribution, invoke the expression given by Eq. (3.16) and deduce that

$$\mathrm{EB}(\Delta) = \frac{\widetilde{\left\langle\overline{\delta^2_{\mathcal{C}}(\Delta)}\right\rangle^2} - \widetilde{\left\langle\overline{\delta^2_{\mathcal{C}}(\Delta)}\right\rangle}^2}{\widetilde{\left\langle\overline{\delta^2_{\mathcal{C}}(\Delta)}\right\rangle}^2}. \tag{3.17}$$

Since anisotropy averaged TAMSDs are independent of the measurement time T, evidently EB does not have the dependency on T as well and it solely depends on the lag time Δ. To calculate EB, the second moment of the disorder averaged TAMSD must be calculated. The result is yielded by the evaluation of the following integral

$$\widetilde{\left\langle\overline{\delta^2_{\mathcal{C}}(\Delta)}\right\rangle^2} = \Xi \int_{||\mathrm{c}||}^{\infty} 4h^4 \left(1 - \exp\left[-\frac{\mathcal{D}\Delta^{2/d_w}}{||\mathcal{C}||^{2/d_f}}\right]\right)^2 ||\mathcal{C}||^{4/d_f + 1 - \tau} d\,||\mathcal{C}||, \tag{3.18}$$

which yields

$$\widetilde{\left\langle\overline{\delta^2_{\mathcal{C}}(\Delta)}\right\rangle^2} = (\tau-2)||\mathfrak{c}||^{\tau-2}\left\{\frac{4d_f h^4||\mathfrak{c}||^{4d_f+2-\tau}}{4+d_f(2-\tau)} - 4d_f h^4 \mathcal{D}^{2+\frac{d_f}{2}(2-\tau)}\right.$$
$$\times\left[-2^{1+\frac{d_f}{2}(2-\tau)}\gamma\left(-2-\frac{d_f}{2}(2-\tau), \frac{2\mathcal{D}\Delta^{2/d_w}}{||\mathfrak{c}||^{2/d_f}}\right)\right.$$
$$\left.\left.+\gamma\left(-2-\frac{d_f}{2}(2-\tau), \frac{\mathcal{D}\Delta^{2/d_w}}{||\mathfrak{c}||^{2/d_f}}\right)\right]\Delta^{\frac{4+d_f(2-\tau)}{d_w}}\right\}. \tag{3.19}$$

It holds equally true as for the first moment of the disorder averaged TAMSD that, when Δ^{2/d_w} is significantly larger than $||\mathfrak{c}||^{2/d_f}/\mathcal{D}$, the second moment of the disorder averaged TAMSD scales as a power of Δ where the power is given by $\frac{4+d_f(2-\tau)}{d_w}$.

It is evident that the full expression for EB is too cumbersome to be written in a full closed analytical form, nor would it provide much insight regarding its behaviour. Yet, there are two essential conclusions one could draw from the generic expression governing the behaviour of EB. Firstly, EB is independent of the measurement time T as both the first and second moments of disorder averaged TAMSD are independent of T. Secondly, for large lag times Δ, EB scales as

$$\text{EB} \approx A\Delta^{d_f(\tau-2)/d_w} - 1, \tag{3.20}$$

where A is a constant. From the first observation one concludes that for an ensemble of random walk processes in an ensemble of open clusters near the critical point, the fluctuation of time averaged quantities is independent of the measurement time T and it is persistent. The amplitude of these fluctuations depends solely on Δ and grows as a power of Δ. The second observation is that the exponent of Δ is smaller than unity, implying that the larger Δ becomes, EB becomes more insensitive to the alternation in the lag time[3]. Furthermore, by invoking the hyperscaling relation mentioned earlier, the exponent of Δ in the equation above can be rewritten as

$$\text{EB} \approx A\Delta^{(d-d_f)/d_w} - 1. \tag{3.21}$$

It is noteworthy to mention that the exponent of Δ in the equation above depends only on the topological factors. Moreover, observe that for large Δ the ratio of the second and first

[3] Δ cannot be arbitrarily large as it is bounded by T from above. Secondly, in order to have a plausible statistical inferences for the first moment of TAMSD, Δ must be smaller than $T/2$ [49]. Generally, for the $2m$ moment of TAMSD, Δ must be smaller than $T/2m$ where $m \in \mathbb{Z}^+$.

moments of disorder averaged TAMSD scales as $\sim \Delta^{2/d_w}$. As predicted by the dynamical scaling theory [18], this exponent is called the *gap exponent* which suggests that the ratio of different moments of a specific quantity concerning the independent variable scales as a power of that variable and the exponent is given by the gap exponent. In this case the gap exponent is $1/d_w$ and since the first and second moments of disorder averaged TAMSD measure the second and fourth power of the position, the ratio between them yields twice the gap exponent.

Interestingly, the exponent of Δ in Eq. (3.20) is the same as the one suggested in [59] to tell apart a fractional Brownian motion from a random walk process on an incipient infinite cluster. The authors therein, suggested a $\log\left(S(t)/\left\langle\overline{\delta^2_{\mathcal{C}^*}(\Delta)}\right\rangle^{d/2}\right)$ as a measure to distinguish the two processes. For a random walk process on an incipient infinite cluster near the critical point, this measure is found to be $(d-d_f)/d_w \neq 0$. Obviously, when the topology of the phase space is Euclidean, $d_f = 2$ and thus this measure would be zero; this would be the case for the fractional Brownian motion.

Chapter 4

Simulation Results

4.1 Simulation Parameters

As it was mentioned throughout the earlier chapters, the lattice considered for the simulations is the square lattice. To study the behaviour of disorder averaged MSD and TAMSD in an ensemble of open clusters near the critical point, the size of the lattice is set to 4096×4096 augmented by the periodic boundary condition.

The critical percolation density p_c for the square lattice is 0.59279 [20]. To fulfil the Kesten theorem [19] p is set to 0.6. For each realisation of a percolation process, each site of the lattice is assigned to be in the state of being unblocked with probability p or left in the state of being blocked with the probability $1 - p$. The centre of the lattice is then either occupied - in this case, the nearest open site is chosen for the ant to parachute - or it is open. In either case, the site on which the ant has parachuted may belong either to a finite size open cluster or to the incipient infinite one. An instance of an incipient infinite cluster is depicted in Fig. 4.1. For the illustration of a finite size open cluster refer to Fig. 2.2. For simulating random walk processes, the landed ant takes T steps which is referred to as the length of the trajectory and is set to 10^6. On each realisation of a percolation process, 5×10^2 random walk processes are simulated for numerically analysing the MSD and TAMSD. These trajectories are recorded for each realisation of a percolation process. In total 10^4 percolation processes were simulated and subsequently, MSDs and TAMSDs were averaged to yield the disorder averaged MSD and TAMSD for this ensemble of open clusters.

To analyse the exponent of Δ which governs the growth of disorder averaged TAMSD, it is necessary to numerically estimate the Fisher exponent τ, the fractal dimension d_f and the random walk dimension d_w. To extract the value of τ, for each realisation of a percolation process, the frequency of open clusters appearing with different sizes was counted. Afterwards, by recalling that near the critical point, scaling theory predicts that the

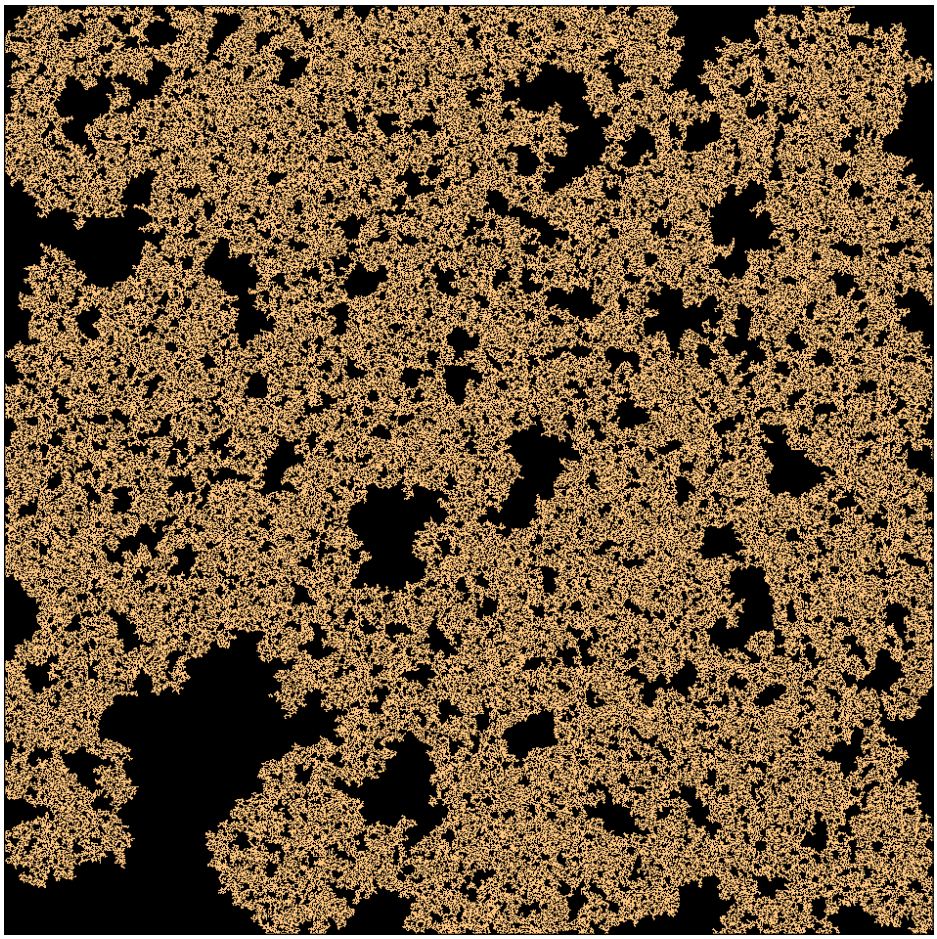

Figure 4.1 An instance of an incipient infinite cluster on a square lattice at $p = 0.6$, depicted in copper orange. The size of the lattice is 4096×4096. The other unblocked sites are not shown.

cluster size distribution should scale as a power law i.e. $||\mathcal{C}||^{-\tau}$, a fit was made to find the value of τ. In total, from 10^4 percolation processes τ was estimated to be 2.03 ± 0.01. Bear in mind that the theoretical value agreed upon is $187/91 \approx 2.05$ for the square lattice [20].

Estimating numerically the values of d_w and d_f is more cumbersome as one has to evaluate their values for the incipient infinite clusters. In order to identify the incipient infinite clusters for each percolation process, Hoshen-Kopelman algorithm [60] was used to first label each open cluster in a percolation process and then select the largest cluster in that realisation. Since labelling each site of a percolation process is computationally expensive, the size of the lattice in this particular case is set to 1024×1024. In total 7×10^2 of such clusters were extracted. The fractal dimension of these incipient infinite clusters were estimated by utilising the box-counting method [25]. The fractal dimension was found to be 1.9 ± 0.1 whereas theoretically it is $91/48 \approx 1.89$ [20]. On each one of these clusters 5×10^2 random walk processes were simulated to estimate d_w since it is predicted by the dynamical scaling theory that MSD scales as t^{2/d_w}. By this means, d_w was estimated to be 2.7 ± 0.1 compared to the widely accepted value 2.87 [33].

4.2 Phenomenological Analogy: Ornstein-Uhlenbeck Process and Random Walk Process on Finite Size Open Clusters

After extracting these essential exponents, the next step would be to justify the phenomenological conjecture raised regarding the analogy between the Ornstein-Uhlenbeck process and the random walk process on finite size open clusters. To conclude the validity of the expressions of MSD and TAMSD given in Eq. (2.21) and Eq. (3.6) respectively, the cluster shown in Fig. 4.2 was chosen. The centre of the mass of this cluster was found to be located at $(513.74, 518.20)$ along the x and y axes. The second power of the radius of gyration, R_g^2, was also found to be 346.33. Two initial conditions were considered to validate the aforementioned expressions for MSD and TAMSD (i) fixed initial condition where the ant always parachutes at the centre of the lattice (ii) the ant could parachute randomly and land on any of the available open sites within the boundary of the cluster with the probability 1/793 which refers to the equilibrium initial condition. In this scenario, 8×10^3 random walk processes were simulated for each one of the initial conditions. As the cluster is distinct from the topological structure of the incipient infinite clusters, the exponent d_f and d_w are different. By fitting the expression given in Eq. (2.21), it was found for this particular open cluster $d_f \approx 1.60$, $d_w \approx 2.44$, $\mathcal{D} \approx 1.60$ and $h \approx 0.29$. The numerical result and the

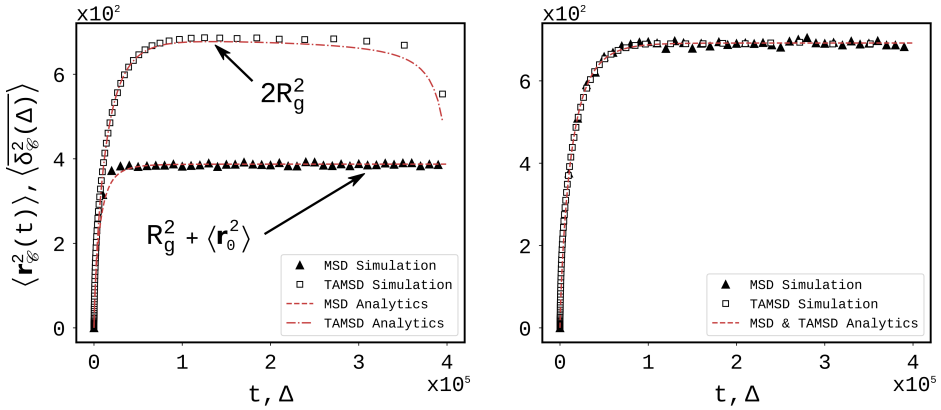

Figure 4.2 MSD and TAMSD for a cluster of size 793 depicted in Fig. 2.2. On the right side the initial condition is fixed to the centre of the lattice. Contrarily, on the left side the equilibrium initial condition is asserted. In total 8×10^3 random walk processes were simulated.

analytical expressions given by Eq. (2.21) and Eq. (3.6) for MSD and TAMSD respectively are demonstrated in Fig. 4.2 on the left panel. The visible gap between MSD and TAMSD for the case where the initial condition is fixed to the centre of the lattice originates from the way they are defined. On the other hand, this gap vanishes if the equilibrium initial condition is asserted which is evident on the right panel of Fig. 4.2. Under equilibrium initial condition, observe that Eq. (2.21) and Eq. (3.6) are simplified to Eq. (2.13) and Eq. (3.2) respectively and MSD and TAMSD coincide. All in all, this simulation result should justify the validity of the conjecture which implies the analogy between the Ornstein-Uhlenbeck and the random walk process on finite size open clusters [63].

4.2.1 Disorder Averaged TAMSD and the Ergodic Property of the Random Walk Process

For capturing the behaviour of the first and second moments of disorder averaged TAMSD, approximately 5×10^6 trajectories, which together encompasses 10^4 percolation processes and 5×10^2 random walk processes were simulated. Refer to Eq. (3.14) and Eq. (3.19) and observe that for large lag times Δ, the first and second moments of disorder averaged TAMSD grow as a power of Δ. Therefore, in logarithmic scale, their growth versus Δ must be linear which is evident in Fig. 4.3. The figure further demonstrates that the estimated values for d_f, d_w and τ have sufficient precision to estimate the exponent of Δ for the first and second moments of disorder averaged TAMSD such that one could grasp fully their linear trend in logarithmic scale. The lag time spans an interval between 10^2 to 10^5. The lower bound is to ensure that the ant has been given enough time to perceive the fractal structure of the cluster

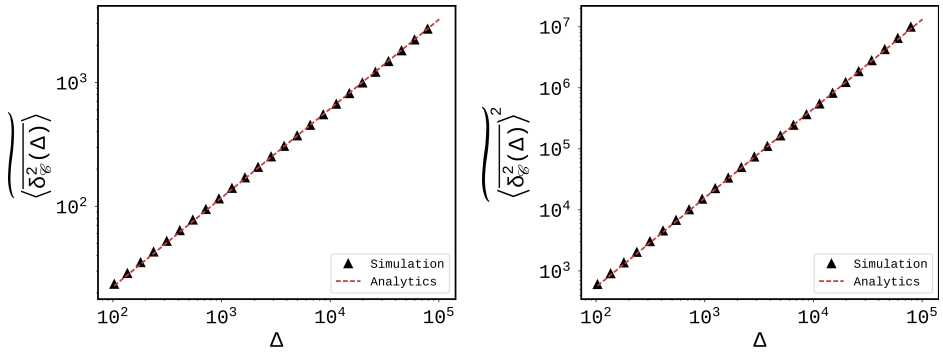

Figure 4.3 First moment (right) and second moment (left) of disorder averaged TAMSD in logarithmic scale. It is clear that their trend is linear with respect to Δ and the slope of the straight lines are $\frac{2+d_f(2-\tau)}{d_w}$ and $\frac{4+d_f(2-\tau)}{d_w}$ respectively.

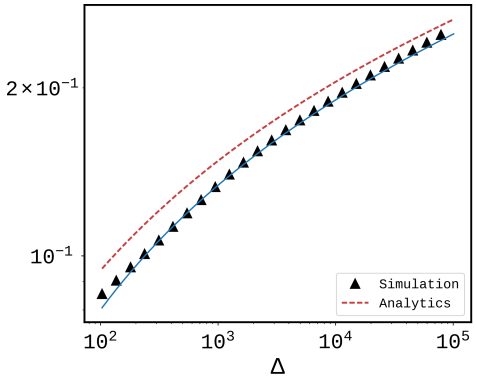

Figure 4.4 EB versus Δ in logarithmic scale. The simulation result is depicted by black triangles while the analytical result is achieved by substituting Eq. (3.14) and Eq. (3.19) into Eq. (3.17). There is a slight discrepancy between the two results. The blue solid line represents the analytical result shifted downwards. It indicates that the trend is captured correctly.

(recall that the cluster becomes homogeneous for length scales larger than the correlation length) and the upper bound is to limit Δ to values smaller than $T/2$ [49].

Furthermore, the behaviour of EB versus Δ is demonstrated in Fig. 4.4 in a logarithmic scale for the same time span of Δ. Therein, it is seen that there is a slight discrepancy between the analytical expression of EB, which is achieved by substituting Eq. (3.14) and Eq. (3.19) into Eq. (3.17), and the simulation result. The solid blue line represents exactly the analytical curve shown by the dashed red line but shifted downwards to lie on top of the simulation curve to demonstrate that the analytical expression governing the behaviour of EB in terms of Δ captures the trend plausibly. Further, notice that since the exponent of Δ is relatively small, the growth of EB is very slow. Moreover, to demonstrate that EB is independent of the measurement time T, Fig. 4.5 is provided to show that EB versus T

sharply drops to a terminal value which solely depends on Δ. One may infer that EB still depends on T but it has to be emphasised that, as mentioned earlier, sampling all the possible configurations of clusters with the same size is computationally impossible and further, note that the disorder averaged TAMSD is independent of T if the anisotropy average could have been taken over all possible configurations of clusters with the same size. Therefore, a slight dependence of EB on T is expected.

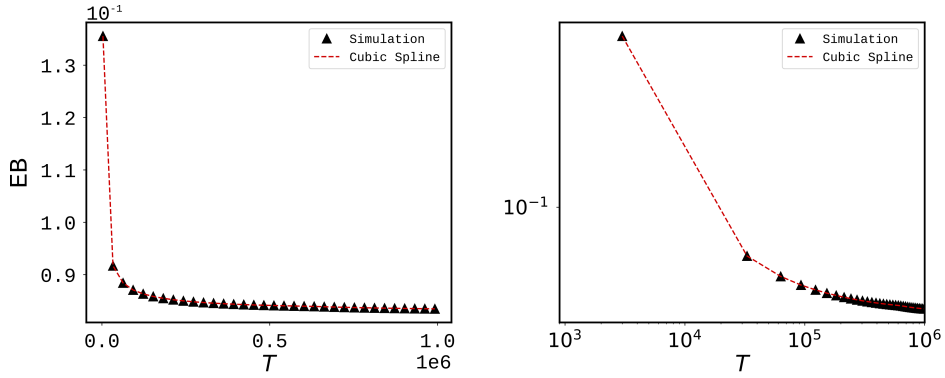

Figure 4.5 The dependence of EB on the measurement time T. The measurement time varies from 10^4 to 10^6 while the lag time Δ is set to 10^2. Observe the insignificant change in EB while T changes two orders of magnitude which implies that EB is insensitive to T or in other words independent of it. The variation in EB could be inferred as the imperfect anisotropy average. The dashed red line is a cubic spline interpolation of the simulation result.

Chapter 5

Conclusions

To address and provide an analytical solution for MSD and ensemble averaged TAMSD for the random walk process on finite-size open clusters near the critical point, a phenomenological analogy was made to the Ornstein-Uhlenbeck process. It was justified by the means of simulations that such an analogy is sound and sensible. To establish this analogy, space and time were rescaled according to the Hausdorff measure. The rescaling of space and time is dictated explicitly by the parameters d_f and d_w respectively. This approach is quite similar to the renormalisation approach bearing in mind that the measure suitable for space and time is the Hausdorff measure.

The possibility to establish such an analogy between the two processes, provides the means to model systems in which crowded environments impose a geometry constraint on the dynamics of the diffusive particles, which quite often, this topology exhibits a fractal nature. Nonetheless, it is worth mentioning that there are other models to address the motion of such particles in crowded environments, such as *fractional Brownian Motion* where the driving noise is modelled by the *fractional Gaussian Noise* [61, 39]. Interestingly, the *velocity autocorrelation function* of the random walk process in topologies modelled by the percolation process is cunningly similar to the case of fractional Brownian Motion [62]. It becomes even more interesting to remind the reader that the random walk process on finite-size open clusters is a Markov process, au contraire, fractional Brownian motion is non-Markovian. Also to explore further the difference between the two cases, the author tried to address some of the essential behaviours of the fractional Ornstein-Uhlenbeck process, which is addressed in [63].

Another interesting result which was central to this work, was the interplay and interconnection between the measurement time T and the anisotropic (topological) property of the finite size open clusters. Even though it was demonstrated that starting with a non-equilibrated initial condition, ensemble averaged TAMSD on a finite-size open cluster with a

certain size depends on the measurement time T, averaging over all other configurations of the clusters with the same size, the anisotropy averaged TAMSD does no longer depend on time T. In other words, for such an ensemble, anisotropy averaged TAMSD corresponds to an ergodic-stationary system. This property, as mentioned earlier is the sole consequence of translational invariance of the lattices. Due to this invariance, averaging over clusters of the same size but with different configurations resembles the equilibrium initial condition.

Though ergodic on the level of anisotropy average, another interesting observation was that the EB parameter had a persistent value, independent of the measurement time T. The finite value of EB depends on the power of the lag time Δ. The power of Δ given by $(d-d_f)/d_w$ indicates that this growth is very weak as the difference between the embedding Euclidean dimension d and the fractal dimension d_f is very small. Furthermore, rewriting this exponent in terms of the spectral dimension reveals that invariably of the underlying lattice structure, the persistent value of EB at a given Δ for a given d remains the same. The same behaviour was observed for the disorder averaged TAMSD but only in the case of $d = 2$, where the exponent of Δ solely depended on the spectral dimension d_s. This implies that disorder averaged TAMSD when $d = 2$, exhibits the same behaviour for large Δ regardless of the underlying lattice structure.

As a closure to this work, some remarks are mentioned that could possibly be guidelines for further research and investigations. The conjecture made to establish the phenomenological correspondence between the Ornstein-Uhlenbeck process and the random walk process in random fractal environments is of utmost importance. It must be either proven or rejected rigorously. If the conjecture holds true, it would provide a powerful tool to approach the ant in labyrinth problem. As the second remark, it should be noted that the random walk process in random environments is ubiquitous in biological realm [64]. The crowd which hinders the movement of the particles could be considered as a *dynamical percolation* model [65]. The author would like to claim audaciously that the model presented here, though static, corresponds to this dynamical model. This further, could be extended to a dynamical percolation model where the diffusion coefficient would be temporarily and spatially dependent. Such a model could be considered as a generalisation of diffusing diffusivity and random walk processes in heterogeneous environments [66]. Another interesting observation is the appearance of the least fluctuation in Eq. (3.14) and Eq. (3.19) which solely depends on the size of the smallest cluster in the continuum limit, d_f and τ. The physical significance of this least contribution remains unknown to the author and a further investigation on its meaning could provide insights into the behaviour of the random walk process within the smallest time and length scales of the process.

With these remarks I would conclude this chapter and dissertation with the hope it would lead to opening new chapters of research and investigations in this *labyrinth*.

Bibliography

[1] Pólya, G., 1921. *Über eine Aufgabe der Wahrscheinlichkeitsrechnung betreffend die Irrfahrt im Straßennetz*. Mathematische Annalen, 84(1), pp.149-160.

[2] Fischer, H., 2010. *A history of the central limit theorem: From classical to modern probability theory*. Springer Science & Business Media.

[3] Broadbent, S.R. and Hammersley, J.M., 1957, July. *Percolation processes: I. Crystals and mazes*. In Mathematical Proceedings of the Cambridge Philosophical Society (Vol. 53, No. 3, pp. 629-641). Cambridge University Press.

[4] Kohn, G.C., 2007. *Encyclopedia of plague and pestilence: from ancient times to the present*. Infobase Publishing.

[5] Gottfried, R.S., 2010. *Black Death*. Simon and Schuster.

[6] Britannica, E., 2019. *Black Death*. Encyclopædia Britannica Online.

[7] Lukowski, J. and Zawadzki, H., 2019. *A concise history of Poland*. Cambridge University Press.

[8] Davies, N., 2005. *God's Playground A History of Poland: Volume 1: The Origins to 1795 (Vol. 1)*. Oxford University Press.

[9] Sienkiewicz, W., 2006. *Ilustrowany atlas historii Polski*. Demart.

[10] Richardson, T.O., Christensen, K., Franks, N.R., Jensen, H.J. and Sendova-Franks, A.B., 2011. *Ants in a labyrinth: a statistical mechanics approach to the division of labour*. PLoS One, 6(4), p.e18416.

[11] Hufnagel, L., Brockmann, D. and Geisel, T., 2004. *Forecast and control of epidemics in a globalized world*. Proceedings of the National Academy of Sciences, 101(42), pp.15124-15129.

[12] Mardoukhi, A., Mardoukhi, Y., Hokka, M. and Kuokkala, V.T., 2017. *Effects of strain rate and surface cracks on the mechanical behaviour of Balmoral Red granite*. Philosophical Transactions of the Royal Society A: Mathematical, Physical and Engineering Sciences, 375(2085), p.20160179.

[13] Mardoukhi, A., Mardoukhi, Y., Hokka, M. and Kuokkala, V.T., 2017. *Effects of heat shock on the dynamic tensile behavior of granitic rocks*. Rock mechanics and rock engineering, 50(5), pp.1171-1182.

[14] Mardoukhi, A., Mardoukhi, Y., Hokka, H. and Kuokkala, V.T., (Submitted 2019). *Effects of test temperature and low temperature thermal cycling on the dynamic behavior of granitic rocks*. Rock Mechanics and Rock Engineering.

[15] Ilachinski, A., 2001. *Cellular automata: a discrete universe*. World Scientific Publishing Company.

[16] Fisher, M.E., 1961. *Critical probabilities for cluster size and percolation problems*. Journal of Mathematical Physics, 2(4), pp.620-627.

[17] Kesten, H., 1982. *Percolation theory for mathematicians (Vol. 423)*. Boston: Birkhäuser.

[18] Grimmett, G., 1999. *Percolation*. Springer, Berlin, Heidelberg.

[19] Kesten, H., 1986. *The incipient infinite cluster in two-dimensional percolation*. Probability theory and related fields, 73(3), pp.369-394.

[20] Stauffer, D. and Aharony, A., 2018. *Introduction to percolation theory*. Taylor & Francis.

[21] Fisher, M.E., 1967. *The theory of condensation and the critical point*. Physics Physique Fizika, 3(5), p.255.

[22] Cantor, G., 1883. *Über unendliche, lineare Punktmannichfaltigkeiten*. Mathematische Annalen, 21(4), pp.545-591.

[23] Halmos, P.R., 2013. *Measure Theory*. Springer.

[24] Edgar, G., 2007. *Measure, topology, and fractal geometry*. Springer Science & Business Media.

[25] Schroeder, M. and Herbich, M., 1996. *Fractals, chaos, power laws*. Pure and Applied Geophysics, 147(3), pp.601-601.

[26] Hughes, B.D, 1996. *Random Walks and Random Environments: Random Environments Volume 2*. Clarendon Press Oxford.

[27] de Gennes, P.G., 2009. *La percolation: un concept unificateur*. La Recherche, 7(72), pp. 919-927.

[28] Mandelbrot, B.B., 1983. *The fractal geometry of nature (Vol. 173, p. 51)*. New York: WH freeman.

[29] Mitescu, C.D. and Rossenq, J., 1983. *Diffusion on percolation clusters*. Percolation structures and processes. Annals of the Israel Physical Society, 5, pp.81-100.

[30] Mitescu, C.D. and Roussenq, J., 1976. *Une fourmi dans un labyrinth: diffusion dans un systeme de percolation*. Comptes Rendus de l'Académie des Sciences (Paris) A, 283, p.999.

[31] Majid, I., Ben-Avraham, D., Havlin, S. and Stanley, H. E., 1984. *Exact enumeration approach to random walks on percolation clusters in two dimensions*. Physical Review B, 30(3), p.1626.

[32] Jacobs, D. and Nakanishi, H., 1990. *Autocorrelation functions for discrete random walks on disordered lattice*. Physical Review A, 41(2), p.706.

[33] Havlin, S. and Ben-Avraham, D., 1987. *Diffusion in disordered media*. Advances in Physics, 36(6), pp.695-798.

[34] Saxton, M.J., 1994. *Anomalous diffusion due to obstacles: a Monte Carlo study*. Biophysical journal, 66(2), pp.394-401.

[35] Sahimi, M., 1993. *Fractal and superdiffusive transport and hydrodynamic dispersion in heterogeneous porous media*. Transport in porous Media, 13(1), pp.3-40.

[36] Chubynsky, M.V. and Slater, G.W., 2014. Diffusing diffusivity: a model for anomalous, yet Brownian, diffusion. Physical review letters, 113(9), p.098302.

[37] Sposini, V., Chechkin, A.V., Seno, F., Pagnini, G. and Metzler, R., 2018. *Random diffusivity from stochastic equations: comparison of two models for Brownian yet non-Gaussian diffusion*. New Journal of Physics, 20(4), p.043044.

[38] Cherstvy, A.G., Chechkin, A.V. and Metzler, R., 2013. *Anomalous diffusion and ergodicity breaking in heterogeneous diffusion processes*. New Journal of Physics, 15(8), p.083039.

[39] Sokolov, I.M., 2012. *Models of anomalous diffusion in crowded environments*. Soft Matter, 8(35), pp.9043-9052.

[40] Alexander, S. and Orbach, R., 1982. *Density of states on fractals:«fractons»*. Journal de Physique Lettres, 43(17), pp.625-631.

[41] Mitescu, C.D., Ottavi, H. and Roussenq, J., 1978, April. *Diffusion on percolation lattices: The labyrinthine ant*. In AIP Conference Proceedings (Vol. 40, No. 1, pp. 377-381). AIP.

[42] Pandey, R.B., 1984. *Classical diffusion, drift, and trapping in random percolating systems*. Physical Review B, 30(1), p.489.

[43] Fassnacht, J.C., 1983. Journal of Undergraduate Reports in Physics, 2, p.23.

[44] Giona, M. and Roman, H.E., 1992. *Fractional diffusion equation for transport phenomena in random media*. Physica A: Statistical Mechanics and its Applications, 185(1-4), pp.87-97.

[45] Metzler, R., Glöckle, W.G. and Nonnenmacher, T.F., 1994. *Fractional model equation for anomalous diffusion*. Physica A: Statistical Mechanics and its Applications, 211(1), pp.13-24.

[46] Rammal, R. and Toulouse, G., 1983. *Random walks on fractal structures and percolation clusters*. Journal de Physique Lettres, 44(1), pp.13-22.

[47] O'Shaughnessy, B. and Procaccia, I., 1985. *Analytical solutions for diffusion on fractal objects*. Physical Review Letters, 54(5), p.455.

[48] Uhlenbeck, G.E. and Ornstein, L.S., 1930. *On the theory of the Brownian motion*. Physical Review, 36(5), p.823.

[49] Cherstvy, A.G., Thapa, S., Mardoukhi, Y., Chechkin, A.V. and Metzler, R., 2018. *Time averages and their statistical variation for the Ornstein-Uhlenbeck process: Role of initial particle distributions and relaxation to stationarity*. Physical Review E, 98(2), p.022134.

[50] Hida, T. and Hitsuda, M., 1993. *Gaussian Processes*. American Mathematical Soc..

[51] Papoulis, A. and Pillai, S.U., 2002. *Probability, random variables, and stochastic processes*. Tata McGraw-Hill Education.

[52] Metzler, R., Jeon, J.H., Cherstvy, A.G. and Barkai, E., 2014. *Anomalous diffusion models and their properties: non-stationarity, non-ergodicity, and ageing at the centenary of single particle tracking*. Physical Chemistry Chemical Physics, 16(44), pp.24128-24164.

[53] Norregaard, K., Metzler, R., Ritter, C.M., Berg-Sørensen, K. and Oddershede, L.B., 2017. *Manipulation and motion of organelles and single molecules in living cells*. Chemical Reviews, 117(5), pp.4342-4375.

[54] Mardoukhi, Y., Chechkin, A. V., Metzler, R., 2020. *Spurious ergodicity breaking in normal and fractional Ornstein-Uhlenbeck process*. New Journal of Physics.

[55] Redelmeier, D.H., 1981. *Counting polyominoes: yet another attack*. Discrete Mathematics, 36(2), pp.191-203.

[56] Barkai, E., Garini, Y. and Metzler, R., 2012. *Strange kinetics of single molecules in living cells*. Physics Today, 65(8), p.29.

[57] Burov, S., Jeon, J.H., Metzler, R. and Barkai, E., 2011. *Single particle tracking in systems showing anomalous diffusion: the role of weak ergodicity breaking*. Physical Chemistry Chemical Physics, 13(5), pp.1800-1812.

[58] Rytov, S.M., Kravtsov, Y.A. and Tatarskii, V.I., 1988. *Principles of statistical radiophysics 2. Correlation theory of random processes*. Springer-Verlag, Berlin, FR Germany.

[59] Meroz, Y., Sokolov, I.M. and Klafter, J., 2013. *Test for determining a subdiffusive model in ergodic systems from single trajectories*. Physical Review Letters, 110(9), p.090601.

[60] Hoshen, J. and Kopelman, R., 1976. *Percolation and cluster distribution. I. Cluster multiple labeling technique and critical concentration algorithm*. Physical Review B, 14(8), p.3438.

[61] Mandelbrot, B.B. and Van Ness, J.W., 1968. *Fractional Brownian motions, fractional noises and applications*. SIAM review, 10(4), pp.422-437.

[62] Mardoukhi, Y., Jeon, J.H. and Metzler, R., 2015. *Geometry controlled anomalous diffusion in random fractal geometries: looking beyond the infinite cluster*. Physical Chemistry Chemical Physics, 17(44), pp.30134-30147.

[63] Mardoukhi Y, Chechkin A.V. and Metzler R., 2020. *Spurious weak ergodicity breaking in the case of (fractional) Ornstein-Uhlenbeck process*.

[64] Höfling, F. and Franosch, T., 2013. *Anomalous transport in the crowded world of biological cells*. Reports on Progress in Physics, 76(4), p.046602.

[65] Saxton, M.J., 1987. *Lateral diffusion in an archipelago*. The effect of mobile obstacles. Biophysical journal, 52(6), pp.989-997.

[66] Bassler, K.E., McCauley, J.L. and Gunaratne, G.H., 2007. *Nonstationary increments, scaling distributions, and variable diffusion processes in financial markets*. Proceedings of the National Academy of Sciences, 104(44), pp.17287-17290.

Appendix A

PCCP

PAPER

View Article Online
View Journal | View Issue

Cite this: *Phys. Chem. Chem. Phys.*, 2018, **20**, 20427

Fluctuations of random walks in critical random environments

Yousof Mardoukhi,[a] Jae-Hyung Jeon,[bc] Aleksei V. Chechkin[ad] and Ralf Metzler *[a]

Received 20th May 2018,
Accepted 19th July 2018

DOI: 10.1039/c8cp03212b

rsc.li/pccp

Percolation networks have been widely used in the description of porous media but are now found to be relevant to understand the motion of particles in cellular membranes or the nucleus of biological cells. Random walks on the infinite cluster at criticality of a percolation network are asymptotically ergodic. On any finite size cluster of the network stationarity is reached at finite times, depending on the cluster's size. Despite of this we here demonstrate by combination of analytical calculations and simulations that at criticality the disorder and cluster size average of the ensemble of clusters leads to a non-vanishing variance of the time averaged mean squared displacement, regardless of the measurement time. Fluctuations of this relevant experimental quantity due to the disorder average of such ensembles are thus persistent and non-negligible. The relevance of our results for single particle tracking analysis in complex and biological systems is discussed.

I. Introduction

Fractals gained immense popularity after Benoît Mandelbrot published his famous book *The fractal geometry of nature* which contains the by now iconic phrase "Clouds are not spheres, mountains are not cones, coastlines are not circles, and bark is not smooth, nor does lightning travel in a straight line".[1] Indeed, natural objects in most cases cannot be characterised by a single scale but exhibit some sort of statistical self-similarity. For instance, the length of the coastlines of Britain or Norway varies as function of the applied yard stick, and similar features appear on different scales.[1–3]

Yet self-similarity is typically not sufficient to describe natural objects, either. Thus, mathematical (deterministic) fractals such as the well known Cantor set (or the multi-dimensional Cantor dust),[4] the von Koch snowflake,[5] or the Sierpiński gasket[6] are composed of exact iterations of an identical operation, such as the removal of the middle third of a line segment for the Cantor set. The resulting symmetries appear artificial. To combine self-similarity—on a statistical, not deterministic sense—with the non-perfect structures of mountains or coastlines, random fractals have been considered such as landscapes created by (fractional) Brownian trajectories.[1,2]

A breakthrough in statistical physics was the conception of percolation theory originally proposed by Broadbent and Hammersley.[7] In the language of site percolation, imagine that on a discrete lattice each lattice site is occupied with probability p and left vacant otherwise. Nearest occupied (or vacant) neighbours on the lattice are considered to be connected, and each set of connected occupied (or vacant) lattice sites forms an occupied (or vacant) cluster. Here we will focus on open clusters $\mathcal{C}$ formed by vacant sites, their size being denoted by $\|\mathcal{C}\|$. Statistical analysis shows that there exists a critical percolation probability p_c at which an open cluster arises which spans the entire lattice, the incipient infinite percolation cluster. If we place a particle randomly on a vacant lattice site, it will either be on the infinite cluster or on any of the finite-sized open clusters. Notably, at criticality the percolation network is a random fractal whose Hausdorff dimension can be calculated for a number of lattice types and dimensions by renormalisation arguments.[2,8] On a square lattice, the centre of the current study, the fractal dimension is $d_f = 91/48$, while the distribution of cluster sizes is characterised by the Fisher exponent $\tau = 187/91$.[9] An example for a finite open cluster is shown in Fig. 1.

A random walker moving on fractal open clusters at criticality continuously encounters dead ends and has to pass through bottlenecks, a situation that was pictorially characterised as the motion of "an ant in a labyrinth" by de Gennes.[10] In fact the fractal nature of the geometric constraints effect a power-law growth of the mean squared displacement (MSD)

$$\langle |\mathbf{r}(t) - \mathbf{r}(0)|^2 \rangle \simeq t^{\alpha}, \qquad (1)$$

on the infinite cluster, where the scaling exponent can be expressed as $\alpha = 2/d_w$ in terms of the fractal walk dimension $d_w \approx 2.87$ on the square lattice.[9] The resulting value $\alpha \approx 0.70$ demonstrates that the motion of the random walker is subdiffusive,[11] that is, indicating less efficient spreading than on a fully accessible Euclidean lattice, for which $d_w = 2$ and thus the diffusion is normal, $\alpha = 1$.

[a] *Institute of Physics and Astronomy, University of Potsdam, 14476 Potsdam-Golm, Germany. E-mail: rmetzler@uni-potsdam.de*
[b] *School of Physics, Korea Institute for Advanced Study, Seoul 02455, Republic of Korea*
[c] *Department of Physics, Pohang University of Science and Technology, Pohang 37673, Republic of Korea*
[d] *Akhiezer Institute for Theoretical Physics, Kharkov 61108, Ukraine*

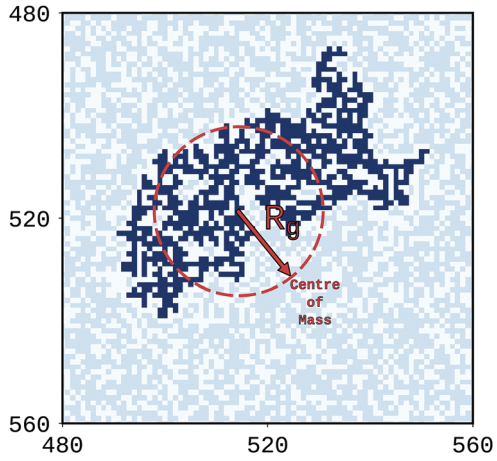

Fig. 1 Finite open cluster of size $\|\mathcal{C}\| = 793$ represented by Oxford blue on a square lattice at criticality. The arrow starts at the centre of mass of the cluster, and its tip defines a circle whose radius is the radius of gyration R_g of the open cluster. The co-ordinates show the lattice points of the entire network. Sky blue sites represent other vacant lattice sites, the powder blue (off-white) sites are occupied. Note that we consider the motion of particles on connected vacant lattice sites.

The emerging subdiffusion on a critical percolation network on a square lattice was demonstrated experimentally by field gradient NMR methods of water diffusion in thin plastic sheets, into which the cluster geometry was milled.[12,13]

Percolation networks have classically been used as model systems for porous media.[8,14,15] More recently single particle tracking experiments monitoring the motion of protein channels in membranes of living biological cells showed that these particles were confined to move on a fractal, percolation-like support.[16] From a modelling perspective percolation networks have been employed to characterise the diffusive motion of, typically submicron, tracer particles in the crowded cytoplasm of biological cells or in their membranes.[17–20] We also mention applications of studies on adaptive growth and branching of plants in heterogeneous environments[21] and to labour division in economic contexts.[22] While the majority of studies focuses on the motion on the infinite cluster, only relatively few consider the impact of the co-existing finite sized clusters.[8,23]

To analyse particle tracking experiments or simulations involving percolation networks at criticality, it is important to have available precise analytical tools to quantify the observed dynamics. Typically, single particle trajectories are evaluated in terms of time averaged mean squared displacements (TAMSDs),[24–28] see eqn (3) below. The prime question in this context is whether the information encoded in the TAMSD is equivalent to that of the ensemble MSD (1) or not. This question is related to ergodicity in the weaker sense that sufficiently long time averages of a physical quantity are equivalent to the corresponding ensemble average.[24,25,29]

Non-stationary anomalous diffusion processes such as the famed continuous time random walk, in which successive motion events are interspersed with immobile periods with scale-free distribution of waiting times[15,25,30] or heterogeneous diffusion processes with space-dependent mobility[31–33] are inherently non-ergodic and exhibit fundamental differences between the MSD and TAMSD,[24,25,34–36] which was indeed shown experimentally.[16,37–39] They also exhibit pronounced ageing effects.[16,25,38–43] Conversely, processes dominated by viscoelastic effects driven by long-range correlated fractional Gaussian noise—stationary in their increments—are ergodic and do not age.[16,37,44–48]

Random walks on the infinite percolation cluster were demonstrated to be ergodic.[49,50] Moreover, it was shown that the increment correlation function for diffusion on a critical square percolation network is indistinguishable from the one for (overdamped) viscoelastic diffusion.[49,50] In our previous analysis[51] we went one step further and took all, incipient infinite and the full ensemble of finite clusters into account. We demonstrated that below, above, as well as at the percolation threshold the average over TAMSDs over a large set of particles indeed converged to the MSD. However, we also showed that due to the random seeding, the TAMSDs of those particles diffusing on finite clusters were eventually dominated by the finite size, and thus intrinsically different from each other. As a particle seeded on a finite cluster cannot jump to another cluster this is some form of strong ergodicity breaking in the sense that the phase space is topologically disconnected. Only the disorder average including the full ensemble of geometries restores ergodicity on this level. In particular, we obtained that even after both ensemble and disorder averages were taken, the amplitude fluctuations of the TAMSD quantified by the ergodicity breaking parameter were characterised by a finite variance.

Here we further analyse the fluctuations of the TAMSD on a critical percolation network. We carefully separate the behaviour of the trajectory on a single cluster, from that of the disorder averaged dynamics. In what follows, after defining the fundamental quantities of MSD and TAMSD on a given topology we conjecture the analogy of the current problem with the Ornstein–Uhlenbeck process. This formal correspondence is then used to calculate the ensemble averages of the MSD and TAMSD. In a further step we then take the disorder average, based on which we quantify the amplitude fluctuations of the TAMSD. Our results are put into perspective in the Discussion section, particular, with respect to single particle tracking analysis in complex and biological systems, before collecting some details in the Methods section.

II. Results

A. Random walks and percolation

For an ensemble of random walkers on a given open cluster $\mathcal{C}$ of the percolation network the MSD is defined as

$$\langle \mathbf{r}_{\mathcal{C}}^2(t)\rangle = \left\langle |\mathbf{r}(t) - \mathbf{r}(0)|^2 \right\rangle, \qquad (2)$$

where the angular brackets indicate an ensemble average over random walks sampled over that specific cluster. The TAMSD for the same ensemble of random walks on this cluster is defined as[24,25,34]

$$\left\langle \overline{\delta c^2(\Delta)} \right\rangle = \frac{1}{T-\Delta}\int_0^{T-\Delta} \left\langle |\mathbf{r}(t+\Delta) - \mathbf{r}(t)|^2 \right\rangle \mathrm{d}t, \qquad (3)$$

where T is the overall length of the measured time series and Δ is called the lag time.

An essential complication for evaluating these quantities is the lack of full knowledge of the probability density function for diffusion on random fractals. Despite scaling arguments based on the radial distribution of the mass of the fractal support[52] or attempts to reproduce the scaling behaviour of the probability density function in terms of fractional diffusion equations,[53,54] this question has remained elusive. A more promising approach is based on dynamical scaling theories, which address questions on the scaling behaviour of statistical quantities of random walks averaged over all clusters, relating them to the geometrical exponents of percolation clusters.[9,55] This is basically the approach chosen here to study random walk processes for the full ensemble of clusters at criticality.

Assume an ensemble of open clusters onto which random walkers parachute. Randomly, they may either land on the incipient infinite cluster or on a finite-sized open cluster. Denote the linear size explored by a random walker after infinitely many steps by R_∞, then the MSD assumes the value,[55,56]

$$\frac{R_\infty^2 - \langle \mathbf{r}_\mathcal{C}^2(t)\rangle}{R_\infty^2} \sim \exp\left(-\left[\frac{t}{\chi}\right]^w\right). \tag{4}$$

Here w is a positive definite exponent which depends on the underlying topology only, and χ is a characteristic time needed by the random walkers such that they will eventually feel the effective linear size of the underlying cluster $\mathcal{C}$.[55] Note that when the underlying cluster tends to be the incipient infinite cluster, then $\chi \to \infty$ and one observes that $\langle \mathbf{r}_\mathcal{C}^2(t)\rangle \simeq t^w$.

In their work Mitescu *et al.* originally assumed w to be unity,[57] but later simulation studies of Fassnacht and Pandey revealed a value smaller than unity in three dimension.[58,59] While the general form of eqn (4) was qualitatively confirmed by simulations, numerical analyses performed by Jacobs *et al.*, based on transition probability matrix formalism, estimated w to be $2/d_w$.[56]

For a finite size cluster $\mathcal{C}$ it is evident that the MSD or TAMSD will eventually reach a saturation plateau, the time needed to reach the plateau depending on the size of the cluster. For such a cluster, at saturation the MSD, averaged over equilibrium initial positions with equal weight $1/\|\mathcal{C}\|$ is twice the squared of the radius of gyration R_g of that cluster.[60,61] Hence we rewrite eqn (4) in the form

$$\langle \mathbf{r}_\mathcal{C}^2(t)\rangle = 2R_g^2\left(1 - \exp\left[-\left(\frac{t}{\chi}\right)^{2/d_w}\right]\right). \tag{5}$$

Here the subscript eq. refers to the equilibrium initial condition. Due to the time invariance at equilibrium the TAMSD $\left\langle \overline{\delta_\mathcal{C}^2(\Delta)}\right\rangle$ is identical to $\langle \mathbf{r}_\mathcal{C}^2(t)\rangle$, with time t replaced by lag time Δ,

$$\left\langle \overline{\delta_\mathcal{C}^2(\Delta)}\right\rangle = 2R_g^2\left(1 - \exp\left[-\left(\frac{\Delta}{\chi}\right)^{2/d_w}\right]\right). \tag{6}$$

Analogy between Ornstein–Uhlenbeck process and random walks on finite size open clusters. However, what happens when the initial seeding of random walkers is different from the above-assumed equilibrium initial condition? This situation will be of relevance for many real systems whose experimental preparation coincides with the start of the measurement at $t = 0$. For instance, in a porous matrix a single colloidal particle is released at a specific point on the cluster, a drop of a tracer chemical trickles down into a soil aquifer from above, or a neuronal synapse sends a signal pulse in a neural network. In our simulations delineated below we adopt this non-equilibrium stance and always seed the random walker at the centre of the lattice. We therefore need to seek a new set of equations for the MSD and TAMSD to address non-equilibrium initial conditions, the purpose of this section. We achieve this by using the analogy between the generic Ornstein–Uhlenbeck processes and random walks on finite size open clusters based on the universal form of eqn (4).

As discussed earlier the precise form of the probability density function for diffusion on a random fractal is unknown. That makes it arduous to approach random walk processes on finite size open clusters by standard methods such as solving the stochastic differential equation associated to the processes and its corresponding Fokker–Planck equation with appropriate boundary conditions, or to employ path integral methods. Looking at eqn (4) one may note that such a form for the MSD for $w = 1$ corresponds to the relaxation dynamics of a random walker in the Ornstein–Uhlenbeck process (diffusion in an harmonic potential).[62,63]

As addressed in ref. 63 the Langevin equation for the Ornstein–Uhlenbeck process in two dimensions with positive parameters χ and σ and a randomly distributed initial condition $\mathbf{r}_0$ in the presence of the white and zero-mean Gaussian noise $\boldsymbol{\xi}(t)$ is given by

$$\frac{\mathrm{d}\mathbf{r}}{\mathrm{d}t} = -\frac{\mathbf{r}}{\chi} + \sigma\boldsymbol{\xi}(t), \quad \langle \xi_i(t_1)\xi_j(t_2)\rangle = \delta_{ij}\delta(t_1 - t_2); \quad i,j \in \{x,y\}. \tag{7}$$

For such processes the MSD and TAMSD are found to be[63]

$$\langle \mathbf{r}_{\mathrm{OU}}^2(t)\rangle = \langle \mathbf{r}_0^2\rangle\left(1 - \exp\left[-\left(\frac{t}{\chi}\right)\right]\right)^2 + \chi\sigma^2\left(1 - \exp\left[-2\left(\frac{t}{\chi}\right)\right]\right), \tag{8a}$$

$$\left\langle \overline{\delta_{\mathrm{OU}}^2(\Delta)}\right\rangle = 2\chi\sigma^2\left(1 - \exp\left[-\left(\frac{\Delta}{\chi}\right)\right]\right) + \left(\langle \mathbf{r}_0^2\rangle - \chi\sigma^2\right) \times \left(1 - \exp\left[-\left(\frac{\Delta}{\chi}\right)\right]\right)^2 \left(\frac{1 - \exp\left[-2\left(\frac{T-\Delta}{\chi}\right)\right]}{2\left(\frac{T-\Delta}{\chi}\right)}\right). \tag{8b}$$

To identify the similarity between Ornstein–Uhlenbeck processes and random walks on finite size open clusters, it is sufficient to consider the equilibrium initial condition for $\mathbf{r}_0$, which implies $\langle \mathbf{r}_0^2\rangle = \chi\sigma^2$.[63] Such a condition then yields

$$\langle \mathbf{r}_{\mathrm{OU}}^2(t)\rangle_{\mathrm{eq.}} = 2\chi\sigma^2\left(1 - \exp\left[-\left(\frac{t}{\chi}\right)\right]\right), \tag{9a}$$

$$\left\langle \overline{\delta_{\mathrm{OU}}{}^2(\Delta)} \right\rangle_{\mathrm{eq.}} = 2\chi\sigma^2\left(1-\exp\left[-\left(\frac{\Delta}{\chi}\right)\right]\right). \tag{9b}$$

One then can immediately relate this set of equations to expressions (5) and (6). Additionally, eqn (8a) and (8b) provide a clear clue to conjecture a new set of relations for the MSD and TAMSD for random walks in finite random environments when the equilibrium initial condition is not satisfied. Thus assume that a random walk on a cluster $\mathcal{C}$ with gyration radius R_g and characteristic time χ is analogous to an Ornstein–Uhlenbeck process with parameters χ and σ, in which $R_g{}^2 = \chi\sigma^2$ and time t is rescaled as t^{2/d_w}. Thus we arrive at the following expressions,

$$\begin{aligned}\left\langle \mathbf{r}_{\mathcal{C}}{}^2(t)\right\rangle = \left\langle \mathbf{r}_0{}^2\right\rangle &\left(1-\exp\left[-\left(\frac{t}{\chi}\right)^{2/d_w}\right]\right)^2 \\ &+ R_g{}^2\left(1-\exp\left[-2\left(\frac{t}{\chi}\right)^{2/d_w}\right]\right),\end{aligned} \tag{10a}$$

$$\begin{aligned}\left\langle \overline{\delta_{\mathcal{C}}{}^2(\Delta)}\right\rangle = {} & 2R_g{}^2\left(1-\exp\left[-\left(\frac{\Delta}{\chi}\right)^{2/d_w}\right]\right) \\ & + \left(\left\langle \mathbf{r}_0{}^2\right\rangle - R_g{}^2\right)\left(1-\exp\left[-\left(\frac{\Delta}{\chi}\right)^{2/d_w}\right]\right)^2 \\ & \times\left(\frac{1-\exp\left[-2\left(\frac{T-\Delta}{\chi}\right)^{2/d_w}\right]}{2\left(\frac{T-\Delta}{\chi}\right)^{2/d_w}}\right).\end{aligned} \tag{10b}$$

We now show that expressions (10), deduced from analogy with the Ornstein–Uhlenbeck process, are consistent with the known limiting behaviours of both the MSD and the TAMSD. Below we will also demonstrate good agreement with simulations results. In the limit of short times $t \ll \chi$ we recover the expected free anomalous diffusion behaviour $\left\langle \mathbf{r}_{\mathcal{C}}{}^2(t)\right\rangle \simeq t^{2/d_w}$ of the MSD, while for $\Delta \ll \chi$ the TAMSD becomes $\left\langle \overline{\delta_{\mathcal{C}}{}^2(\Delta)}\right\rangle \simeq \Delta^{2/d_w}$. Conversely, in the long time limit t, $T \to \infty$, eqn (10) have the following asymptotes,

$$\lim_{t\to\infty}\left\langle \mathbf{r}_{\mathcal{C}}{}^2(t)\right\rangle = \left\langle \mathbf{r}_0{}^2\right\rangle + R_g{}^2 \tag{11a}$$

$$\lim_{T\to\infty}\left\langle \overline{\delta_{\mathcal{C}}{}^2(\Delta)}\right\rangle = \begin{cases} 2R_g{}^2, & \text{if} \quad \chi < \Delta \ll T \\ \left\langle \mathbf{r}_0{}^2\right\rangle + R_g{}^2, & \text{if} \quad \Delta \to T \end{cases}. \tag{11b}$$

This limit indeed produces the expected values.

These asymptotes can alternatively be derived by invoking the generic definition of the MSD and TAMSD given by relations (2) and (3). To demonstrate this for the TAMSD consider a finite size open cluster $\mathcal{C}$. According to eqn (3) for lag times $\Delta \to T$ the TAMSD saturates at a certain level, assuming that $\chi \ll T$, which guarantees that the random walker would have enough time to visit each site of the cluster equally. Then

$$\begin{aligned}\lim_{\Delta\to T}\left\langle \overline{\delta_{\mathcal{C}}{}^2(\Delta)}\right\rangle &= \lim_{\Delta\to T}\frac{1}{T-\Delta}\int_0^{T-\Delta}\left\langle \left|\mathbf{r}(t+\Delta)-\mathbf{r}(t)\right|^2\right\rangle \mathrm{d}t \\ &= \left\langle \left|\mathbf{r}(T)-\mathbf{r}(0)\right|^2\right\rangle.\end{aligned}$$

In the centre of mass co-ordinate system, used here for convenience,

$$\left\langle \left|\mathbf{r}(T)-\mathbf{r}(0)\right|^2\right\rangle = \left\langle \left|\mathbf{r}(T)-\mathbf{r}_{\mathcal{C},\mathrm{cm}}+\mathbf{r}_{\mathcal{C},\mathrm{cm}}-\mathbf{r}(0)\right|^2\right\rangle, \tag{12}$$

where $\mathbf{r}_{\mathcal{C},\mathrm{cm}} = \frac{1}{\|\mathcal{C}\|}\sum_{s=1}^{\|\mathcal{C}\|}\mathbf{r}_{\mathcal{C},s}$ is the centre of mass of the finite size open cluster. Here $\mathbf{r}_{\mathcal{C},s}$ represents the spatial position of site s in the cluster $\mathcal{C}$. In the limit $N \to \infty$, where N is the number of random walk processes on a given cluster, due to the finite cluster size visiting any site $s_j \in \mathcal{C}$ becomes equally probable. Thus $\mathbf{r}(T)$ would be any $\mathbf{r}_{\mathcal{C},s}$, where the probability of visitation is $1/\|\mathcal{C}\|$. Therefore the ensemble average would be equivalent to taking an average over different cluster sites. Hence,

$$\begin{aligned}\lim_{\Delta\to T}\left\langle \overline{\delta_{\mathcal{C}}{}^2(\Delta)}\right\rangle = \frac{1}{\|\mathcal{C}\|}\sum_{s=1}^{\|\mathcal{C}\|}\big[&\left|\mathbf{r}_{\mathcal{C},s}-\mathbf{r}_{\mathcal{C},\mathrm{cm}}\right|^2+\left|\mathbf{r}_{\mathcal{C},\mathrm{cm}}-\mathbf{r}(0)\right|^2 \\ &+2\left(\mathbf{r}_{\mathcal{C},s}-\mathbf{r}_{\mathcal{C},\mathrm{cm}}\right)\cdot\left(\mathbf{r}_{\mathcal{C},\mathrm{cm}}-\mathbf{r}(0)\right)\big].\end{aligned} \tag{13}$$

In the equation above, the square root of the first term is simply the definition of the radius of gyration R_g for a given cluster $\mathcal{C}$ and the third term vanishes. This yields

$$\left\langle \overline{\delta_{\mathcal{C}}{}^2(\Delta)}\right\rangle = R_g{}^2 + \left\langle \left|\mathbf{r}_{\mathcal{C},\mathrm{cm}}-\mathbf{r}(0)\right|^2\right\rangle, \quad \Delta \to T, \tag{14}$$

where $\left|\mathbf{r}(0)-\mathbf{r}_{\mathcal{C},\mathrm{cm}}\right|^2$ (equivalent to $\mathbf{r}_0{}^2$ in eqn (11a)) is a random variable which depends on the initial position of the random walkers.

In the current form of eqn (10a) and (10b) the dependence of χ and R_g on $\mathcal{C}$ is not evident. To find the relation between these quantities, dynamical scaling theory is exploited. The time which is required by a random walker to reach the linear length scale of a cluster $\mathcal{C}$ can be approximated as follows: on length scales smaller than R_g the boundaries of the underlying finite cluster can not yet be reached by the walker, and thus $\left\langle \mathbf{r}_{\mathcal{C}}{}^2(t)\right\rangle = Dt^{2/d_w}$, where D is the anomalous diffusion coefficient.[8,55] Therefore the typical time scale χ required for a random walker to reach a length scale comparable to $\sqrt{2R_g{}^2}$, scales as $\chi = \left(\frac{2}{D}\right)^{d_w/2}R_g^{d_w}$. From this scaling relation and the scaling relation for the mass distribution of fractal objects, $R_g^{d_f} = h^{d_f}\|\mathcal{C}\|$ (where h is a dimensional constant),[9] on the time

scale χ one attains $\chi^{2/d_w} = \frac{2h^2}{D}\|\mathcal{C}\|^{2/d_f}$. Including this relation into eqn (10a) and (10b), we obtain the modified relations

$$\langle \mathbf{r}_{\mathcal{C}}^2(t)\rangle = \langle \mathbf{r}_0^2\rangle\left(1-\exp\left[-\frac{\mathscr{D}t^{2/d_w}}{\|\mathcal{C}\|^{2/d_f}}\right]\right)^2 + h^2\|\mathcal{C}\|^{2/d_f}\left(1-\exp\left[-\frac{2\mathscr{D}t^{2/d_w}}{\|\mathcal{C}\|^{2/d_f}}\right]\right), \quad (15a)$$

$$\left\langle\overline{\delta_{\mathcal{C}}^2(\Delta)}\right\rangle = 2h^2\|\mathcal{C}\|^{2/d_f}\left(1-\exp\left[-\frac{\mathscr{D}\Delta^{2/d_w}}{\|\mathcal{C}\|^{2/d_f}}\right]\right) + \left(\langle \mathbf{r}_0^2\rangle - h^2\|\mathcal{C}\|^{2/d_f}\right)\left(1-\exp\left[-\frac{\mathscr{D}\Delta^{2/d_w}}{\|\mathcal{C}\|^{2/d_f}}\right]\right)^2 \times\left(\frac{1-\exp\left[-2\mathscr{D}\frac{(T-\Delta)^{2/d_w}}{\|\mathcal{C}\|^{2/d_f}}\right]}{2\mathscr{D}\frac{(T-\Delta)^{2/d_w}}{\|\mathcal{C}\|^{2/d_f}}}\right). \quad (15b)$$

Here we introduced $\mathscr{D} = D/(2h^2)$. For validation of this approach based on the analogy with the Ornstein–Uhlenbeck process, by extensive Monte Carlo simulations we refer to Fig. 5.

B. Disorder average: anisotropy and cluster size average

In an ensemble of open clusters, it is not only the size of the clusters that matters but also their topological structure and the distribution of their mass around their centre of mass. These two factors together define the disorder average. Indeed, averaging over the anisotropy of same-sized open clusters yields a result, which is equivalent to averaging over the randomly distributed initial position of the random walks, producing an equilibrium situation. This observation simplifies the rest of the calculations regarding the cluster size average over the ensemble of finite size open clusters.

Anisotropy average of the TAMSD over all possible same-sized clusters. We take a disorder average of the TAMSD in two steps. First we average over all possible clusters of the same size, then we average over the distribution of cluster sizes. In the first step we note that averaging over $\langle \mathbf{r}_0^2\rangle$ yields exactly R_g^2, which is intuitively clear (see also the Methods section). The TAMSD (15b) after anisotropy averaging returns expression (6) corresponding to equilibrium initial conditions.

It is interesting to observe that due to this averaging the T dependence of $\left\langle\overline{\delta_{\mathcal{C}}^2(\Delta)}\right\rangle$ disappears. Indeed, this is not surprising as the average over all clusters of the same size is equivalent to the averaging over the equilibrium initial condition corresponding to the specific system. To clarify the equivalence between these two, recall that the equilibrium initial condition for a cluster $\mathcal{C}$ is realised once the random walk process is initiated randomly with equal weight $1/\|\mathcal{C}\|$ at any possible site in $\mathcal{C}$. Now, instead of choosing the initial position randomly, shift the underlying lattice and choose randomly the centre of the lattice within the cluster $\mathcal{C}$ while keeping the initial position of the random walk at the centre of the lattice. Since the lattice remains the same under translational transformations the new configuration is equal to realisations of different clusters with the same size and shape. Therefore one observes that randomly choosing the initial positions of random walkers is equivalent to randomly choosing the centre of the lattice within the cluster by shifting the underlying lattice. In the Methods section a more formal proof is provided for the anisotropy average over clusters of size three. There it will be demonstrated further that in the simulations this claim also holds true.

Cluster size average of $\left\langle\overline{\delta_{\mathcal{C}}^2(\Delta)}\right\rangle$. For the ensemble of finite size open clusters $\{\mathcal{C}\}$ the cluster size average of $\left\langle\overline{\delta_{\mathcal{C}}^2(\Delta)}\right\rangle$ (eqn (6)) is given by

$$\left\langle\widetilde{\overline{\delta_{\mathcal{C}}^2(\Delta)}}\right\rangle = \sum_{\{\mathcal{C}\}}\mathcal{P}(\|\mathcal{C}\|)\left\langle\overline{\delta_{\mathcal{C}}^2(\Delta)}\right\rangle, \quad (16)$$

where $\mathcal{P}(\|\mathcal{C}\|)$ is the probability for a random walker to land on cluster $\mathcal{C}$. This probability is simply given by the probability of the appearance of such a cluster in a specific realisation of the underlying percolation network, multiplied by the probability that the centre of the lattice would belong to this cluster. The probability distribution for the cluster $\mathcal{C}$ to appear in a specific lattice realisation at the critical percolation density is $\simeq \|\mathcal{C}\|^{-\tau}$, where τ is a scaling exponent called the Fisher exponent.[9] Therefore, the probability that the centre of the lattice would belong to this cluster scales as $\|\mathcal{C}\|^{1-\tau}$,[8] such that

$$\left\langle\widetilde{\overline{\delta_{\mathcal{C}}^2(\Delta)}}\right\rangle = \Xi\sum_{\|\mathcal{C}\|=1}^{\infty}\left\langle\overline{\delta_{\mathcal{C}}^2(\Delta)}\right\rangle\|\mathcal{C}\|^{1-\tau}. \quad (17)$$

Here Ξ is a normalisation constant. Taking the continuum limit of the summation (see ref. 9, eqn (21)) and substituting relation (6), the evaluation of the integral yields the cluster size average of $\left\langle\overline{\delta_{\mathcal{C}}^2(\Delta)}\right\rangle$,

$$\left\langle\widetilde{\overline{\delta_{\mathcal{C}}^2(\Delta)}}\right\rangle = \Xi\int_{\|\mathfrak{c}\|}^{\infty}2h^2\left(1-\exp\left[-\frac{\mathscr{D}\Delta^{2/d_w}}{\|\mathcal{C}\|^{2/d_f}}\right]\right)\|\mathcal{C}\|^{2/d_f+1-\tau}d\|\mathcal{C}\|, \quad (18)$$

where $\|\mathfrak{c}\|$ is the smallest cluster in $\{\mathcal{C}\}$. Substituting the argument of the exponential function we evaluate the integral, producing

$$\left\langle\widetilde{\overline{\delta_{\mathcal{C}}^2(\Delta)}}\right\rangle = (\tau-2)\|\mathfrak{c}\|^{\tau-2}\left\{-\frac{2d_fh^2}{2+d_f(2-\tau)}\|\mathfrak{c}\|^{2d_f+2-\tau} - d_fh^2\mathscr{D}^{1+\frac{d_f}{2}(2-\tau)}\gamma\left(-1-\frac{d_f}{2}(2-\tau),\frac{\mathscr{D}\Delta^{2/d_w}}{\|\mathfrak{c}\|^{2/d_f}}\right)\Delta^{\frac{2+d_f(2-\tau)}{d_w}}\right\}, \quad (19)$$

where $\gamma(a,x)$ represents the lower incomplete gamma function.

Normalised variance of $\left\langle\overline{\delta_{\mathcal{C}}^2(\Delta)}\right\rangle$. To evaluate the variance of the TAMSD we need to evaluate the cluster size average of $\left\langle\overline{\delta_{\mathcal{C}}^2(\Delta)}\right\rangle^2$. After following the same procedure carried out for

$\left\langle\widetilde{\overline{\delta c^2(\Delta)}}\right\rangle$, we find

$$\widetilde{\left\langle\overline{\delta c^2(\Delta)}\right\rangle^2} = (\tau-2)\|\mathfrak{c}\|^{\tau-2}\left\{-\frac{4d_f h^4\|\mathfrak{c}\|^{4d_f+2-\tau}}{4+d_f(2-\tau)} - 4d_f h^4 \mathscr{D}^{2+\frac{d_f}{2}(2-\tau)} \times\left[-2^{1+\frac{d_f}{2}(2-\tau)}\gamma\left(-2-\frac{d_f}{2}(2-\tau),\frac{2\mathscr{D}\Delta^{2/d_w}}{\|\mathfrak{c}\|^{2/d_f}}\right) + \gamma\left(-2-\frac{d_f}{2}(2-\tau),\frac{\mathscr{D}\Delta^{2/d_w}}{\|\mathfrak{c}\|^{2/d_f}}\right)\right]\Delta^{\frac{4+d_f(2-\tau)}{d_w}}\right\}. \quad (20)$$

In eqn (18) we might set the lower limit of the integral to zero, $\|\mathfrak{c}\| = 0$, as the integral converges. We however find that taking into account the existence of the smallest cluster size $\|\mathfrak{c}\|$ is necessary to grasp the numerical results below. When fitting eqn (19) and (20) to the simulation data with $\|\mathfrak{c}\| = 0$, the remaining two free parameters h and D were found to be insufficient to provide sufficiently good descriptions for $\left\langle\widetilde{\overline{\delta c^2(\Delta)}}\right\rangle$ and $\widetilde{\left\langle\overline{\delta c^2(\Delta)}\right\rangle^2}$. Once a smallest cluster size is considered (we here choose the physical value $\|\mathfrak{c}\| = 1$) h and D can be optimised simultaneously to achieve a good fit to the simulations data.

Eqn (19) and (20) deserve two pertinent remarks. First, it is seen that when $\mathscr{D}\Delta^{2/d_w} \gg \|\mathfrak{c}\|^{2/d_f}$ in the argument of the incomplete gamma function γ, then the quantities $\left\langle\widetilde{\overline{\delta c^2(\Delta)}}\right\rangle$ and $\widetilde{\left\langle\overline{\delta c^2(\Delta)}\right\rangle^2}$ grow as a power of Δ. Within the same limit, division of $\widetilde{\left\langle\overline{\delta c^2(\Delta)}\right\rangle^2}$ by $\left\langle\widetilde{\overline{\delta c^2(\Delta)}}\right\rangle$ yields an exponent for Δ which is twice the gap exponent $1/d_w$, predicted by dynamical scaling theory.[8,64] In particular, both $\left\langle\widetilde{\overline{\delta c^2(\Delta)}}\right\rangle$ and $\widetilde{\left\langle\overline{\delta c^2(\Delta)}\right\rangle^2}$ are independent of the measurement time T. This is due to the averaging over all same-sized open clusters, as already alluded to above. To justify the validity of these scaling relations, D and h were optimised simultaneously for the two equations to achieve the best fit to the simulations results, represented by the dotted line in Fig. 2. The qualitative match between results (19) and (20) with the simulation results in Fig. 2 is quite good, given the conjectural arguments above.

The normalised variance of $\left\langle\overline{\delta c^2(\Delta)}\right\rangle$ for an ensemble of finite size open clusters is given by

$$\mathrm{EB}(\Delta) = \frac{\left(\widetilde{\left\langle\overline{\delta c^2(\Delta)}\right\rangle^2}\right) - \left(\left\langle\widetilde{\overline{\delta c^2(\Delta)}}\right\rangle\right)^2}{\left(\left\langle\widetilde{\overline{\delta c^2(\Delta)}}\right\rangle\right)^2} \geq 0, \quad (21)$$

which is a measure to quantify the amplitude fluctuations of individual results for the TAMSD at a given lag time Δ. We emphasise that in this expression for EB no T-dependence remains due to the anisotropy average over finite-sized open clusters, as discussed above. Apart from the disorder average $\widetilde{\ }$ the quantity (21) has a similar structure as the ergodicity breaking parameter introduced and studied in ref. 24, 25, 34, 44 and 65.

Substituting expressions (19) and (20) into eqn (21) we arrive at an analytical expression for EB. This expression contains a large number of cross-correlation terms such that we restrict ourselves to the limiting behaviour in the case $\mathscr{D}\Delta^{2/d_w} \gg \|\mathfrak{c}\|^{2/d_f}$ in which the incomplete gamma functions reduce to complete gamma functions. We then find that

$$\mathrm{EB} \approx A\Delta^{d_f(\tau-2)/d_w} - 1, \quad (22)$$

where A is a constant. The same result yields from eqn (18) by setting the lower integral limit to zero. Employing the hyperscaling relation between d_f and $\tau = d/d_f + 1$ where d is the embedding Euclidean dimension,[9] the above expression can be written exclusively in terms of d_f and d. Interestingly, the resulting form

$$\mathrm{EB} \approx A\Delta^{(d-d_f)/d_w} - 1, \quad (23)$$

has the same exponent of Δ as the form for the parameter S proposed by Meroz *et al.*[49,50] to distinguish non-ergodic processes from ergodic ones. The difference is that here the ensemble is constituted by a cluster ensemble of different sizes, in contrast to the case addressed in ref. 49 and 50 where only incipient infinite clusters were considered.

The analytical solution (21) for EB with the fit parameters from Fig. 2 is plotted as function of lag time Δ in Fig. 3 along with the results of our Monte Carlo simulations. The match is indeed rather good. What is clear from the double logarithmic plot in Fig. 3 is that for the displayed lag time values we see a crossover to the long-Δ scaling. The intermediate scaling at shorter Δ has a steeper slope.

Another interesting observation is that the exponent of the lag time Δ in eqn (19) can be rewritten in terms of the spectral dimension $d_s = 2d_f/d_w$.[8,66] Recalling the hyperscaling relation stated earlier between d_f and the Fisher exponent τ, the expression of the disorder averaged TAMSD of eqn (19) can be rewritten as

$$\left\langle\widetilde{\overline{\delta c^2(\Delta)}}\right\rangle = (\tau-2)\|\mathfrak{c}\|^{\tau-2}\left[-2h^2\|\mathfrak{c}\|^{2d_f+2-\tau} - d_f h^2 \mathscr{D}^{d_f/2} \times\gamma\left(-\frac{d_f}{2},\frac{\mathscr{D}\Delta^{2/d_w}}{\|\mathfrak{c}\|^{2/d_f}}\right)\Delta^{d_s/2}\right]. \quad (24)$$

We emphasise that regardless of the type of the underlying lattice, in two dimensions and for long lag times, $\Delta \to \infty$, the disorder averaged TAMSD grows as $\Delta^{d_s/2}$. This sole dependence on the spectral dimension d_s is a consequence of the two-dimensional embedding.

III. Discussion

We studied the amplitude fluctuations of the TAMSD typically measured in single particle tracking experiments or simulations for diffusion processes on a square percolation network at criticality. In particular we took all clusters of the network into account, not solely the incipient infinite cluster. Based on the conjectural analogy of this process with an Ornstein–Uhlenbeck

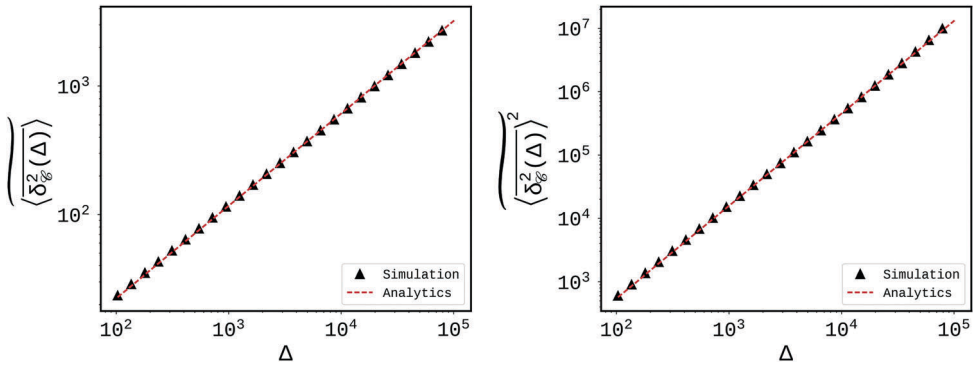

Fig. 2 $\overline{\langle \delta_{\mathcal{C}}^2(\Delta) \rangle}$ (left) and $\overline{\langle \delta_{\mathcal{C}}^2(\Delta) \rangle}^2$ (right) *versus* Δ. Dashed lines indicate the theoretical expressions (19) and (20). The simulation time was $T = 10^6$. The ensemble consists of 5×10^2 lattices of size 4096×4096, on each lattice 50 random walks were simulated with $D = 0.827$ and $h = 0.375$.

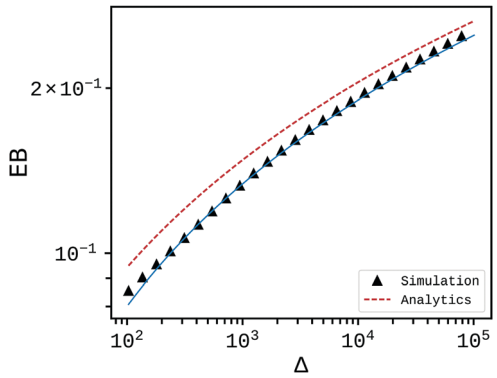

Fig. 3 Ergodicity breaking parameter EB *versus* lag time Δ. The red dashed line represents eqn (21) based on results (19) and (20). The values of the adjustable parameters are $D = 0.827$ and $h = 0.375$, the fit values being taken from Fig. 2. The blue full line is the scaling form of EB given by result (22) with the fitted value $A = 0.98$. The ensemble in the simulations consists of 5×10^2 lattices, where on each 50 random walks were simulated.

process whose known results were rescaled in time we obtained the MSD and TAMSD for the diffusion on the ensemble of percolation clusters, under non-equilibrium initial conditions. The latter are appropriate for many single particle experiments and simulations, in which a tracer is put at a specific place on the percolation network initially. The results based on the analogy with the Ornstein–Uhlenbeck process were shown to be fully consistent with our simulations. Moreover, the expected analytical short and long time behaviours were recovered from the resulting expressions. In addition, it was shown that averaging over the anisotropy of clusters with a specific size yields an expression for the TAMSD which in this anisotropy-averaged sense is independent of the measurement time T. This consequently yielded a result for the normalised variance for the TAMSD, the ergodicity breaking parameter, which is independent of T, as well.

Let us briefly dwell on the connection with our earlier result. Thus, in ref. 51 we empirically suggested from simulations results that EB decays algebraically in T towards a residual value EB_∞ in the form

$$\mathrm{EB}(\Delta) = k\left(\frac{\Delta}{T}\right)^g + \mathrm{EB}_\infty(\Delta), \qquad (25)$$

where k is a constant and g a scaling exponent, whose value for the square lattice was estimated to be 0.8. The constant EB_∞ was found to be an increasing function of the lag time Δ and the percolation density p, as well as to acquire a non-zero value when p approaches the critical value p_c.[51] This form was proposed based on earlier analytical results for other stochastic processes such as Brownian motion, fractional Brownian motion, scaled Brownian motion, and continuous time random walks:[25,34,67–70] there EB decays as a power of T, with different scaling exponents, and, in some cases, attains a residual value. Here we demonstrate that the T dependence vanishes after taking the anisotropy average corresponding to an equilibrium initial condition, for which the dynamics is stationary. Due to computational limitations, however, it is impossible to sample all cluster configurations of the same size by means of Monte Carlo simulations. For instance, even for a small cluster of size 24 there are 10^3 configurations.[71] This is the reason why in our simulations we could observe a T dependence of EB, albeit this dependence is rather weak. This fact is illustrated in Fig. 4 which demonstrates that EB remains practically constant when T varies from 10^4 to 10^6.

It will be interesting to extend the current study to other types of lattices and dimensions. For lattices embedded in two dimensions we would expect that the results obtained here can be transferred to other cases such as the triangular lattice. In higher dimensions it will have to be seen whether the residual, asymptotic value of EB is still relevant, and how the lag time scaling of the different averages of the TAMSD is modified.

As we discussed in the introduction, percolative systems are used as models for the study of protein diffusion in the chromatin of living cells or in the cellular cytoplasm.[18,20] Here the percolation network models areas of the cell that are inaccessible due to molecular crowding. Following recent simulations studies, in particular, in two spatial dimensions demonstrate that in crowded environments the size of the tracer particle itself may renormalise the accessible space.[72] Such effects may be included in more realistic percolation simulations. Moreover, it was shown that essential features of two-dimensional membrane systems consisting of small lipid molecules and large proteins, both mobile, can be mimicked by a static excluded volume system,[73] thus rendering static

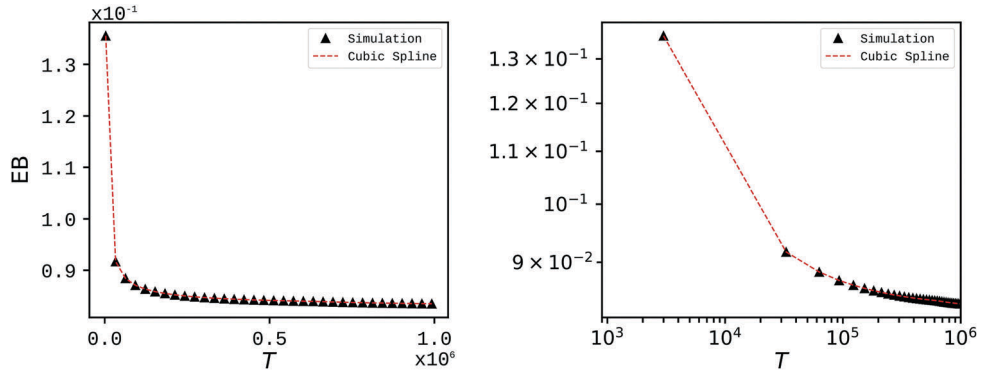

Fig. 4 EB *versus* T at $\Delta = 10^2$. The number of lattices in the ensemble is 10^3 on each of which 2×10^2 random walks were simulated. Note the slight changes in EB while T varies between 10^4 to 10^6.

approaches such as the percolation network applicable also to intrinsically dynamic systems.

Concluding, we are convinced that our results will be of interest not only to the further understanding of dynamics on percolation networks but of special relevance for the interpretation of single particle tracking experiments. In realistic situations one does not always have the flexibility to measure systems under equilibrium initial conditions, and averages of dynamic quantities are affected by inherent disorder in the system. Here our results of physical observables such as the MSD and the amplitude variations expressed in terms of the ergodicity breaking parameter will be easy to implement in data analysis. A particularly relevant area of current research is the single particle tracking of channel proteins in the membranes of living biological cells for which random fractal patterns have been unveiled from the trajectories.[74,75] This behaviour was associated with the self-similar compartmentalisation of the cortical actin meshwork.[76] Similarly relevant will be single particle tracking studies in the nucleus of living cells.[18]

IV. Methods

A. Simulation Scheme

The simulations were carried out on a square lattice, and the nearest neighbours of each site were identified by the von Neumann neighbourhood. The size of the lattice was set to 4096×4096, unless otherwise specified, when the size is set to 1024×1024. Each cell of the lattice is then attributed to be occupied with the percolation probability p or is left vacant otherwise. For the square lattice the critical percolation density p_c is not known analytically but it is, by the means of simulations, confirmed that $p_c = 0.407254$ (note that vacant sites are of interest here).[8,9] In the simulations carried out here we used $p_c = 0.4$.

The initial position of the random walker is located at the centre of the lattice, which may belong to an open cluster or it is an occupied site. In the latter case, the nearest vacant site is chosen as the initial position. Therefore whether a random walker parachutes onto a finite size open cluster or onto an incipient infinite cluster, is random and the associated probability related to the given cluster size $\|\mathcal{C}\|$. For an illustration of such clusters see Fig. 1. The simulation time T is set to 10^6. It is variable only when the dependence of the variance of the disorder averaged TAMSD on T is analysed, when it varies from 10^4 to 10^6. The minimum lag time is $\Delta = 10^2$ to guarantee that the topology of the underlying open clusters are sufficiently sampled.

The fractal dimension d_f was estimated as follows. An ensemble of 7×10^2 incipient infinite clusters are analysed. It is clear that it is not readily observable whether the centre of the lattice belongs to a finite size cluster or to the incipient infinite cluster. Therefore to identify the open clusters and sieve the incipient infinite ones in a lattice realisation, the Hoshen–Kopelman algorithm is used.[77] Afterwards, the box counting method was used to estimate their fractal dimension d_f.[78] On average its corresponding value was found to be $d_f = 1.9 \pm 0.1$, which compares favourably with the predicted value $d_f = 91/48 \approx 1.90$. Yet it should be understood that every cluster has its own fractal dimension due to the unique anisotropy and inhomogeneity of the topology. The same applies to the random walk dimension d_w. To estimate d_w eqn (1) was used to extract the anomalous diffusion exponent α for the incipient infinite clusters, and it was estimated as 2.7 ± 0.1, compared to the known value 2.87. The Fisher exponent τ of the cluster size distribution at p_c is set to 2.03 ± 0.01 based on earlier analyses on the distribution of finite size open clusters.[51] Again, this compares well with the literature value of $\tau = 187/91 \approx 2.05$.

Simulation validation of phenomenological approach. To verify the validity of eqn (5), (6), (10a) and (10b), analyses were performed on some finite size open clusters. Here for instance, a sample open cluster of size 793 on a lattice of size 1024×1024 is demonstrated, see Fig. 1. Two initial conditions were considered: (i) the random walker was fixed to the centre of the underlying lattice at (512, 512), or (ii) the initial position was randomly chosen to be any site within the finite cluster. In total 8×10^3 random walks were simulated and the result is shown in Fig. 5. In the left panel, corresponding to the fixed initial position, we note the gap of width R_g^2 between the MSD and the TAMSD. This is the immediate consequence of how these

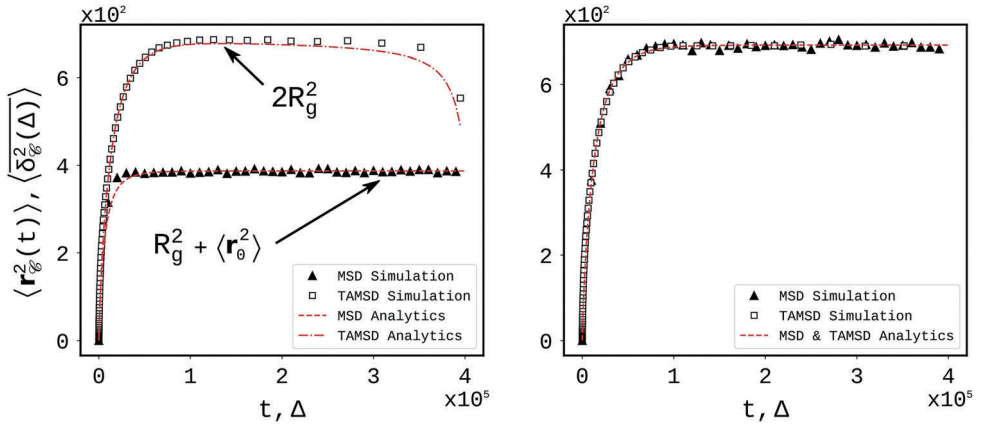

Fig. 5 MSD and TAMSD for fixed initial position (left) and arbitrary initial position (right) on a finite cluster of size 793. 8×10^3 random walks were simulated. The *x* and *y* axes components of the co-ordinate of the centre of mass were found to be 513.74 and 518.20, respectively. $R_g{}^2$ was measured to be 346.33.

quantities are defined in eqn (2) and (3); this is a well known disadvantage of these definitions for the stationary state of a diffusion process, see, for instance, ref. 25 and 79. In contrast, in the right panel, where the initial position was chosen arbitrarily, both reach the same asymptote, namely $2R_g{}^2$. In the procedure $d_f \approx 1.60$ was estimated by the box counting method; the values $d_w \approx 2.44$, $D \approx 0.27$, and $h \approx 0.29$ were determined by best fit with the analytical expressions.

Anisotropy average over same-sized open clusters. To demonstrate that $\langle \mathbf{r}_0{}^2\rangle$, once averaged over the anisotropy of clusters of the same size, is simply $R_g{}^2$, an analytical proof for the case of clusters of size three is provided here. There are two classes of clusters with the size three which are presented in Fig. 6. Note that clusters formed by applying the symmetry groups of the square lattice again belong to these two classes. Define these two classes with [–] and [⌞] (the upper row and the lower row in Fig. 6, respectively).

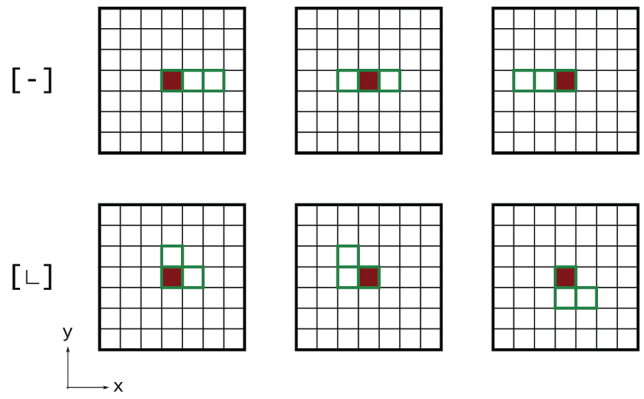

Fig. 6 Two classes of clusters of size three with their different sites positioned at the centre of the lattice. Other clusters which are formed by applying the symmetry groups of the square lattice are equivalent to these two. The *x* and *y* axes show the positive direction of the Cartesian co-ordinate, and the red square cell is the centre of the lattice located at (0, 0).

Consider the class [–], then the following are the calculated values $\langle \mathbf{r}_0{}^2\rangle$ and $R_g{}^2$ for the three possible configurations that appear at the centre of the lattice presented on the leftmost, middle, and rightmost panels of the first row of Fig. 6:

$$\left.\begin{aligned}\langle \mathbf{r}_0{}^2\rangle &= (0-1)^2 = 1\\ R_g{}^2 &= \frac{1}{3}\left[(0-1)^2+(1-1)^2+(2-1)^2\right] = \frac{2}{3}\end{aligned}\right\}\text{(Leftmost)} \tag{26}$$

$$\left.\begin{aligned}\langle \mathbf{r}_0{}^2\rangle &= (0-0)^2 = 0\\ R_g{}^2 &= \frac{1}{3}\left[(-1-0)^2+(0-0)^2+(1-0)^2\right] = \frac{2}{3}\end{aligned}\right\}\text{(Middle)} \tag{27}$$

$$\left.\begin{aligned}\langle \mathbf{r}_0{}^2\rangle &= (-1-0)^2 = 1\\ R_g{}^2 &= \frac{1}{3}\left[(-2+1)^2+(-1+1)^2+(0+1)^2\right] = \frac{2}{3}\end{aligned}\right\}\text{(Rightmost)} \tag{28}$$

Then the anisotropy average over $\langle \mathbf{r}_0{}^2\rangle$ yields $\frac{1+1+0}{3} = \frac{2}{3}$, which is equal to $R_g{}^2$. The same applies to the [⌞] class. Therefore it is supported that in eqn (15b) the quantity $\langle \mathbf{r}_0{}^2\rangle$ is indeed equal to $R_g{}^2$, once averaged over the anisotropy. This should not be surprising since this average is equivalent to an average over different initial positions of the random walks. However, to proof this numerically is practically impossible. For instance among the 9780 lattice realisations only 4 clusters of size 100 were identified. Thus the ensemble of finite clusters with size ranging from 100 to 149 comprised altogether 75. Although the size of these clusters varies somewhat, $\left\langle\overline{\delta c^2(\Delta)}\right\rangle$ maintains practically stationary property for this very ensemble. In Fig. 7 we depict $\left\langle\overline{\delta c^2(\Delta)}\right\rangle$ of these clusters (grey lines). Alongside $\left\langle\overline{\delta c^2(\Delta)}\right\rangle$ is shown (thick black line). Note that there

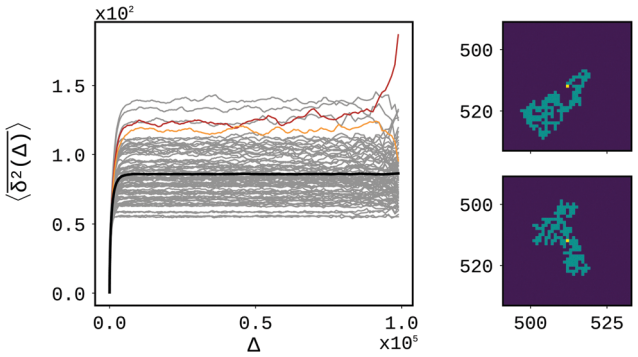

Fig. 7 TAMSD for a set of 75 clusters with size varying between 100 to 149 (grey). The tail of the TAMSD either ascends (red), corresponding to highly anisotropic cluster topologies depicted in the right panel top, or descends (yellow) which corresponds to more isotropic clusters depicted in the right panel bottom. The ensemble average of the TAMSDs are represented by the thick black line whose tail remains levelled. In the right panel the yellow dots represent the centre of the lattice at (512, 512) and the cyan colour depicts the finite cluster.

are two types of $\left\langle \overline{\delta c^2(\Delta)} \right\rangle$ distinguished by their tail, which either ascends or descends (the red and yellow curves). The former corresponds to situations when the topological shape of the cluster is highly anisotropic (Fig. 7 right panel top) and consequently $\langle \mathbf{r}_0{}^2 \rangle > R_g{}^2$. The latter case corresponds to situations when the finite cluster is distributed evenly around the centre of the lattice (Fig. 7 right panel bottom). Such cases imply that $\langle \mathbf{r}_0{}^2 \rangle < R_g{}^2$. The tails of the resulted anisotropy averaged TAMSDs stays constant implying that the quantity (6) is indeed independent of T.

Conflicts of interest

There are no conflicts to declare.

Acknowledgements

A. V. C. and R. M. acknowledge support from Deutsche Forschungsgemeinschaft within project ME 1535/6-1 and ME 1535/7-1. J.-H. J. acknowledges financial support from NRF within project 2017R1C1B2007555. R. M. acknowledges support from the Foundation for Polish Science within an Alexander von Humboldt Polish Honorary Research Scholarship.

References

1 B. B. Mandelbrot, *The Fractal Geometry of Nature*, W.H. Freeman, New York, 1977.
2 J. Feder, *Fractals*, Plenum Press, New York, NY, 1988.
3 H. Takayasu, *Fractals in the physical sciences*, John Wiley & Sons, Chichester, UK, 1992.
4 G. Cantor, Ueber unendliche, lineare Punktmannichfaltigkeiten, *Math. Ann.*, 1883, **21**, 545–591.
5 H. V. Koch, Sur une courbe continue sans tangente, obtenue par une construction géométrique élémentaire, *Ark. Mat., Astron. Fys.*, 1904, **1**, 681–704.
6 W. Sierpiński, Sur une courbe cantorienne dont tout point est un point de ramification, *Comptes Rendues Acad. Sci. Paris*, 1915, **160**, 302.
7 S. R. Broadbent and J. M. Hammersley, Percolation processes: I. Crystals and mazes, in *Mathematical Proceedings of the Cambridge Philosophical Society*, Cambridge University Press, Cambridge, 1957, vol. 53, pp. 629–641.
8 S. Havlin and D. Ben-Avraham, Diffusion in disordered media, *Adv. Phys.*, 1987, **36**, 695–798.
9 D. Stauffer and A. Aharony, *Introduction to Percolation Theory*, CRC Press, 1994.
10 P. G. de Gennes, La percolation: un concept unificateur, *La Recherche*, 1976, **7**, 919–927.
11 R. Metzler and J. Klafter, The random walk's guide to anomalous diffusion: a fractional dynamics approach, *Phys. Rep.*, 2000, **339**, 1.
12 A. Klemm, R. Kimmich and M. Weber, Flow through percolation clusters: NMR velocity mapping and numerical simulations study, *Phys. Rev. E: Stat., Nonlinear, Soft Matter Phys.*, 2001, **63**, 041514.
13 A. Klemm, R. Metzler and R. Kimmich, Diffusion on random site percolation clusters: theory and NMR microscopy experiments with model objects, *Phys. Rev. E: Stat., Nonlinear, Soft Matter Phys.*, 2002, **65**, 021112.
14 M. Sahimi, Fractal and superdiffusive transport and hydrodynamic dispersion in heterogeneous porous media, *Transp. Porous Media*, 1993, **13**, 3–40.
15 J.-P. Bouchaud and A. Georges, Anomalous diffusion in disordered media: statistical mechanisms, models and physical applications, *Phys. Rep.*, 1990, **195**, 127.
16 A. V. Weigel, *et al.*, Obstructed diffusion propagator analysis for single-particle tracking, *Phys. Rev. E: Stat., Nonlinear, Soft Matter Phys.*, 2012, **85**, 041924.
17 C. Loverdo, *et al.*, Quantifying hopping and jumping in facilitated diffusion of DNA-binding proteins, *Phys. Rev. Lett.*, 2009, **102**, 188101.
18 C. C. Fritsch and J. Langowski, Anomalous diffusion in the interphase cell nucleus: the effect of spatial correlations of chromatin, *J. Chem. Phys.*, 2010, **133**, 07B602.
19 M. Krasowska, A. Strzelewicz, A. Rybak, G. Dudek and M. Cieśla, Structure and transport properties of ethylcellulose membranes with different types and granulation of magnetic powder, *Phys. A*, 2016, **452**, 241–250.
20 M. J. Saxton, Anomalous diffusion due to obstacles: a Monte Carlo study, *Biophys. J.*, 1994, **66**, 394–401.
21 B. Oborny, V. Benedek, P. Englert, M. Gulyás and A. G. Hubai, The plant in the labyrinth: adaptive growth and branching in heterogeneous environments, *J. Theor. Biol.*, 2017, **412**, 146–153.
22 T. O. Richardson, K. Christensen, N. R. Franks, H. J. Jensen and A. B. Sendova-Franks, Ants in a labyrinth: a statistical mechanics approach to the division of labour, *PLoS One*, 2011, **6**, e18416.

23 M. J. Saxton, Lateral diffusion in an archipelago. the effect of mobile obstacles, *Biophys. J.*, 1987, **52**, 989–997.
24 E. Barkai, Y. Garini and R. Metzler, Strange Kinetics of Single Molecules in Living Cells, *Phys. Today*, 2012, **65**(8), 29.
25 R. Metzler, J.-H. Jeon, A. G. Cherstvy and E. Barkai, Anomalous diffusion models and their properties: non-stationarity, non-ergodicity, and ageing at the centenary of single particle tracking, *Phys. Chem. Chem. Phys.*, 2014, **16**, 24128–24164.
26 F. Höfling and T. Franosch, Anomalous transport in the crowded world of biological cells, *Rep. Prog. Phys.*, 2013, **76**, 046602.
27 R. Metzler, J.-H. Jeon and A. G. Cherstvy, Non-Brownian diffusion in lipid membranes: experiments and simulations, *Biochim. Biophys. Acta*, 1858, **2451**, 2016.
28 K. Nørregaard, R. Metzler, C. Ritter, K. Berg-Sørensen and L. Oddershede, Manipulation and motion of organelles and single molecules in living cells, *Chem. Rev.*, 2017, **117**, 4342.
29 J.-P. Bouchaud, Weak ergodicity breaking and aging in disordered systems, *J. Phys. I*, 1992, **2**, 1705.
30 H. Scher and E. W. Montroll, Anomalous transit-time dispersion in amorphous solids, *Phys. Rev. B: Condens. Matter Mater. Phys.*, 1975, **12**, 2455.
31 P. Massignan, *et al.*, Nonergodic subdiffusion from Brownian motion in an inhomogeneous medium, *Phys. Rev. Lett.*, 2014, **112**, 150603.
32 A. G. Cherstvy, A. V. Chechkin and R. Metzler, Particle invasion, survival, and non-ergodicity in 2D diffusion processes with space-dependent diffusivity, *Soft Matter*, 2014, **10**, 1591.
33 A. G. Cherstvy, A. V. Chechkin and R. Metzler, Anomalous diffusion and ergodicity breaking in heterogeneous diffusion processes, *New J. Phys.*, 2013, **15**, 083039.
34 Y. He, S. Burov, R. Metzler and E. Barkai, Random time-scale invariant diffusion and transport coefficients, *Phys. Rev. Lett.*, 2008, **101**, 058101.
35 A. Lubelski, I. M. Sokolov and J. Klafter, Nonergodicity mimics inhomegeneity in single particle tracking, *Phys. Rev. Lett.*, 2008, **100**, 250602.
36 S. Burov, R. Metzler and E. Barkai, Aging and non-ergodicity beyond the Khinchin theorem, *Proc. Natl. Acad. Sci. U. S. A.*, 2010, **107**, 13228.
37 J.-H. Jeon, V. Tejedor, S. Burov, E. Barkai, C. Selhuber-Unkel, K. Berg-Sørensen, L. Oddershede and R. Metzler, *In vivo* anomalous diffusion and weak ergodicity breaking of lipid granules, *Phys. Rev. Lett.*, 2011, **106**, 048103.
38 S. M. A. Tabei, *et al.*, Intracellular transport of insulin granules is a subordinated random walk, *Proc. Natl. Acad. Sci. U. S. A.*, 2013, **110**, 4911.
39 C. Manzo, *et al.*, Weak Ergodicity Breaking of Receptor Motion in Living Cells Stemming from Random Diffusivity, *Phys. Rev. X*, 2015, **5**, 011021.
40 J. H. P. Schulz, E. Barkai and R. Metzler, Aging renewal theory and application to random walks, *Phys. Rev. X*, 2014, **4**, 011028.
41 X. Hu, *et al.*, The dynamics of single protein molecules is non-equilibrium and self-similar over thirteen decades in time, *Nat. Phys.*, 2016, **12**, 171.
42 M. S. Song, H. C. Moon, J.-H. Jeon and H. Y. Park, Neuronal messenger ribonucleoprotein transport follows an ageing Lévy walk, *Nat. Commun.*, 2018, **9**, 344.
43 C. Monthus and J.-P. Bouchaud, Models of traps and glass phenomenology, *J. Phys. A*, 1996, **29**, 3847.
44 W. Deng and E. Barkai, Ergodic properties of fractional Brownian-Langevin motion, *Phys. Rev. E: Stat., Nonlinear, Soft Matter Phys.*, 2009, **79**, 011112.
45 J.-H. Jeon, N. Leijnse, L. Oddershede and R. Metzler, Anomalous diffusion and power-law relaxation in wormlike micellar solution, *New J. Phys.*, 2013, **15**, 045011.
46 I. Bronstein, *et al.*, Transient Anomalous Diffusion of Telomeres in the Nucleus of Mammalian Cells, *Phys. Rev. Lett.*, 2009, **103**, 018102.
47 M. Weiss, Single-particle tracking data reveal anticorrelated fractional Brownian motion in crowded fluids, *Phys. Rev. E: Stat., Nonlinear, Soft Matter Phys.*, 2013, **88**, 010101(R).
48 J. F. Reverey, *et al.*, Superdiffusion dominates intracellular particle motion in the supercrowded space of pathogenic *Acanthamoeba castellanii*, *Sci. Rep.*, 2015, **5**, 11690.
49 Y. Meroz, I. M. Sokolov and J. Klafter, Test for determining a subdiffusive model in ergodic systems from single trajectories, *Phys. Rev. Lett.*, 2013, **110**, 090601.
50 Y. Meroz, I. M. Sokolov and J. Klafter, Subdiffusion of mixed origins: when ergodicity and nonergodicity coexist, *Phys. Rev. E: Stat., Nonlinear, Soft Matter Phys.*, 2010, **81**, 010101(R).
51 Y. Mardoukhi, J.-H. Jeon and R. Metzler, Geometry controlled anomalous diffusion in random fractal geometries: looking beyond the infinite cluster, *Phys. Chem. Chem. Phys.*, 2015, **17**, 30134–30147.
52 B. O'Shaughnessy and I. Procaccia, Analytical solutions for diffusion on fractal objects, *Phys. Rev. Lett.*, 1985, **54**, 455.
53 M. Giona and H. E. Roman, Fractional diffusion equation for transport phenomena in random-media, *Physica A*, 1992, **185**, 87.
54 R. Metzler, W. G. Glöckle and T. F. Nonnenmacher, Fractional model equation for anomalous diffusion, *Physica A*, 1994, **211**, 13.
55 B. D. Hughes, *Random Walks and Random Environments*, Clarendon Press Oxford, 1996, vol. 2.
56 D. Jacobs and H. Nakanishi, Autocorrelation functions for discrete random walks on disordered lattice, *Phys. Rev. A: At., Mol., Opt. Phys.*, 1990, **41**, 706.
57 C. D. Mitescu, H. Ottavi and J. Roussenq, Diffusion on percolation lattices: the labyrinthine ant, in *AIP Conference Proceedings*, AIP, 1978, vol. 40, pp. 377–381.
58 R. Pandey, Classical diffusion, drift, and trapping in random percolating systems, *Phys. Rev. B: Condens. Matter Mater. Phys.*, 1984, **30**, 489.
59 C. Fassnacht, *J. Undergrad. Res. Phys.*, 1983, **2**, 23.
60 C. D. Mitescu and J. Rossenq, Diffusion on percolation clusters. Percolation Structures and Processes, *Ann. Isr. Phys. Soc.*, 1983, **5**, 81–100.

61 J. Roussenq, PhD thesis, Université de Provence, Marseille, 1980.
62 G. E. Uhlenbeck and L. S. Ornstein, On the theory of the Brownian motion, *Phys. Rev.*, 1930, **36**, 823.
63 A. G. Cherstvy, Y. Mardoukhi, A. V. Chechkin and R. Metzler, under revision.
64 G. Grimmett, *Percolation*, Springer, 1999.
65 S. M. Rytov, Y. A. Kravtsov and V. I. Tatarskii, *Principles of Statistical Radiophysics: Correlation theory of random processes. Principles of Statistical Radiophysics*, Springer-Verlag, 1987.
66 S. Alexander and R. Orbach, Density of states on fractals: ''fractons'', *J. Phys. (Paris), Lett.*, 1982, **43**, L625–L631.
67 M. Schwarzl, A. Godec and R. Metzler, Quantifying non-ergodicity of anomalous diffusion with higher order moments, *Sci. Rep.*, 2017, **7**, 3878.
68 H. Safdari, *et al.*, Quantifying the non-ergodicity of scaled Brownian motion, *J. Phys. A*, 2015, **48**, 375002.
69 A. Bodrova, *et al.*, Underdamped scaled Brownian motion: (non-)existence of the overdamped limit in anomalous diffusion, *Sci. Rep.*, 2016, **6**, 30520.
70 A. G. Cherstvy and R. Metzler, Ergodicity breaking, ageing, and confinement in generalized diffusion processes with position and time dependent diffusivity, *J. Stat. Mech.: Theory Exp.*, 2015, **2015**, P05010.
71 D. H. Redelmeier, Counting polyominoes: yet another attack, *Discrete Math.*, 1981, **36**, 191–203.
72 S. Ghosh, A. G. Cherstvy, D. Grebenkov and R. Metzler, Anomalous, non-Gaussian tracer diffusion in heterogeneously crowded environments, *New J. Phys.*, 2016, **18**, 013027.
73 J.-H. Jeon, M. Javanainen, H. Martinez-Seara, R. Metzler and I. Vattulainen, Protein crowding in lipid bilayers gives rise to non-Gaussian anomalous lateral diffusion of phospholipids and proteins, *Phys. Rev. X*, 2016, **6**, 021006.
74 A. V. Weigel, B. Simon, M. M. Tamkun and D. Krapf, Ergodic and nonergodic processes coexist in the plasma membrane as observed by single molecule tracking, *Proc. Natl. Acad. Sci. U. S. A.*, 2011, **108**, 6438.
75 D. Krapf, Mechanisms underlying anomalous diffusion in the plasma membrane, *Curr. Top. Membr.*, 2015, **75**, 167.
76 S. Sadegh, J. L. Higgins, P. C. Mannion, M. M. Tamkun and D. Krapf, Plasma membrane is compartmentalized by a self-similar cortical actin meshwork, *Phys. Rev. X*, 2017, **7**, 011031.
77 J. Hoshen and R. Kopelman, Percolation and cluster distribution. i. cluster multiple labeling technique and critical concentration algorithm, *Phys. Rev. B: Condens. Matter Mater. Phys.*, 1976, **14**, 3438.
78 K. Falconer, *Fractal geometry*, John Wiley & Sons, Chichester, UK, 1990.
79 J.-H. Jeon and R. Metzler, Inequivalence of time and ensemble averages in ergodic systems: exponential *versus* power-law relaxation in confinement, *Phys. Rev. E: Stat., Nonlinear, Soft Matter Phys.*, 2012, **85**, 021147.

Appendix B

PCCP

PAPER

View Article Online
View Journal | View Issue

Cite this: *Phys. Chem. Chem. Phys.*, 2015, **17**, 30134

Geometry controlled anomalous diffusion in random fractal geometries: looking beyond the infinite cluster

Yousof Mardoukhi,†[ab] Jae-Hyung Jeon†[bc] and Ralf Metzler*[ab]

We investigate the ergodic properties of a random walker performing (anomalous) diffusion on a random fractal geometry. Extensive Monte Carlo simulations of the motion of tracer particles on an ensemble of realisations of percolation clusters are performed for a wide range of percolation densities. Single trajectories of the tracer motion are analysed to quantify the time averaged mean squared displacement (MSD) and to compare this with the ensemble averaged MSD of the particle motion. Other complementary physical observables associated with ergodicity are studied, as well. It turns out that the time averaged MSD of individual realisations exhibits non-vanishing fluctuations even in the limit of very long observation times as the percolation density approaches the critical value. This apparent non-ergodic behaviour concurs with the ergodic behaviour on the ensemble averaged level. We demonstrate how the non-vanishing fluctuations in single particle trajectories are analytically expressed in terms of the fractal dimension and the cluster size distribution of the random geometry, thus being of purely geometrical origin. Moreover, we reveal that the convergence scaling law to ergodicity, which is known to be inversely proportional to the observation time T for ergodic diffusion processes, follows a power-law $\sim T^{-h}$ with $h < 1$ due to the fractal structure of the accessible space. These results provide useful measures for differentiating the subdiffusion on random fractals from an otherwise closely related process, namely, fractional Brownian motion. Implications of our results on the analysis of single particle tracking experiments are provided.

Received 19th June 2015,
Accepted 2nd October 2015

DOI: 10.1039/c5cp03548a

www.rsc.org/pccp

1 Introduction

Roughly a century after Jean Perrin's groundbreaking experiments on Brownian motion using an elaborate single particle tracking method in 1908,[1] nowadays sophisticated single particle tracking of submicron tracer particles and even single molecules have become a routine tool in the study of passive and active transport dynamics in living biological cells as well as in various crowded fluids *in vitro*.[2] Distinguished from traditional ensemble averaging experiments single particle tracking enables one to directly access the diffusive properties of the tracer particles without any loss of information due to ensemble averaging. Based on the single particle tracking technique it was revealed that the tracer motion in 'superdense'[3] biological or complex environments often exhibits anomalous diffusion such that its ensemble averaged mean squared displacement (MSD) grows non-linearly with time in the form

$$\langle \mathbf{r}^2(t) \rangle \simeq t^{\alpha} \tag{1}$$

with the anomalous diffusion exponent α. We distinguish subdiffusion for $0 < \alpha < 1$ and superdiffusion with $\alpha > 1$. Examples for subdiffusion include the diffusion of messenger RNA molecules[3] and lipid granules in living cells,[4–7] and the motion of phospholipid molecules and proteins in the membranes of living cells or *in silico* membranes.[8–12] As examples from *in vitro* systems we mention the anomalous diffusion of microbeads in polymer networks or gels[13–16] and in artificially crowded media[17,18] as well as colloidal suspensions.[19,20] Examples for superdiffusion due to active motion in living cells were provided in ref. 21–25. Effective superdiffusion on surfaces is also observed due to bulk mediation effects.[26,27]

Theoretically an anomalous diffusion process characterised by the law (1) may be governed by different stochastic models, each of them underlying a unique physical process.[28–30] Despite the common scaling (1) of the ensemble averaged MSD some of these processes are ergodic in the Boltzmann–Khinchin sense that the long time average of physical observables such as the

[a] *Institute of Physics and Astronomy, University of Potsdam, 14476 Potsdam-Golm, Germany. E-mail: rmetzler@uni-potsdam.de*
[b] *Department of Physics, Tampere University of Technology, FI-33101 Tampere, Finland*
[c] *School of Physics, Korea Institute for Advanced Study, Seoul 02455, Republic of Korea. E-mail: jeonjh@kias.re.kr*
† YM and JHJ contributed equally to this work.

MSD converges to the corresponding ensemble average while in other, weakly non-ergodic processes both kinds of averages remain disparate.[28–32] One process, that was identified as stochastic mechanism behind the motion of tracers in living biological cells and structured environments is the continuous time random walk.[33] Continuous time random walks give rise to weakly non-ergodic subdiffusion due to multiple binding or caging events characterised by a long-tailed distribution of waiting times between successive motion events which features a diverging mean waiting time.[28,29,31] Fractional Brownian motion and the associated fractional Langevin equation describe Gaussian processes in which the power-law correlated displacements give rise to anomalous diffusion.[34–40] Such self-affine Gaussian processes have a fractal path and are ergodic, and they were shown to occur in viscoelastic environments.[40,41] Another popular ergodic model, which in many ways appears similar to fractional Brownian motion, are random walks on fractal structures.[28–30,42,43] Fractals with their scale-free geometry were popularised by Mandelbrot in the 1980's to more closely resemble natural objects such as mountains or coastlines than do classical geometrical bodies.[44] De Gennes coined the concept of ant in the labyrinth:[45] random fractals such as the statistically self-similar continuum or discrete percolation models effect the subdiffusion of a random walker due to the existence of bottlenecks and cul-de-sacs on all scales.[42,43,46–49] Among a variety of applications, this model was used to describe the obstructed diffusion in highly crowded random environments, for instance, the cytoplasm of cells, cell nuclei, and biological membranes.[15,50–55] Recently models of mixed origins of anomalous diffusion processes were also suggested.[29]

Following the advances in single particle tracking techniques it has become possible to garner sufficient evidence to diagnose the statistical characteristics of a stochastic process on the single trajectory level. To identify a specific anomalous diffusion process behind observed data allows one to learn more about the physical nature of the system and predict secondary quantities such as the first passage behaviour responsible for (bio)chemical reactions.[29,31,56–59] Weakly non-ergodic processes in Bouchaud's sense exhibit the above-mentioned disparity between the ensemble averaged MSD (1) and the time averaged MSD defined below, even in the limit of long measurement times. Moreover, these processes exhibit ageing, the dependence of observables on the time span between initiation of the process and start of the measurement, and the amplitude of individual time averages fluctuates significantly. This behaviour is shared by continuous time random walks[31,60–64] and its variants[65–67] as well as heterogeneous diffusion processes with space dependent diffusivity.[68–70] In contrast, stochastic motion driven by power-law correlated Gaussian noise and the random motion on fractals are the key ergodic anomalous diffusion processes.[29,71] Another class of weakly non-ergodic processes corresponds to scaled Brownian motion with a power-law time dependent noise strength.[72–75] It is known that the discrimination between them based on data analysis is challenging, as both models share the same asymptotic scaling behaviour of the velocity autocorrelation functions.[76] Theoretical tests differentiating the two were recently proposed on the ground that the fractal dimension—or the number of visited sites—is smaller than the dimensionality of the embedding Euclidean space—or the total number of sites in space.[56,77] We here explore in more detail the exact ergodic properties of de Gennes' random ant-in-the-labyrinth motion. Specifically, we analyse the single particle diffusion on two-dimensional percolation clusters at varying densities. Special emphasis is put on the ergodic properties of the motion revealed by the time averaged MSD. Remarkably, our simulations reveal that the fluctuations in the time averaged MSD have a unique statistical feature of geometrical origin which is significantly different from that of fractional Brownian motion.

This paper is organised as follows. In Section 2 we gather the information on the simulation procedure, the definitions of the averaging procedures used in our analysis, and the well known diffusion dynamics on percolation clusters in the framework of ensemble averages. In Section 3 we present our simulation results on the single trajectory level including the time averaged MSD, the amplitude scatter distribution of the time averaged MSD, and the ergodicity breaking parameter. In particular, we analyse the rôle of clusters other than the infinite cluster. In Section 4 we discuss our results and conclude.

2 Methods

2.1 Simulation scheme

Our study is based on a two-dimensional square lattice with periodic boundary conditions, as commonly used in other studies.[50,77,78] On this underlying structure we generate our random percolation environments. The system size varies depending on the load of the simulations. For instance, to simulate individual trajectories for analysis in terms of the time averaged MSD a lattice of 4096×4096 is considered whereas in more computationally expensive simulations such as labelling clusters with different sizes, the lattice size is set to 1024×1024. Each site is either filled with probability p or vacant with probability $1 - p$. Here we follow the convention that p refers to the obstacle density in space.[50]

Percolation theory states that as the percolation density p approaches the critical value p_c from above—that is for decreasing obstacle size—separated finite clusters merge and the correlation length $\bar{\xi}$ of clusters diverges as $\bar{\xi} \sim |p - p_c|^{-\nu}$ with $\nu = 5/36$.[48] At the percolation threshold p_c and for lower obstacle densities $p < p_c$ there exists an infinite cluster of empty sites spanning the entire volume.[42,48] The probability that a given site belongs to the infinite cluster at criticality scales as $P_\infty \sim (p - p_c)^\beta$ where $\beta = 43/18$.[42,48] Concurrently as $p \to p_c$ the crossover length r_c from anomalous to normal diffusion used below diverges as $r_c \sim |p - p_c|^{-\nu+\beta/2}$. Thus at $p = p_c$ anomalous diffusion of the form (1) prevails at all times.[42,48,50] Simultaneously the percolation geometry forms scale-free fractal objects over all length scales larger than the lattice constant.[42,48,50,79] ‡ For obstacle percolation considered here the critical percolation threshold is $p_c = 0.407256$.[48] § This critical case is depicted in Fig. 1.

‡ Note that for finite sized fractals with lower and upper bound the power-law behaviour levels off at both ends in sigmoidal fashion.[80]

§ Often one considers the percolation of accessible sites, in that case the percolation threshold is $1 - p_c \approx 0.59$.

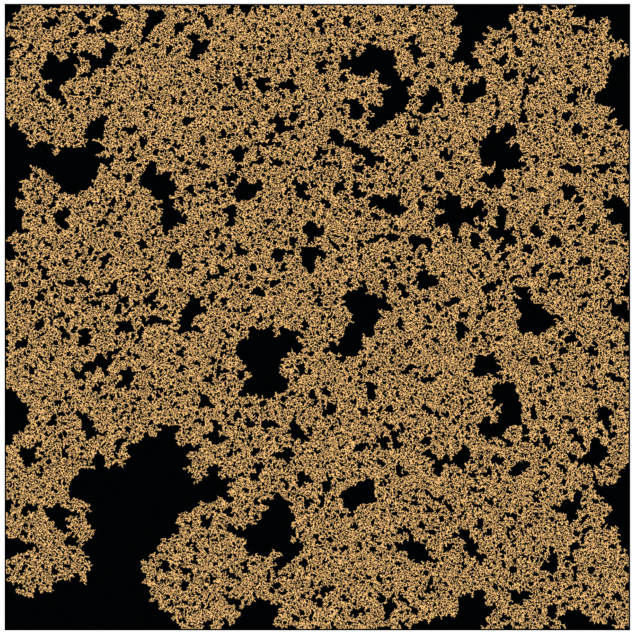

Fig. 1 Sample realisation of a random percolation geometry at the percolation threshold $p = p_c$ on a square lattice of size 1024 × 1024. The copper coloured structure representing the vacant sites of an infinite cluster accessible to the random walker constitutes a statistically scale-free, fractal object.

In our simulations, after a random geometry with label ζ of given density p is generated a tracer particle starts to diffuse at its centre if it is vacant. Otherwise a randomly chosen vacant site close to the centre is chosen. In our Monte Carlo simulation, at every unit time step $\delta t = 1$ the tracer particle jumps to the nearest vacant site with probability 1/4 on our two-dimensional lattice. Uniform random numbers were generated by the `ran()` function taken from Numerical Recipes.[81] On an isolated unit cluster no move is allowed and the random walker becomes completely localised. In the limit of $p \to 0$ the diffusivity of the tracer particle is that of a free two-dimensional lattice, $K = \frac{a^2}{4\delta t}$ where a is the lattice constant. Our typical simulation time was 10^6 time steps, unless indicated otherwise. For the evaluation of physical observables N_ζ random percolation geometries were generated at a given percolation density p, and N tracer trajectories for each percolation geometry were recorded. For the efficiency of the simulation study, the number N_ζ was varied from 50 to 10 000 and N from 3 to 1000 depending on the observables. In each case sufficiently large samples were chosen to ensure a proper statistical convergence. Information on N_ζ and N used in the evaluation of each observable are provided in the text and in the figure captions.

2.2 Ensemble averaged mean square displacement

Let us first address the potential ambiguity in defining ensemble averages in percolation systems.[42] For a given fractal geometry ζ the MSD of an ensemble of particles starting at the origin at time $t = 0$ is given by

$$\langle \mathbf{r}(t)^2 \rangle_\zeta = \frac{1}{N} \sum_i^N \mathbf{r}_i(t)^2 \qquad (2)$$

where we choose the coordinate systems such that $\mathbf{r}_i(0) = 0$. The MSD $\langle \mathbf{r}(t)^2 \rangle_\zeta$ will in general assume different values for different realisations ζ.¶ To avoid the dependence on the specific realisation, an additional (disorder) average of the form

$$\langle \widetilde{\mathbf{r}^2(t)} \rangle = \frac{1}{N_\zeta} \sum_\zeta^{N_\zeta} \left\langle \mathbf{r}(t)^2 \right\rangle_\zeta, \qquad (3)$$

is defined, where N_ζ counts the different realisation ζ over which the average is taken. In what follows we refer to this quantity as the ensemble averaged MSD. We note that we did not average over initial positions for a given realisation ζ, however, we expect this averaging to be equivalent to the disorder averaging over different ζ. We also note that similar questions on the averaging arise in the analysis of diffusion in quenched energy landscapes.[82]

Prior to our study of single trajectories below we here briefly summarise the ensemble averaged MSD for particles diffusing in percolation geometries, and we compare these results with our current Monte Carlo simulation. The ensemble averaged MSD has two distinct scaling regimes over time for percolation densities below the percolation threshold p_c, namely[42,43,47,48,50]

$$\langle \widetilde{\mathbf{r}^2(t)} \rangle \simeq \begin{cases} t^{2/d_w}, & |\mathbf{r}| < r_c \\ t, & |\mathbf{r}| > r_c \end{cases}. \qquad (4)$$

Thus, the diffusion is transiently anomalous below the crossover length $r_c(p)$, corresponding to times shorter than the crossover time $t_c \simeq r_c^{d_w}$. Here the classical notation involves the walk dimension d_w of the diffusing particle. Generally $d_w > 2$ implying subdiffusion with $0 < \alpha = 2/d_w < 1$. In the simplest case when we have no obstacles ($p = 0$) all sites are accessible to the random walker and we have normal diffusion at all times. In this case the crossover length r_c vanishes. This case is shown in Fig. 2(a). At finite percolation densities below the percolation threshold, $0 < p < p_c$, the crossover length roughly corresponds to the average cluster size of locally fractal structures: local bottlenecks and cul-de-sacs generate anomalous diffusion, which eventually crosses over to normal diffusion when the typical distance travelled by the random walker exceeds r_c. This case is shown in Fig. 2(b). We note that compared to the obstacle-free case $p = 0$, the effective diffusion coefficient in the case $0 < p < p_c$ has a reduced value. At the percolation threshold $p = p_c \approx 0.407256$ the percolation geometry is fractal on all available scales, and the crossover length r_c diverges. Concurrently, the anomalous diffusion regime ranges over all time scales.‖ For the square lattice the anomalous diffusion exponent is $2/d_w \approx 0.7$,[50] which is again confirmed by our simulations, see Fig. 2. Indeed, Fig. 2(c) documents the anomalous diffusion at criticality. Anomalous diffusion in effectively two dimensional geometries was indeed verified by NMR measurements

¶ Only for random walker exclusively seeded on the infinite cluster, that is, for obstacle percolation densities $p \leq p_c$, the MSD $\langle \mathbf{r}(t)^2 \rangle_\zeta$ for different realisations ζ of the geometry will converge to approximately the same value.

‖ More accurately, anomalous diffusion is observed when the random walker samples distances above several lattice constants a and will be eventually terminated in our periodic boundary conditions when the percolation structure is fully sampled.

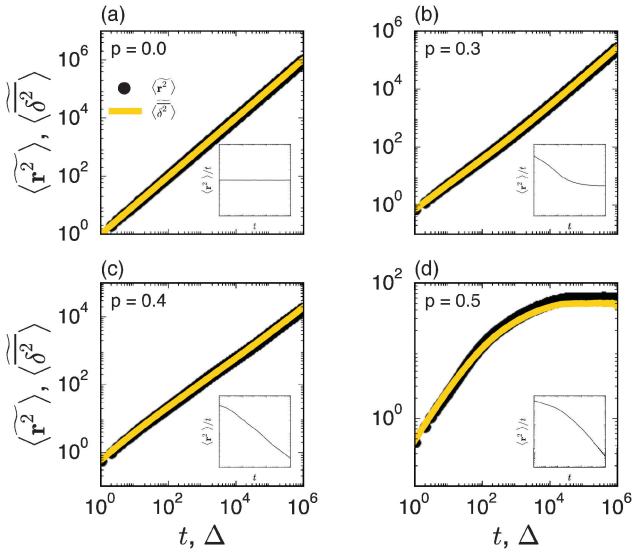

Fig. 2 Ensemble averaged MSD $\langle \mathbf{r}^2(t) \rangle$ (black circles) and mean time averaged MSD $\left\langle \overline{\delta^2(\Delta)} \right\rangle$ (yellow solid line) for four different percolation densities: (a) $p = 0$, (b) $p < p_c$, (c) $p \approx p_c$, and (d) $p > p_c$. In each panel the inset depicts $\langle \mathbf{r}^2(t) \rangle / t$ *versus* t on a double logarithmic scale, the slope is $\alpha - 1$. Note the terminal Brownian scaling for $p < p_c$ with a reduced diffusivity for the finite percolation density (b). The numbers of the random geometries and trajectories used for the plot are $N_\zeta = 50$ and $N = 1000$.

in computer generated percolation clusters milled into stacked plastic sheets.[83,84] Above the percolation threshold the diffusion is more and more reduced. In particular, only finite, disjunct clusters remain such that the MSD eventually saturates to a plateau, see Fig. 2(d).

3 Probing the ergodic behaviour of diffusion on percolation geometries

3.1 Time averaged mean squared displacement

To explore the ergodic properties of the diffusion process on percolation clusters in addition to the ensemble averaged MSD we now consider the time averaged MSD defined in terms of the moving average

$$\overline{\delta^2(\Delta)} = \frac{1}{T-\Delta}\int_0^{T-\Delta} [\mathbf{r}(t+\Delta) - \mathbf{r}(t)]^2 \mathrm{d}t \qquad (5)$$

of a single trajectory $\mathbf{r}(t)$.[28,29,31] Here Δ is the lag time corresponding to the width of the window slid along the time series, and T is the total observation (measurement) time. The time averaged MSD (5) provides information on the diffusive properties of a single particle and is routinely applied to evaluate experimental single particle tracking data. Typically diffusive processes, that are ergodic in the Boltzmann–Khinchin sense, have the property that for sufficiently long observation times T (formally, $T \to \infty$), the time and ensemble averaged MSDs converge to each other,

$$\lim_{T\to\infty} \overline{\delta^2(\Delta)} = \langle \mathbf{r}^2(\Delta) \rangle. \qquad (6)$$

In agreement with previous numerical studies,[77] our simulations indeed demonstrate that this ergodicity relation is satisfied for our random walker on the percolation geometry for any percolation density if we average the time averaged MSD over both N individual simulated trajectories (index i) and over an ensemble of N_ζ percolation geometries ζ,

$$\left\langle \widetilde{\overline{\delta^2(\Delta)}} \right\rangle = \frac{1}{N \times N_\zeta} \sum_{i,\zeta} \overline{\delta_{i,\zeta}{}^2(\Delta)}. \qquad (7)$$

As seen in Fig. 2, this mean time averaged MSD—represented by the yellow solid line—coincides with the ensemble averaged MSD (black circles) for all cases. The equivalence between the two quantities for $N_\zeta = 50$ is not significantly improved when the sample size is increased tenfold to $N_\zeta = 500$ (not shown).

However, the equality between the ensemble averaged MSD (7) and individual long time averaged MSDs is not always fulfilled. To demonstrate this fact we show in Fig. 3 individual time averaged MSD traces $\overline{\delta^2(\Delta)}$ along with the ensemble average $\left\langle \widetilde{\overline{\delta^2(\Delta)}} \right\rangle$ (black solid line) from Fig. 2. As long as $p < p_c$ the individual $\overline{\delta^2(\Delta)}$ follow nicely the mean $\left\langle \widetilde{\overline{\delta^2(\Delta)}} \right\rangle$ except for long lag times $\Delta \approx T$ when the statistic for the time averaging becomes insufficient (Fig. 3(a) and (b)). In this case the cluster turns from a fully accessible two-dimensional lattice at $p = 0$ to a geometry with growing but localised clusters of obstacles at $0 < p < p_c$. The connectivity remains high such that, independent of the initial position, eventually the random walker explores the entire structure, apart from inaccessible areas of sufficiently small measure. Right at the percolation threshold $p = p_c$ shown in Fig. 3(c) we already observe significant deviations from the mean $\left\langle \widetilde{\overline{\delta^2(\Delta)}} \right\rangle$: a smaller number of

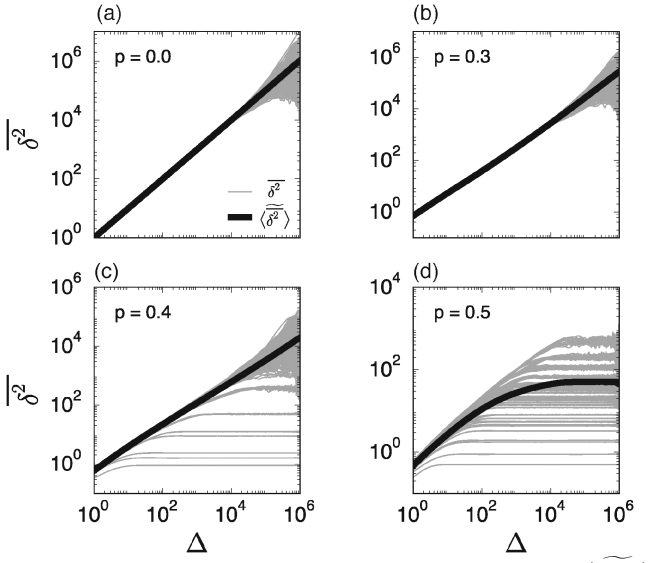

Fig. 3 Individual time averaged MSD curves $\overline{\delta^2(\Delta)}$ and their mean $\left\langle \widetilde{\overline{\delta^2(\Delta)}} \right\rangle$ (thick black curve, as already shown in Fig. 2). In each panel the variation of the individual time averaged MSD curves represents 10 different trajectories on each of the overall 50 different simulated percolation geometries.

traces $\overline{\delta^2(\Delta)}$ show confinement leading $\overline{\delta^2(\Delta)}$ to enter a plateau much earlier than the crossover time of $\left\langle\widetilde{\overline{\delta^2(\Delta)}}\right\rangle$. This is due to the fact that at criticality, when the percolation geometry is fractal, the size of the accessible regions is scale-free and finite accessible clusters of all sizes are created in addition to the incipient infinite cluster. When seeded on such a finite cluster the time averaged MSD of the emanating trajectory will show a plateau depending on the very size of the visited cluster. We thus encounter a non-ergodic scenario in which the irreproducibility of trajectories stems from the quenched geometry. This non-ergodic behaviour is strengthened above the percolation threshold, $p > p_c$, as shown in Fig. 3(d). Individual traces $\overline{\delta^2(\Delta)}$ exhibit a pronounced scatter around the average $\left\langle\widetilde{\overline{\delta^2(\Delta)}}\right\rangle$. In the sense of Bouchaud's definition[32] the fact that once seeded on a specific cluster the random walker cannot pass to an unconnected cluster is referred to as strong ergodicity breaking. It denotes the case when the phase space of a system consists of disjoint subvolumes and access to each subvolume is determined by the initial position of the particle. It is intrinsic for the percolation system in that it is reproducible when simulations are performed with the same number of runs for given trajectory length T. Moreover, a typical scatter of amplitudes of the plateaus always occurs at any trajectory length T. It is in fact noteworthy that albeit these features of individual tracer motion the ensemble average remains ergodic within the error of our simulations.

Subdiffusive continuous time random walks[31,60,65,67,85,86] show ageing in the sense that the particle encounters longer and longer waiting times on its motion due to the scale free nature of the distribution of waiting times. The amplitude of the time averaged MSD given by the effective diffusivity therefore becomes a decaying function of the observation time T. Analogous ageing effects occur for scaled Brownian motion,[87] heterogeneous diffusion processes,[68] and their combination. Apart from transient ageing[88] the Gaussian processes with correlated increments of the fractional Brownian motion and fractional Langevin equation motion types do not exhibit such effects.[9] In Fig. 4 we analyse the dependence of the time averaged MSD on the observation time T using the data from Fig. 3 for fixed lag time $\Delta = 100$. As can be seen no significant ageing can be detected, the traces settle towards a constant function of T. The figure also illustrates the relatively small amplitude scatter below and at the percolation threshold, $p \leq p_c$, as compared to the behaviour at the higher percolation density, $p > p_c$.

3.2 Time averaged occupation probability

To gather more quantitative clues on the above observations of the time averaged MSD we determine the profile of individual time averaged MSDs and explore how it is related to the particles' random paths on a given percolation geometry ζ. To this end we introduce the time averaged occupation probability $\overline{P_\zeta(\mathbf{r})}$ at the lattice point $\mathbf{r}$ for a given fractal geometry ζ in the form

$$\overline{P_\zeta(\mathbf{r})} = \frac{t_\mathbf{r}}{T} \tag{8}$$

where $t_\mathbf{r}$ is the accumulated residence time of the particle at the lattice site $\mathbf{r}$ averaged over the observation time T.

Fig. 5 presents typical patterns of the time average $\overline{P_\zeta(\mathbf{r})}$ obtained from simulations with $N = 10^4$. For the fully accessible two-dimensional lattice ($p = 0$) the time averaged occupation probability is smoothly spread out from the origin with a uniform radial distribution of bell shape. This is a typically expected result for Brownian motion as well as for other ergodic processes in which the ensemble averaged occupation probability $\langle P_\zeta(\mathbf{r})\rangle$ is identical with its time averaged counterpart. This case is shown in Fig. 5(a). For growing percolation densities below the percolation threshold we therefore observe similar patterns, albeit local fine structure will appear due to the existence of a finite correlation range of obstacles measured by the radius r_c introduced above. In particular, growing p will increasingly limit the accessible range for the random walker, that is, the occupation probability at finite T will decay faster from the initial position. At the percolation threshold $p = p_c$ the pattern of the time averaged occupation probability $\overline{P_\zeta(\mathbf{r})}$ exhibits a structural fingerprint of the specific underlying fractal geometry. Interestingly, we find that $\overline{P_\zeta(\mathbf{r})}$ may assume two distinct patterns at the percolation threshold. Thus, while Fig. 5(b) reveals an emerging fractal spreading pattern, Fig. 5(c) shows a uniform distribution within a localised region—note the different scales of the panels. How can this come about? This phenomenon is again related to the fractal nature of the

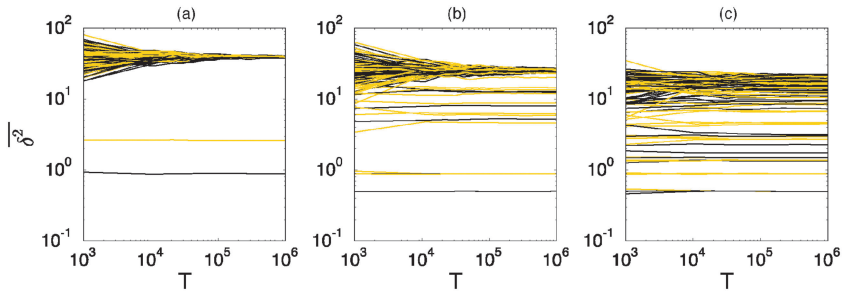

Fig. 4 Time averaged MSD curves $\overline{\delta^2(\Delta)}$ at fixed lag time Δ as a function of the observation time T for $N_\zeta = 2000$ and $N = 3$. We here plot the same data as in Fig. 3, for (a) $p = 0.3$, (b) 0.4, and (c) 0.5. For all cases $\Delta = 100$ was chosen. No significant dependence on T is visible for any sufficiently small value of Δ/T. The distinct, much lower lines in (a) corresponds to a very rare case of confinement. These cases become increasingly likely in (b) and (c).

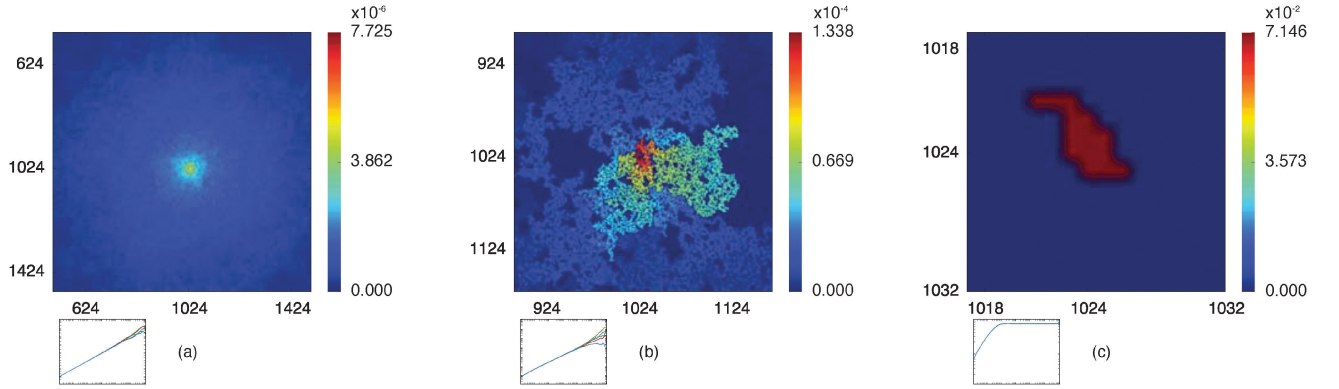

Fig. 5 Time averaged occupation probability $\overline{P_\zeta(\mathbf{r})}$, eqn (8), distributed over three given percolation geometries. This quantity is sampled from an ensemble of 10^4 particle traces on the same percolation geometry ζ starting from the same initial site. We show results for a two-dimensional lattice corresponding to (a) $p = 0.1$, (b) at the percolation threshold with $p = p_c$ with an emerging fractal pattern, and (c) at the percolation threshold with a localised pattern. The outsets show examples of the corresponding time averaged MSD curves for those particles.

percolation geometry at criticality. In the former case, the tracer particle diffuses on the infinite incipient fractal cluster of vacant sites whose linear size is only limited by the size of the simulated lattice. Thus the corresponding time averaged MSD exhibits the anomalous scaling law (1) and the ergodic property $\lim_{T\to\infty}\overline{\delta^2(\Delta)} = \langle \mathbf{r}^2(\Delta)\rangle$ is satisfied.[77] The quantity $\overline{P_\zeta(\mathbf{r})}$ also provides information on how the tracer particle diffuses away from its starting site. It is noteworthy that the spatial gradient of $\overline{P_\zeta(\mathbf{r})}$ has no obvious discontinuous shape. This means that there are no sites at which the particle is significantly trapped for much longer times than at other neighbouring sites. In contrast to this, the latter case corresponding to Fig. 5(c) represents the case in which over the observation time T the particle visits repeatedly a small range of sites. These are either extremely poorly connected to the infinite cluster or completely separated. Accordingly the corresponding time averaged MSD saturates (outset). As seen in our previous analysis above the percentage of such complete confinement is relatively low compared to the situation above the percolation threshold. In the latter case $p > p_c$ confinement will always occur, as no infinite cluster of vacant sites remains. Patterns such as those shown in Fig. 5(c) will then emerge for clusters of varying size. On average clusters of decreasing size emerge when p is increased (not shown).

3.3 Amplitude scatter distribution

We now quantify the amplitude fluctuations of individual time averaged MSDs seen in Fig. 3 by measuring the normalised distribution $\phi(\xi)$ as functions of the lag time Δ and the observation time T in terms of the dimensionless variable[28,29,60,89]

$$\xi = \frac{\overline{\delta^2(\Delta)}}{\left\langle \overline{\delta^2(\Delta)} \right\rangle}. \tag{9}$$

Fig. 6 shows the variation of the scatter distribution $\phi(\xi)$ at two different values of Δ and for fixed $T = 10^6$. As anticipated from the time averaged MSD traces in Fig. 3 the distribution for $p < p_c$ represented by Fig. 3(a) and (b), has a narrow, bell-shaped form.

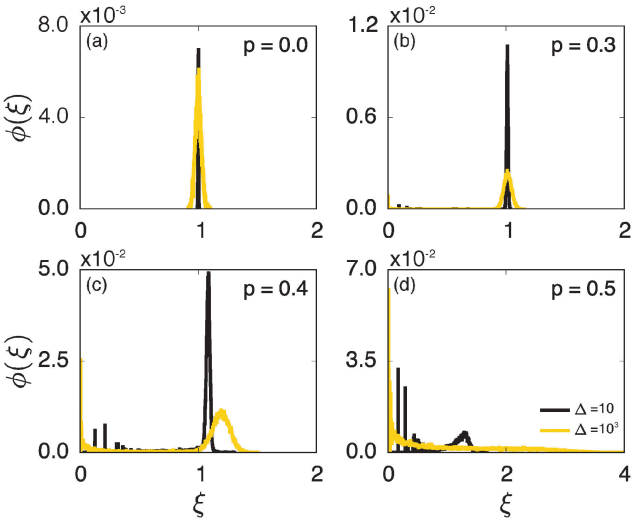

Fig. 6 Normalised scatter distribution $\phi(\xi)$ as function of the dimensionless variable $\xi = \overline{\delta^2(\Delta)} \Big/ \left\langle \overline{\delta^2(\Delta)} \right\rangle$ for four different percolation densities. In each panel the curves represent $\phi(\xi)$ for the lag times $\Delta = 10$ (black) and 10^3 (yellow), each obtained from 30 000 simulation runs corresponding to $N_\zeta = 10\,000$ random geometries and $N = 3$ different trajectories performed on each geometry. Each single run is of length $T = 10^6$.

Its centre is located at the ergodic value $\xi = 1$, and the width becomes broader at larger lag times. This is a typical behaviour for ergodic diffusion.[89] At and above the percolation threshold $p \geq p_c$ this behaviour changes drastically, and the scatter distribution reveals unique features that are not expected from an ergodic diffusion process, nor are these features known from other weakly non-ergodic processes. Consider first the longer lag time $\Delta = 10^3$ at $p = p_c$. We first observe an additional peak showing up at around $\xi = 0$ (Fig. 6(c)). This means that there is a finite contribution from traces in which the particles undergo severely confined diffusion on finite clusters of vacant sites. This peak corresponds to the localised and uniformly distributed time averaged occupation probabilities $\overline{P_\zeta(\mathbf{r})}$ shown in Fig. 5(c). Note that this peak at $\xi = 0$ is not a statistical error due to an insufficient number of simulation runs.

Our further investigation demonstrates that this peak is still observed in larger simulation sets. Second, the position of the main peak is shifted to a larger value above $\xi = 1$ while the bell-shaped profile is preserved. For the shorter lag time $\Delta = 10$ the shift is less severe, however, one can distinguish a fine structure of different peaks for ξ values closer to zero. These correspond to clusters of different size, which can be resolved here when the overall values of the MSD are smaller.

Remarkably, when the percolation density exceeds the critical value p_c the profile of $\phi(\xi)$ changes again significantly. In this overcrowded situation vacant sites exist in the form of finite clusters, forcing the tracer particles to undergo confined diffusion. At the shorter lag time, over which the tracer's motion is not seriously hampered by confinement corresponding to Fig. 6(d) at $\Delta = 10$, the distribution ϕ has a dominant contribution at $\xi \approx 1$. Concurrently, several peaks close to $\xi = 0$ reveal again a distribution of cluster sizes. However, at longer lag times the main peak disappears, and the distribution is monotonically decreasing with ξ: localised motion becomes dominant for the statistic.

In Fig. 7 we investigate the variation of the scatter distribution at the percolation threshold, $p = p_c$ with changing observation times T for fixed lag time. It shows that the position of the main peak remains largely unchanged while the peak gets increasingly sharper as T is increased. In contrast the height and width of the peak at $\xi \approx 0$ is quite insensitive to T. Naively speaking this population splitting of different trajectories into a distribution around ergodic motion $\xi = 1$ and an almost immobile fraction again results from the coexistence of the two distinct diffusion modes induced by the geometry: unrestricted motion on large (infinite) clusters and confined diffusion on small, finite clusters. The propensities of occurrence depend on the lag time Δ as well as the percolation density p. At criticality both modes are significant. We note that this behaviour is a geometry controlled analogue of the dynamic population splitting into mobile and immobile particles in subdiffusive continuous time random walks[85,86] and heterogeneous diffusion processes.[90]

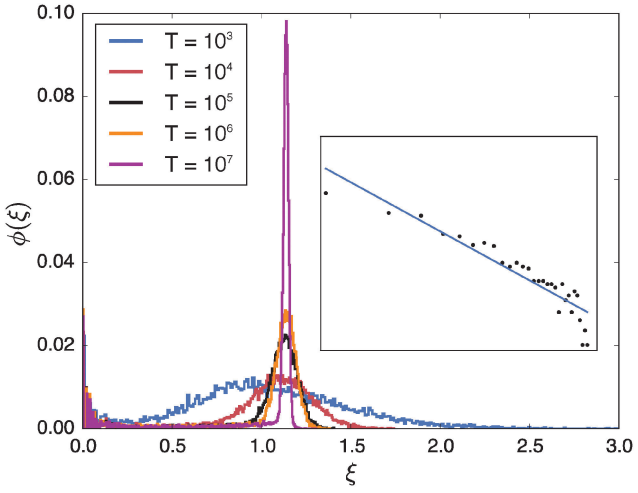

Fig. 7 Dependence of the scatter distribution $\phi(\xi)$ on the observation time T at the percolation threshold $p = p_c$ and for the lag time $\Delta = 10^2$. Each distribution was obtained from 30 000 sample trajectories. The inset shows the double-logarithmic plot of the part of the scatter distribution at small ξ for $T = 10^6$. The straight line is a fit with the power-law function x^{-b}, see text.

Let us spin this idea forward with some analytical considerations based on the cluster size (area) distribution (s). Imagine the situation in which a random walker moves on a finite cluster of size s and radius of gyration $R_s \equiv \sqrt{\frac{1}{(2s^2)} \times \sum_{i,j}^{s} |\mathbf{r}_i - \mathbf{r}_j|^2}$.[48] In the limit of sufficiently long trajectories $(T \to \infty)$ and for lag times $\Delta \geq \Delta_s$, where Δ_s is implicitly defined by the equivalence $\overline{\delta^2(\Delta_s)} = {R_s}^2$ of the time averaged MSD and the squared gyration radius, the time averaged MSD is saturated to the value $\overline{\delta^2(\Delta)} \simeq {R_s}^2$. As the cluster appears fractal on length scales smaller than R_s, it can be reasonably assumed that the size of the cluster is $s \simeq R_s^{d_f}$ close to the percolation threshold, where d_f is the fractal dimension. We then relate the distribution of the saturation value of the time averaged MSD to the cluster size distribution $\mathscr{P}(s)$ in terms of

$$P\left(\overline{\delta^2}\right) \simeq \frac{d_f}{2} s^{2-2/d_f} \mathscr{P}(s), \tag{10}$$

where we used that $\overline{\delta^2} \simeq s^{2/d_f}$ omitting a proportionality constant. Given this latter scaling relation between the saturation value of the time averaged MSD and the size of a cluster, we can use both quantities interchangeably.

Now assume that there are N long $(T \to \infty)$ trajectories of tracer particles that performed a random walk on a randomly generated fractal cluster and have a value $\overline{\delta^2}$ governed by the distribution P. At a given finite lag time Δ, a tracer particle will perform anomalous diffusion of the form $\overline{\delta^2_\Delta} \equiv 4K_\alpha \Delta^\alpha$ as long as the walker has not yet fully sampled the cluster of size s or, equivalently, the time averaged MSD $\overline{\delta^2_\Delta}$ has not reached the saturation value $\overline{\delta^2}$. Among N sample trajectories the fraction showing unrestricted anomalous diffusion will be

$$N_u = \frac{d_f N}{2} \int_{\overline{\delta^2_\Delta}}^{\infty} \overline{\delta^2}^{d_f - 1} \mathscr{P}\left(\overline{\delta^2}^{d_f/2}\right) \mathrm{d}\overline{\delta^2}. \tag{11}$$

The remainder $N - N_u$ then corresponds to saturated diffusion. As demonstrated in Fig. 7 the scatter distribution for the free diffusion part will be a δ peak as T is increased to infinity. Thus in the long time limit this part corresponds to the contribution $\frac{N_u}{N}\delta\left(\overline{\delta^2} - \overline{\delta^2_\Delta}\right)$. For the complementary, confined fraction the scatter distribution will be proportional to $\left(1 - \frac{N_u}{N}\right) P\left(\overline{\delta^2}\right)$. Therefore the normalised scatter distribution in the long time limit can be written as

$$\phi\left(\overline{\delta^2}\right) = \begin{cases} \frac{N_u}{N}\delta\left(\overline{\delta^2} - \overline{\delta^2_\Delta}\right) + \frac{1 - N_u/N}{\mathscr{N}} \\ \qquad \times \overline{\delta^2}^{d_f - 1} \mathscr{P}\left(\overline{\delta^2}^{d_f/2}\right), & \overline{\delta^2} \leq \overline{\delta^2_\Delta} \\ 0, & \overline{\delta^2} > \overline{\delta^2_\Delta} \end{cases} \tag{12}$$

in terms of the variable $\overline{\delta^2}$. Here

$$\mathscr{N} = \int_0^{\overline{\delta^2_\Delta}} \overline{\delta^2}^{d_f-1} \mathscr{P}\left(\overline{\delta^2}^{d_f/2}\right) \mathrm{d}\overline{\delta^2} \tag{13}$$

is a normalisation constant. From eqn (12) the averaged value of the time averaged MSD is calculated to be

$$\begin{aligned}\left\langle \widetilde{\overline{\delta^2(\Delta)}} \right\rangle &= \int_0^\infty \phi\left(\overline{\delta^2}\right) \overline{\delta^2} \mathrm{d}\overline{\delta^2} \\ &= \frac{N_u}{N} \overline{\delta^2_\Delta} + \frac{1 - N_u/N}{\mathscr{N}} \\ &\quad \times \int_0^{\overline{\delta^2_\Delta}} \overline{\delta^2}^{d_f} \mathscr{P}\left(\overline{\delta^2}^{d_f/2}\right) \mathrm{d}\overline{\delta^2}.\end{aligned} \tag{14}$$

Although the exact form of $\mathscr{P}$ is unknown, the fact that $\mathscr{P}(s)$ is a monotonically decaying distribution leads to the relation $\left\langle \widetilde{\overline{\delta^2(\Delta)}} \right\rangle < \overline{\delta^2_\Delta}$ found in Fig. 6 and 7. Eqn (12) tells us that the fluctuations of the time averaged MSD given by ϕ is fully determined by the cluster size $\mathscr{P}$ distribution as well as the lag time Δ. In percolation theory the form

$$\mathscr{P}(s) \propto s^{-\tau} f\left[(p - p_c) s^\sigma\right] \tag{15}$$

based on the scaling function $f(x)$ is invoked where τ and σ are two scaling exponents.[48,91] At the percolation threshold $p = p_c$ the cluster size distribution asymptotically has the power-law form $\mathscr{P}(s) \simeq s^{-\tau}$ with $2 < \tau < 3$.[48] Using this information we find that

$$N_u \simeq \frac{N}{\tau - 2} \overline{\delta^2_\Delta}^{d_f(2-\tau)/2} \simeq \Delta^{\alpha d_f(2-\tau)/2}. \tag{16}$$

Thus N_u slowly decreases with increasing Δ as $\tau = 187/91 \approx 2.05$ at $p = p_c$ on the square lattice. The sharp peak in $\phi(\xi)$ is observed even for long lag times, as evidenced in the plot for $p = p_c$ in Fig. 6. For the distribution of finite size clusters, with the above we find the following simplified expression of eqn (10),

$$P\left(\overline{\delta^2}\right) = \frac{d_f}{2} \overline{\delta^2}^{d_f(2-\tau)/2-1}. \tag{17}$$

The theoretical value of the scaling exponent of $\overline{\delta^2}$ in this relation can be evaluated from the numerical estimation of d_f and τ in our simulations. From approximately 25 000 clusters of various size s extracted from 9480 percolation geometries ζ, the fractal dimension d_f is estimated via the scaling law $s \simeq R_s^{d_f}$ of the gyration radius as $d_f \approx 1.865$ with the confidence interval (1.824, 1.905) and $\tau \approx 2.03$ from eqn (15).** This measurement leads to the prediction that the exponent is given by -1.028 with the confidence interval $(-1.027, -1.029)$. In the inset of Fig. 7 the decaying part of the distribution $\phi(\xi)$ at $\Delta = 10^3$ is plotted in on a logarithmic scale (black circles). The slope of the linear fit (blue line) is -1.063 with the confidence interval $(-1.226, -0.899)$, agreeing well with the theoretically predicted value.

** The box counting method gives the estimation $d_f \equiv 1.9191 \pm 0.0095$ from 10 000 infinite clusters in our simulation while the accepted values in literatures are $d_f = 91/48$ and $\tau = 187/91 \approx 2.05495$, respectively.

Above the obstacle percolation threshold, $p > p_c$, when only finite, disjunct cluster remain, the cluster size distribution $\mathscr{P}(s)$ has the asymptotic form

$$\mathscr{P}(s) \simeq s^{-\tau} \mathrm{e}^{-cs} \tag{18}$$

where $1/c$ is the characteristic cluster size.[48] From this result we obtain that

$$N_u = N c^{\tau-2} \Gamma\left(2 - \tau, c\overline{\delta^2_\Delta}^{d_f/2}\right) \simeq N c^{\tau-2} \Gamma\left(2 - \tau, c\overline{\delta^2_\Delta}\right), \tag{19}$$

in terms of the incomplete Gamma function $\Gamma(\cdot,\cdot)$. The last transformation follows from the fact that for $p > p_c$ the fractal dimension $d_f = 2$ equals the embedding Euclidean dimension, that is $d = 2$ here, corresponding to the locally fully connected, finite clusters. Consequently in this situation we face the scaling $\overline{\delta^2} \simeq s$. At large lag times Δ satisfying the criterion $\overline{\delta^2_\Delta} \gg 1/c$, N_u is approximated as

$$N_u \approx \frac{N}{c} \overline{\delta^2_\Delta}^{1-\tau} \exp\left(-c\overline{\delta^2_\Delta}\right), \tag{20}$$

and thus we obtain $N_u \ll N$. Therefore in eqn (12) the second term involving the cluster size distribution $\mathscr{P}$ will dominate the scatter distribution ϕ. This argument supports the monotonically decaying profiles of ϕ at $\Delta = 10^3$ and 10^5 in the plot for $p = 0.5$ displayed in Fig. 7 which is accordingly the very profile of $\mathscr{P}$. This also underlines the fact that at time scales for which $\overline{\delta^2_\Delta} \gg 1/c$ almost all tracer particles undergo confined diffusion. In the opposite case, at short lag times satisfying $\overline{\delta^2_\Delta} \ll 1/c$, we see that $N_u \approx \frac{N}{\tau - 2} \overline{\delta^2_\Delta}^{2-\tau}$, which is the same as N_u at $p = p_c$ with the replacement $d_f \to 2$. This means that there are particles performing free diffusion over short lag times Δ. Thus ϕ should have a peak around the ergodic value, as shown in the case of $\Delta = 10$ for $p = 0.5$ in Fig. 6.

3.4 Ergodicity breaking parameter

We now study the functional behaviour of the fluctuations of the time averaged MSD as the observation time T is increased. For this purpose, we use the ergodicity breaking (EB) parameter[28,29,31,60]

$$\mathrm{EB}(\Delta) = \frac{\left\langle \left(\widetilde{\overline{\delta^2(\Delta)}}\right)^2 \right\rangle - \left(\left\langle \widetilde{\overline{\delta^2(\Delta)}} \right\rangle\right)^2}{\left(\left\langle \widetilde{\overline{\delta^2(\Delta)}} \right\rangle\right)^2} = \widetilde{\langle \xi^2 \rangle} - 1. \tag{21}$$

Here the ensemble average $\widetilde{\langle\cdot\rangle}$ again means the ensemble average over the set of trajectories as well as over the fractal geometries ζ at given lag time Δ and the observation time T, similar to our definition of the ensemble averaged MSD $\widetilde{\langle \mathbf{r}^2 \rangle}$ above.

Fig. 8 shows the EB parameter as function of the observation time T for four distinct cases. In each panel two EB curves are plotted at lag times $\Delta = 10$ and 10^2. At given percolation density p the EB curves are shown on linear (left column) and double logarithmic (right column) scales. At $p = 0$ when the accessible

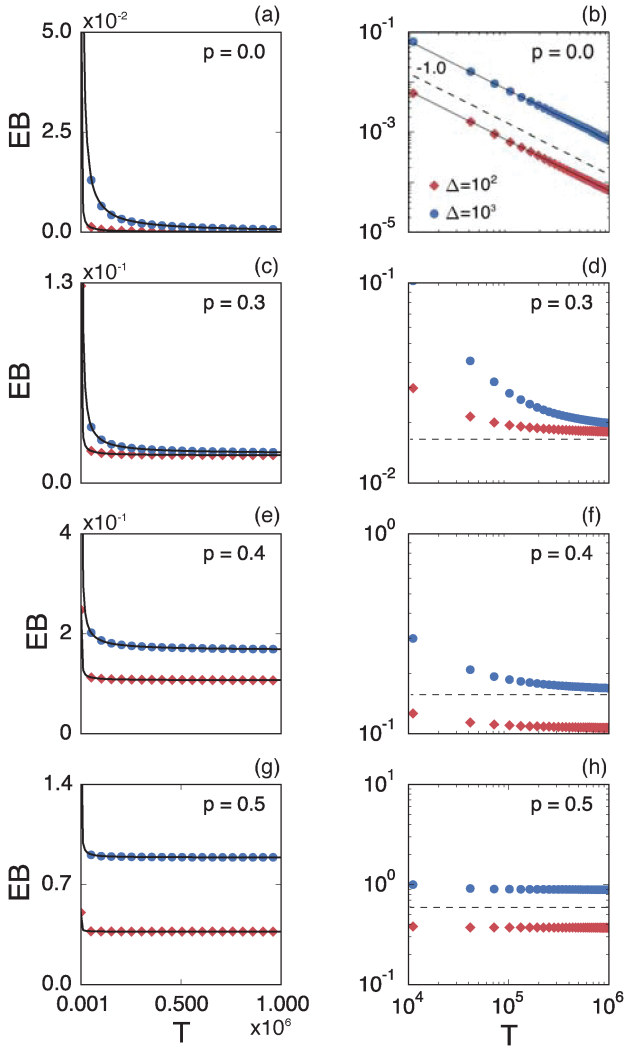

Fig. 8 Ergodicity breaking parameter EB on linear scales (left column) and on double logarithmic scales (right column) as function of the observation time T. The red curves correspond to $\Delta = 10^2$ and the blue curves represent $\Delta = 10^3$. The black solid lines depict the best fits with eqn (23). The grey lines in the double logarithmic plot for $p = 0$ (b), correspond to the EB parameter for normal Brownian motion with $\Delta = 10^2$ and 10^3. The dashed lines in the double logarithmic plots show the asymptotic behaviour of EB. The results are from $N_\xi = 3000$ percolation geometries and $N = 3$ trajectories.

space is the full two-dimensional square lattice the EB parameter displays the theoretically expected scaling behaviour $\mathrm{EB}(\Delta) \sim \frac{2}{3}\frac{\Delta}{T}$ for two-dimensional Brownian motion shown by the dashed slope in the double logarithmic panel for $p = 0$, see Fig. 8(b).[29,92] In this case the fluctuation of the time averaged MSD tend to zero as $T \to \infty$: for this ergodic process the time averaged MSD becomes identical to the ensemble averaged MSD. This conventional convergence continues if the space is filled with obstacles with a concentration p well below the percolation threshold p_c, as evidenced for the case $p = 0.3$ in Fig. 8(d).

However, the convergence of the EB parameter behaves quite differently when we approach the percolation threshold at $p = p_c$. In this case EB does not converge to zero when T goes to infinity but, as demonstrated in Fig. 8(d), EB converges to the finite residual value

$$\mathrm{EB}_\infty = \int_0^\infty \xi^2 \phi(\xi) \mathrm{d}\xi - 1 \qquad (22)$$

shown by the dotted horizontal line. This value was numerically estimated from the scatter distribution in Fig. 6. The geometrically induced fluctuations in the time averaged MSD due to the existence of finite clusters do not vanish even in the limit of infinite observation time.

The EB curves shown in Fig. 8 converge towards EB_∞ in good agreement with the algebraic form

$$\mathrm{EB}(\Delta) = k\left(\frac{\Delta}{T}\right)^h + \mathrm{EB}_\infty. \qquad (23)$$

Here h and $\mathrm{EB}_\infty \geq 0$ are, respectively, the associated scaling exponent and the limiting value of EB at $T \to \infty$, and k is a proportionality constant. In Fig. 10 we show the functional relations of the exponent h and of EB_∞ *versus* the percolation density p as estimated from the EB curves. In Fig. 8 (left) the solid lines depict the best fit to eqn (23). We mention the following noteworthy aspects of the results: (i) for percolation densities p sufficiently below the percolation threshold p_c the EB parameter follows that of normal Brownian diffusion, that is, $h = 1$ and $\mathrm{EB}_\infty = 0$, as mentioned above. (ii) For the opposite regime of high obstacle densities, $p > p_c$, we find $h = 1$ and a non-zero value EB_∞ of the residual EB parameter that tends to increase with the percolation density p. In this regime the Brownian convergence speed $\mathrm{EB} \sim T^{-1}$ is derived from the long time confined Brownian motion of tracer particles. The value $\mathrm{EB}_\infty \neq 0$ is attributed to the heterogeneity of the saturation values of the time averaged MSD and is thus geometry controlled. This statement is also consistent with the fact that EB_∞ depends on the lag time Δ in Fig. 8(g) and (h), due to the different resolution set by the value $\overline{\delta^2_\Delta}$. (iii) Close to the percolation threshold p_c the behaviour of the EB parameter is distinguished from these two regimes. As p is increased towards the critical point p_c, h consistently decreases from unity. Thus when the space becomes fractal on all length scales we find that $h \approx 0.80$ and $\mathrm{EB}_\infty \neq 0$.

We emphasise that the estimated value $h < 1$ at p_c is a genuine convergence property due to the fractal structure of the explored space. To rule out the possibility that the value $h \approx 0.8 < 1$ is due to the small finite clusters responsible for $\mathrm{EB}_\infty \neq 0$, we plot in Fig. 9 the EB curves after excluding the contribution of the smallest clusters of size $s = 1$. The unit sized clusters are the most dominant contribution among the finite clusters, see the form of $\mathscr{P}(s)$, and results in the vanishing time averaged MSD, $\overline{\delta^2} = 0$. Fig. 9 shows that after removing these unit size clusters the EB parameter always converges to $\mathrm{EB}_\infty = 0$ for all p values. However, the convergence exponent h remains at $h \approx 0.8$, compare also Fig. 10. We note that the convergence law of the EB parameter is not the same as that of fractional Brownian motion, although both models share the same anomalous diffusion scaling (1) and are ergodic (for the present

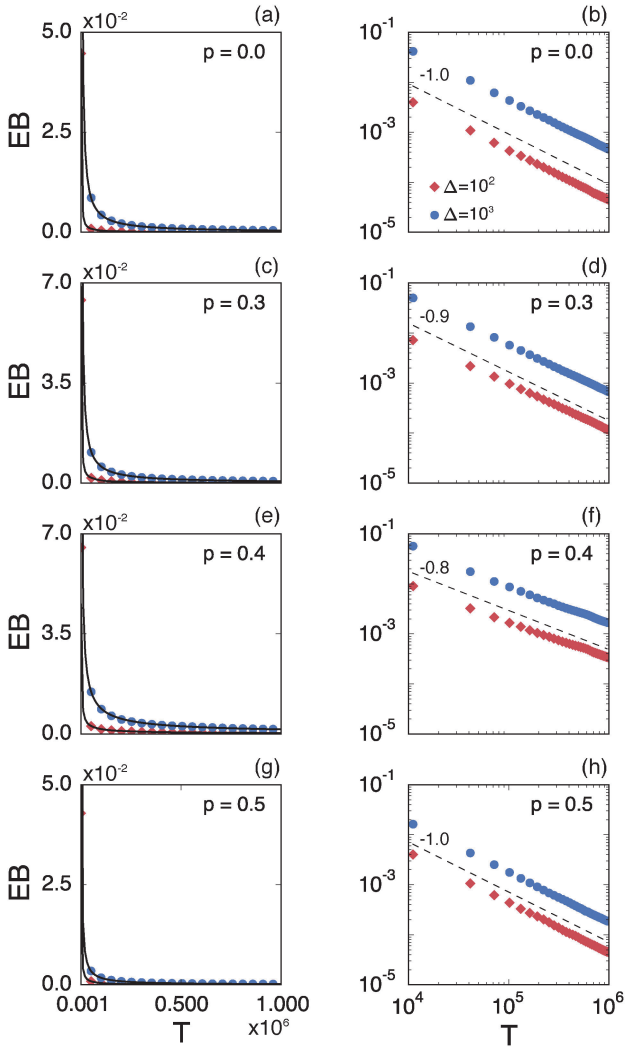

Fig. 9 Ergodicity breaking parameter as a function of the observation time T when clusters with $s = 1$ are removed. The double logarithmic plot shows a linear behaviour of EB *versus* the observation time T, independent of the percolation density p. The red curve corresponds to $\Delta = 10^2$ and the blue curve represents $\Delta = 10^3$. The black solid lines for the linear scales plots are the best fits to eqn (23), the dashed black lines in the double logarithmic plots show the slope of the EB curves. Same numbers for N_ζ and N as in Fig. 8.

case in the sense of the disorder average). For fractional Brownian motion EB was found to have the convergence form $\mathrm{EB} \sim \frac{\Delta}{T}$ for $0 < \alpha < \frac{3}{2}$, $\mathrm{EB} \sim \frac{\Delta}{T}\log T$ for $\alpha = \frac{3}{2}$, and $\mathrm{EB} \sim \left(\frac{\Delta}{T}\right)^{4-2\alpha}$ for $\frac{3}{2} < \alpha < 2$.[92–94] Thus, compared to fractional Brownian motion the fractal geometry-induced subdiffusion has a slower convergence to ergodicity. The observed characters of the EB parameter also differ from those of other diffusion models such as scaled Brownian motion, heterogeneous diffusion processes, and continuous time random walk.[60,68,95] Therefore, the EB convergence law provides useful information for unveiling the physical origins of anomalous diffusion processes found in complex random media.

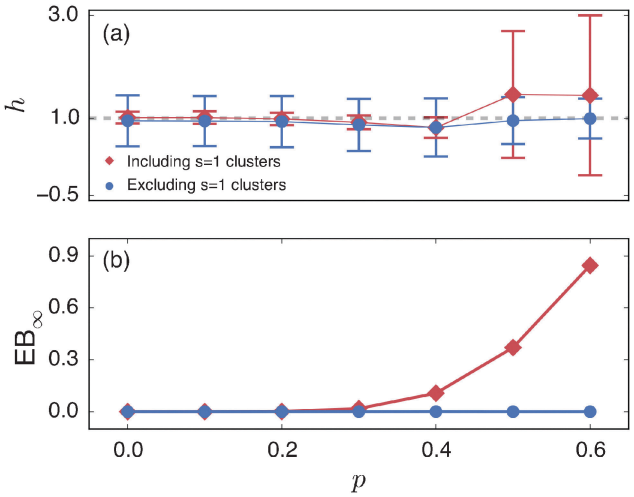

Fig. 10 (a) Variation of the scaling exponent h and (b) the residual ergodicity breaking parameter EB_∞ as function of the percolation density p. Values from fit of the scaling function (23) to the EB curves in Fig. 8 and 9. The results are reported for $\Delta = 10$. Red diamonds: fit from Fig. 8 including the smallest clusters of size $s = 1$. Blue circles: fit from Fig. 9 neglecting the smallest clusters.

4 Conclusion

Based on extensive Monte Carlo simulations we studied the ergodic properties of single particles diffusing in random two-dimensional fractal geometries modelled by a percolation geometry at varying percolation density of obstacles. While the asymptotic equality between the ensemble averaged MSD $\langle\widetilde{\mathbf{r}^2(\Delta)}\rangle$ and the time averaged MSD $\left\langle\widetilde{\overline{\delta^2(\Delta)}}\right\rangle$ averaged over all individual trajectories and many percolation geometries is observed at any percolation density, individual time averaged MSDs do not always behave like this average and are thus non-ergodic. As we showed here this non-ergodic behaviour is geometry controlled and thus corresponds to strong ergodicity breaking due to a topologically disconnected phase space. Thus, at low obstacle densities $p \ll p_c$ the single particle diffusion exhibits typical ergodic behaviour as seen in the scaling law of the time averaged MSDs, their scatter distribution, and the ergodicity breaking parameter. In this case, the ensemble averaged MSD shows no disparity with individual time averaged MSDs as long as the observation time is sufficiently long. Close to the percolation threshold $p \approx p_c$, however, such a typical ergodic character is no longer observed. There exists a fraction of time averaged MSDs which significantly deviate from the averaged curve $\left\langle\widetilde{\overline{\delta^2(\Delta)}}\right\rangle$. Using the time averaged occupation probability $\overline{P_\zeta(\mathbf{r})}$ we demonstrated that these outliers correspond to trajectories when the particles motion is restricted on finite clusters of gyration radius R_s significantly smaller than the system size. Other particles moving on the infinite cluster at criticality, however, do show the convergence to the ensemble averaged MSD $\langle\widetilde{\mathbf{r}^2(\Delta)}\rangle$ on the single trajectory level. We thus observe ergodic motion for a fraction of particles conditioned to move on the infinite

incipient cluster, as reported earlier.[77] Due to the mix of confined and freely diffusing trajectories, the scatter distribution of the amplitudes of individual time averaged MSDs shown in Fig. 6 and 7 acquires an asymmetric bell shaped form around the main peak at $\overline{\delta^2(\Delta)}\Big/\left\langle\overline{\delta^2(\Delta)}\right\rangle = 1$ and a second peak at $\overline{\delta^2(\Delta)}\Big/\left\langle\overline{\delta^2(\Delta)}\right\rangle \sim 0$. As shown in Fig. 7, upon increase of the observation time T the latter part is preserved while the main peak around the ergodic value $\overline{\delta^2(\Delta)}\Big/\left\langle\overline{\delta^2(\Delta)}\right\rangle = 1$ becomes a sharp, almost δ function like peak. Relating the cluster size distribution to the distribution of the time averaged MSDs by eqn (12) we qualitatively explained the observed behaviour of the scatter distribution ϕ. An interesting behaviour is also observed for the ergodicity breaking parameter defined in eqn (21). From numerical analysis we found that EB generally follows an algebraic decay $[\mathrm{EB}(\Delta) - \mathrm{EB}_\infty] \sim T^{-h(p)}$ towards the finite residual EB parameter EB_∞ reached at $T \to \infty$, and h is a scaling exponent. The exact value of EB_∞ depends on the percolation density p. As p is increased to p_c the decay of the EB parameter thus deviates from that for typical ergodic diffusion, for which $h = 1$ and $\mathrm{EB}_\infty = 0$. Importantly, on approximating the percolation threshold, $p \approx p_c$, the EB parameter has a slower convergence with scaling exponent $h \approx 0.8 < 1$ as well as a nonzero value $\mathrm{EB}_\infty > 0$ due to the contribution of confined particles.

Above p_c the particle diffusion always takes place on confined clusters. Large fluctuations from the average $\left\langle\overline{\delta^2(\Delta)}\right\rangle$ are present in individual time averaged MSDs. The profile of the scatter distribution $\phi(\xi)$ is quite different from those for critical and lower than critical percolation densities, see Fig. 6. At sufficiently long lag times Δ the distribution decays almost monotonically with the variable ξ, due to the exclusive presence of finite clusters with an exponentially decaying distribution of cluster sizes. This is a purely geometrical effect, as revealed in the distribution of the time averaged MSD which turns out to be independent of the observation time T. In both Fig. 8 and 9 the EB parameter was shown to decay as T^{-1}, corresponding to the convergence to zero of a Brownian particle. This is due to the fact that in this overcrowded obstacle regime the particle explores small clusters with local Euclidean geometries. We note that while the specific values for the scaling exponents and percolation thresholds vary for different lattice types and dimensionality of the embedding dimension the generic features revealed here remain unchanged. This claim is supported by preliminary studies on cubic and hexagonal lattices (not shown).

Anomalous diffusion in a fractal geometry is a non-Gaussian process[42,43,48] and therefore different from the Gaussian fractional Brownian motion on a fundamental level. However, except for the Gaussianity the difference between these two processes has not been studied in detail. In particular, it has been said that both models share the same ergodic behaviour. However, as revealed in our study the ergodic properties of diffusion on fractals displays distinctly different behaviour due to the quenched nature of the underlying geometry. Only in certain cases (low obstacle concentration or conditional seeding of the particle exclusively on the infinite cluster close to criticality) we observe ergodic behaviour. While the statistical fluctuations in the time averaged MSD are homogeneous for fractional Brownian motion, the fractal geometry-induced anomalous diffusion is heterogeneous, and the strength and character of the heterogeneity depend on the obstacle density. Therefore the detailed analysis of the ergodic properties is indeed a useful measure to differentiate the type of ant-in-the-labyrinth motion from other models, along with recently developed theoretical tools estimating the fractal dimension d_f.[56,77] An advantage of the method developed herein studying ergodic properties is more feasible than estimating the fractal dimension d_f.

As experimental single particle tracking studies become increasingly popular our results are expected to be helpful in analysing and interpreting experimental results for various problems of anomalous diffusion in complex environments. In the case of lateral diffusion in phospholipid membranes some recent simulation studies reported that lipid diffusion is a two dimensional fractional Brownian motion[9,37] while conventionally it was understood as diffusion on fractal lattices.[43,50,96] In addition for more complex membranes the lateral diffusion exhibits non-ergodic continuous time random walk type motion[97] or was identified as the combination of motion on a fractal and continuous time random walks.[8] Also fairly complex non-Gaussian ergodic motion types were reported.[98] Such a stochastic variety in the lateral diffusion dynamics seems to be natural given the fact that biological membranes have a composition dependent, wide range of structural complexities. From the trajectory analyses presented in this work one can have additional insight about the lateral dynamics and static structural complexity of a membrane system under investigation. For instance, if the plot of EB *versus* T gives the scaling exponent $h < 1$ it gives a signature that the lateral anomalous diffusion is not of fractional Brownian motion type. Then the ageing test for the time averaged MSDs along with the moment ratio evaluation further differentiates the fractal induced subdiffusion from non-ergodic continuous time random walk process. The distribution of saturated TA MSDs and a non-vanishing EB_∞ may be used to obtain information on the size distribution of confining domains in a membrane, if any. Our analysis can also be applied to nano-particle transport in porous media.[52,99] From the profile of the distribution of the time averaged MSD one may obtain information on the pore size distribution as well as the porosity of a medium. Additionally the ageing test for the time averaged MSD shown in Fig. 4 appears to be informative to examining the nano-particle-pore interactions: if the motion exhibits features of ageing it is likely that there are nonspecific interactions between the particles and a porous medium which give rise to the temporal heterogeneity in the time averaged MSD.

Acknowledgements

JHJ and RM acknowledge financial support from the Academy of Finland (Suomen Akatemia) within the Finland Distinguished Professor (FiDiPro) programme awarded to RM.

References

1 J. Perrin, *Acad. Sci., Paris, C. R.*, 1908, **146**, 967.
2 *Single particle tracking and single molecule energy transfer*, ed. C. Bräuchle, D. C. Lamb and J. Michaelis, Wiley-VCH, Weinheim, 1908.
3 I. Golding and E. C. Cox, Physical nature of bacterial cytoplasm, *Phys. Rev. Lett.*, 2006, **96**, 098102.
4 I. M. Tolić-Nørrelykke, E.-L. Munteanu, G. Thon, L. Oddershede and K. Berg-Sørensen, Anomalous diffusion in living yeast cells, *Phys. Rev. Lett.*, 2004, **93**, 078102.
5 J.-H. Jeon, V. Tejedor, S. Burov, E. Barkai, C. Selhuber-Unkel, K. Berg-Sørensen, L. Oddershede and R. Metzler, *Phys. Rev. Lett.*, 2011, **106**, 048103.
6 M. A. Taylor, J. Janousek, V. Daria, J. Knittel, B. Hage, H.-A. Bachor and W. P. Bowen, Biological measurement beyond the quantum limit, *Nat. Photonics*, 2013, **7**, 229.
7 S. M. Tabei, S. Burov, H. Y. Kim, A. Kuznetsov, T. Huynh, J. Jureller, L. H. Philipson, A. R. Dinner and N. F. Scherer, Intracellular transport of insulin granules is a subordinated random walk, *Proc. Natl. Acad. Sci. U. S. A.*, 2013, **110**, 4911.
8 A. V. Weigel, B. Simon, M. M. Tamkun and D. Krapf, Ergodic and nonergodic processes coexist in the plasma membrane as observed by single-molecule tracking, *Proc. Natl. Acad. Sci. U. S. A.*, 2011, **108**, 6438.
9 J.-H. Jeon, H. M.-S. Monne, M. Javanainen and R. Metzler, Anomalous diffusion of phospholipids and cholesterols in a lipid bilayer and its origins, *Phys. Rev. Lett.*, 2012, **109**, 188103.
10 G. R. Kneller, K. Baczynski and M. Pasenkiewicz-Gierula, Consistent picture of lateral subdiffusion in lipid bilayers: Molecular dynamics simulation and exact results, *J. Chem. Phys.*, 2011, **135**, 141105.
11 M. Javanainen, H. Hammaren, L. Monticelli, J.-H. Jeon, M. S. Miettinen, H. Martinez-Seara, R. Metzler and I. Vattulainen, Anomalous and normal diffusion of proteins and lipids in crowded lipid membranes, *Faraday Discuss.*, 2013, **161**, 397.
12 S. J. Sahl, M. Leutenegger, M. Hilbert, S. W. Hell and C. Eggeling, Fast molecular tracking maps nanoscale dynamics of plasma membrane lipids, *Proc. Natl. Acad. Sci. U. S. A.*, 2010, **107**, 6829.
13 I. Y. Wong, M. L. Gardel, D. R. Reichman, E. R. Weeks, M. T. Valentine, A. R. Bausch and D. A. Weitz, Anomalous diffusion probes microstructure dynamics of entangled F-actin networks, *Phys. Rev. Lett.*, 2004, **92**, 178101.
14 J.-H. Jeon, N. Leijnse, L. B. Oddershede and R. Metzler, Anomalous diffusion and power-law relaxation of the time averaged mean squared displacement in worm-like micellar solutions, *New J. Phys.*, 2013, **15**, 045011.
15 N. Fatin-Rouge, K. Starchev and J. Buffle, Size effects on diffusion processes within agarose gels, *Biophys. J.*, 2004, **86**, 2710.
16 A. Godec, M. Bauer and R. Metzler, Collective dynamics effect transient subdiffusion of inert tracers in gel networks, *New J. Phys.*, 2014, **16**, 092002.
17 D. S. Banks and C. Fradin, Anomalous diffusion of proteins due to molecular crowding, *Biophys. J.*, 2005, **89**, 2960.
18 J. Szymanski and M. Weiss, Elucidating the origin of anomalous diffusion in crowded fluids, *Phys. Rev. Lett.*, 2009, **103**, 038102.
19 S. Burov, S. M. Ali Tabei, T. Huynh, M. P. Murrell, L. H. Philipson, S. A. Rice, M. L. Gardel, N. F. Scherer and A. R. Dinner, Distribution of directional change as a signature of complex dynamics, *Proc. Natl. Acad. Sci. U. S. A.*, 2013, **110**, 19689.
20 T. Turiv, I. Lazo, A. Brodin, B. I. Lev, V. Reiffenrath, V. G. Nazarenko and O. D. Lavrentovich, Effect of collective molecular reorientations on Brownian motion of colloids in nematic liquid crystal, *Science*, 2013, **342**, 1351.
21 J. F. Reverey, J.-H. Jeon, M. Leippe, R. Metzler and C. Selhuber-Unkel, Superdiffusion dominates intracellular particle motion in the supercrowded space of pathogenic Acanthamoeba castellanii, *Sci. Rep.*, 2015, **5**, 11690.
22 A. Caspi, R. Granek and M. Elbaum, Enhanced Diffusion in Active Intracellular Transport, *Phys. Rev. Lett.*, 2000, **85**, 5655.
23 N. Gal and D. Weihs, Experimental evidence of strong anomalous diffusion in living cells, *Phys. Rev. E: Stat., Nonlinear, Soft Matter Phys.*, 2010, **81**, 020903(R).
24 D. Robert, Th. H. Nguyen, F. Gallet and C. Wilhelm, *In vivo* determination of fluctuating forces during endosome trafficking using a combination of active and passive microrheology, *PLoS One*, 2010, **4**, e10046.
25 I. Goychuk, V. O. Kharchenko and R. Metzler, Molecular motors pulling cargos in the viscoelastic cytosol: power strokes beat subdiffusion, *Phys. Chem. Chem. Phys.*, 2014, **16**, 16524.
26 G. Campagnola, K. Nepal, B. W. Schroder, O. B. Peersen and D. Krapf, Superdiffusion in supported lipid bilayers, E-print arXiv:1506.03795.
27 A. V. Chechkin, I. M. Zaid, M. A. Lomholt, I. M. Sokolov and R. Metzler, Bulk-mediated diffusion on a planar surface: full solution, *Phys. Rev. E: Stat., Nonlinear, Soft Matter Phys.*, 2012, **86**, 041101.
28 S. Burov, J.-H. Jeon, R. Metzler and E. Barkai, Single particle tracking in systems showing anomalous diffusion: the role of weak ergodicity breaking, *Phys. Chem. Chem. Phys.*, 2011, **13**, 1800.
29 R. Metzler, J.-H. Jeon, A. G. Cherstvy and E. Barkai, Anomalous diffusion models and their properties: non-stationarity, non-ergodicity and ageing at the centenary of single particle tracking, *Phys. Chem. Chem. Phys.*, 2014, **16**, 24128.
30 I. M. Sokolov, Models of anomalous diffusion in crowded environments, *Soft Matter*, 2012, **8**, 9043.
31 E. Barkai, Y. Garini and R. Metzler, Strange kinetics of single molecules in living cells, *Phys. Today*, 2012, **65**(8), 29.
32 C. Monthus and J.-P. Bouchaud, Models of traps and glass phenomenology, *J. Phys. A: Math. Gen.*, 1996, **29**, 3847.
33 H. Scher and E. W. Montroll, Anomalous transit-time dispersion in amorphous solids, *Phys. Rev. B: Solid State*, 1975, **12**, 2455.
34 P. Hänggi, Correlation functions and masterequations of generalized (non-Markovian) Langevin equations, *Z. Phys. B: Condens. Matter*, 1978, **31**, 407.
35 P. Hänggi and F. Mojtabai, Thermally activated escape rate in presence of long-time memory, *Phys. Rev. A: At., Mol., Opt. Phys.*, 1982, **26**, 1168.

36 R. Kubo, The fluctuation-dissipation theorem, *Rep. Prog. Phys.*, 1966, **29**, 255.
37 G. Kneller, A scaling approach to anomalous diffusion, *J. Chem. Phys.*, 2014, **141**, 041105.
38 B. B. Mandelbrot and J. W. van Ness, Fractional Brownian motions, fractional noises and applications, *SIAM Rev.*, 1968, **10**, 422.
39 A. M. Yaglom, *Correlation theory of stationary and related random functions*, Springer, Heidelberg, 1987.
40 I. Goychuk, Viscoelastic subdiffusion: from anomalous to normal, *Phys. Rev. E: Stat., Nonlinear, Soft Matter Phys.*, 2009, **80**, 046125.
41 J.-H. Jeon, N. Leijnse, L. B. Oddershede and R. Metzler, *New J. Phys.*, 2013, **15**, 045011.
42 S. Havlin and D. Ben-Avraham, Diffusion in disordered media, *Adv. Phys.*, 1987, **36**, 695.
43 F. Höfling and T. Franosch, Anomalous transport in the crowded world of biological cells, *Rep. Prog. Phys.*, 2013, **76**, 046602.
44 B. B. Mandelbrot, *The fractal geometry of nature*, W. H. Freeman, New York, NY, 1982.
45 P. G. de Gennes, *La Recherche*, 1976, **7**, 919.
46 J. C. Angles d'Auriac, A. Benoit and R. Rammal, Random walk on fractals: numerical studies in two dimensions, *J. Phys. A: Math. Gen.*, 1983, **16**, 4039.
47 J.-P. Bouchaud and A. Georges, Anomalous diffusion in disordered media: statistical mechanisms, models and physical applications, *Phys. Rep.*, 1990, **195**, 127.
48 D. Stauffer and A. Aharony, *Introduction to percolation theory*, Taylor and Francis, London, 2nd edn, 1992.
49 F. Höfling, T. Franosch and E. Frey, Localization transition of the three-dimensional Lorentz model and continuum percolation, *Phys. Rev. Lett.*, 2006, **96**, 167901.
50 M. J. Saxton, Anomalous diffusion due to obstacles: a Monte Carlo study, *Biophys. J.*, 1994, **66**, 394.
51 L. E. Sereshki, M. A. Lomholt and R. Metzler, A solution to the subdiffusion-efficiency paradox: inactive states enhances reaction efficiency at subdiffusion conditions in living cells, *Europhys. Lett.*, 2012, **97**, 20008.
52 H. Sanabria, Y. Kubota and M. N. Waxham, Multiple diffusion mechanisms due to nanostructuring in crowded environments, *Biophys. J.*, 2007, **92**, 313.
53 M. Hellmann, D. W. Heermann and M. Weiss, Enhancing phosphorylation cascades by anomalous diffusion, *EPL*, 2012, **97**, 58004.
54 C. C. Fritsch and J. Langowski, *J. Chem. Phys.*, 2010, **133**, 025101.
55 C. Loverdo, O. Bénichou, R. Voituriez, A. Biebricher, I. Bonnet and P. Desbiolles, Quantifying Hopping and Jumping in Facilitated Diffusion of DNA-Binding Proteins, *Phys. Rev. Lett.*, 2009, **102**, 188101.
56 V. Tejedor, O. Bénichou, R. Voituriez, R. Jungmann, F. Simmel, C. Selhuber-Unkel, L. Oddershede and R. Metzler, Quantitative analysis of single particle trajectories: mean maximal excursion method, *Biophys. J.*, 2010, **98**, 1364.
57 K. Burnecki, E. Kepten, Y. Garini, G. Sikora and A. Weron, Estimating the anomalous diffusion exponent for single particle tracking data with measurement errors – an alternative approach, *Sci. Rep.*, 2015, **5**, 11306.
58 E. Kepten, A. Weron, G. Sikora, K. Burnecki and Y. Garini, Guidelines for the Fitting of Anomalous Diffusion Mean Square Displacement Graphs from Single Particle Tracking Experiments, *PLoS One*, 2015, **10**, e0117722.
59 A. Robson, K. Burrage and M. C. Leake, Inferring diffusion in single live cells at the single-molecule level, *Philos. Trans. R. Soc., B*, 2012, **368**, 20120029.
60 Y. He, S. Burov, R. Metzler and E. Barkai, Random Time-Scale Invariant Diffusion and Transport Coefficients, *Phys. Rev. Lett.*, 2008, **101**, 058101.
61 A. Lubelski, I. M. Sokolov and J. Klafter, Nonergodicity Mimics Inhomogeneity in Single Particle Tracking, *Phys. Rev. Lett.*, 2008, **100**, 250602.
62 I. M. Sokolov, E. Heinsalu, P. Hänggi and I. Goychuk, Universal fluctuations in subdiffusive transport, *EPL*, 2009, **86**, 30009.
63 M. J. Skaug, A. M. Lacasta, L. Ramirez-Piscina, J. M. Sancho, K. Lindenberg and D. K. Schwartz, Single molecule diffusion in a periodic potential at a solid-liquid interface, *Soft Matter*, 2014, **10**, 753.
64 M. Khoury, A. M. Lacasta, J. M. Sancho and K. Lindenberg, Weak disorder: anomalous transport and diffusion are normal yet again, *Phys. Rev. Lett.*, 2011, **106**, 090602.
65 J.-H. Jeon, E. Barkai and R. Metzler, Noisy continuous time random walks, *J. Chem. Phys.*, 2013, **139**, 121916.
66 V. Tejedor and R. Metzler, Anomalous diffusion in correlated continuous time random walks, *J. Phys. A: Math. Gen.*, 2010, **43**, 082002.
67 M. Magdziarz, R. Metzler, W. Szczotka and P. Zebrowski, Correlated Continuous Time Random Walks in External Force Fields, *Phys. Rev. E: Stat., Nonlinear, Soft Matter Phys.*, 2012, **85**, 051103.
68 A. G. Cherstvy, A. V. Chechkin and R. Metzler, Anomalous diffusion and ergodicity breaking in heterogeneous diffusion processes, *New J. Phys.*, 2013, **15**, 083039.
69 A. V. Cherstvy, A. V. Chechkin and R. Metzler, Particle invasion, survival, and non-ergodicity in 2D diffusion processes with space-dependent diffusivity, *Soft Matter*, 2014, **10**, 1591.
70 A. G. Cherstvy, A. V. Chechkin and R. Metzler, Ageing and confinement in non-ergodic heterogeneous diffusion processes, *J. Phys. A: Math. Gen.*, 2014, **47**, 485002.
71 Y. Meroz and I. M. Sokolov, A toolbox for determining subdiffusive mechanisms, *Phys. Rep.*, 2015, **573**, 1.
72 S. C. Lim and S. V. Muniandi, *Phys. Rev. E*, 2002, **66**, 021114.
73 F. Thiel and I. M. Sokolov, *Phys. Rev. E*, 2014, **89**, 012115.
74 J.-H. Jeon, A. V. Chechkin and R. Metzler, Scaled Brownian motion: a paradoxical process with a time dependent diffusivity for the description of anomalous diffusion, *Phys. Chem. Chem. Phys.*, 2014, **16**, 15811.
75 A. Bodrova, A. V. Chechkin, A. G. Cherstvy and R. Metzler, *Phys. Chem. Chem. Phys.*, 2015, **17**, 21791.

76 D. Jacobs and H. Nakanishi, Autocorrelation functions for discrete random walks on disordered lattice, *Phys. Rev. A: At., Mol., Opt. Phys.*, 1990, **41**, 706.
77 Y. Meroz, I. M. Sokolov and J. Klafter, Test for determining a subdiffusive model in ergodic systems from single trajectories, *Phys. Rev. Lett.*, 2013, **110**, 090601.
78 Y. Meroz, I. M. Sokolov and J. Klafter, Subdiffusion of mixed origins: When ergodicity and nonergodicity coexist, *Phys. Rev. E: Stat., Nonlinear, Soft Matter Phys.*, 2010, **81**, 010101(R).
79 K. Falconer, *Fractal geometry*, John Wiley & Sons, Chichester, UK, 1990.
80 J. W. Dollinger, R. Metzler and T. F. Nonnenmacher, Bi-asymptotic fractals: fractals between lower and upper bounds, *J. Phys. A: Math. Gen.*, 1998, **31**, 3839.
81 W. H. Press, S. A. Teukolsky, W. T. Vetterling and B. P. Flannery, *Numerical recipes in C: the art of scientific computing*, Cambridge University Press, 2nd edn, 1992.
82 A. Godec, A. V. Chechkin, E. Barkai, H. Kantz and R. Metzler, Localization and universal fluctuations in ultraslow diffusion processes, *J. Phys. A: Math. Gen.*, 2014, **47**, 492002.
83 A. Klemm, H.-P. Müller and R. Kimmich, NMR microscopy of pore-space backbones in rock, sponge, and sand in comparison with random percolation model objects, *Phys. Rev. E: Stat. Phys., Plasmas, Fluids, Relat. Interdiscip. Top.*, 1997, **55**, 4413.
84 A. Klemm, R. Metzler and R. Kimmich, Diffusion on random-site percolation clusters: theory and NMR microscopy experiments with model objects, *Phys. Rev. E: Stat., Nonlinear, Soft Matter Phys.*, 2002, **65**, 021112.
85 J. Schulz, E. Barkai and R. Metzler, Ageing effects in single particle trajectory averages, *Phys. Rev. Lett.*, 2013, **110**, 020602.
86 J. H. P. Schulz, E. Barkai and R. Metzler, Aging renewal theory and application to random walks, *Phys. Rev. X*, 2014, **4**, 011028.
87 H. Safdari, A. V. Chechkin, G. Jafari and R. Metzler, Aging Scaled Brownian Motion, *Phys. Rev. E: Stat., Nonlinear, Soft Matter Phys.*, 2015, **91**, 042107.
88 J. Kursawe, J. H. P. Schulz and R. Metzler, Transient ageing in fractional Brownian and Langevin equation motion, *Phys. Rev. E: Stat., Nonlinear, Soft Matter Phys.*, 2013, **88**, 062124.
89 J.-H. Jeon and R. Metzler, Analysis of short subdiffusive time series: scatter of the time averaged mean squared displacement, *J. Phys. A: Math. Gen.*, 2010, **43**, 252001.
90 A. G. Cherstvy and R. Metzler, Population splitting, trapping, and non-ergodicity in heterogeneous diffusion processes, *Phys. Chem. Chem. Phys.*, 2013, **15**, 20220.
91 J. Hoshen, D. Stauffer, G. H. Bishop, R. J. Harrison and G. D. Quinn, Monte Carlo experiments on cluster size distribution in percolation, *J. Phys. A: Math. Gen.*, 1979, **12**, 1285.
92 W. Deng and E. Barkai, Ergodic properties of fractional Brownian-Langevin motion, *Phys. Rev. E: Stat., Nonlinear, Soft Matter Phys.*, 2009, **79**, 011112.
93 J.-H. Jeon and R. Metzler, Fractional Brownian motion and motion governed by the fractional Langevin equation in confined geometries, *Phys. Rev. E: Stat., Nonlinear, Soft Matter Phys.*, 2010, **81**, 021103.
94 J.-H. Jeon and R. Metzler, Inequivalence of time and ensemble averages in ergodic systems: exponential *versus* power-law relaxation in confinement, *Phys. Rev. E: Stat., Nonlinear, Soft Matter Phys.*, 2012, **85**, 021147.
95 J.-H. Jeon, A. V. Chechkin and R. Metzler, Scaled Brownian motion: a paradoxical process with a time dependent diffusivity for the description of anomalous diffusion, *Phys. Chem. Chem. Phys.*, 2014, **16**, 15811.
96 M. J. Saxton, Lateral diffusion in an archipelago: the effect of mobile obstacles, *Biophys. J.*, 1987, **52**, 989.
97 T. Akimoto, E. Yamamoto, K. Yasuoka, Y. Hirano and M. Yasui, Non-Gaussian fluctuations resulting from power-law trapping in a lipid bilayer, *Phys. Rev. Lett.*, 2011, **107**, 178103.
98 J.-H. Jeon, M. Javanainen, H. Martinez-Seara, I. Vattulainen and R. Metzler, manuscript in preparation.
99 M. J. Skaug and D. K. Schwartz, Tracking nanoparticle diffusion in porous filtration media, *Ind. Eng. Chem. Res.*, 2015, **54**, 4414.

Appendix C

Spurious ergodicity breaking in normal and fractional Ornstein-Uhlenbeck process

Yousof Mardoukhi[†], Aleksei Chechkin[†,‡] and Ralf Metzler[†]

† Institute of Physics and Astronomy, University of Potsdam, 14476 Potsdam-Golm, Germany.

‡ Akhiezer Institute for Theoretical Physics, Kharkov 61108, Ukraine

E-mail: Corresponding author: rmetzler@uni-potsdam.de

Abstract. The Ornstein-Uhlenbeck process is a stationary and ergodic Gaussian process, that is fully determined by its covariance function and mean. We show here that the generic definitions of the ensemble- and time-averaged mean squared displacements fail to capture these properties consistently, leading to a spurious ergodicity breaking. We propose to remedy this failure by redefining the mean squared displacements such that they reflect unambiguously the statistical properties of any stochastic process. In particular we study the effect of the initial condition in the Ornstein-Uhlenbeck process and its fractional extension. For the fractional Ornstein-Uhlenbeck process representing typical experimental situations in crowded environments such as living biological cells, we show that the stationarity of the process delicately depends on the initial condition.

1. Introduction

The Ornstein-Uhlenbeck process is one of the most fundamental physical processes, originally devised to describe the velocity distribution and relaxation of a Brownian particle under the influence of a velocity-dependent friction. The Ornstein-Uhlenbeck process belongs to the class of Gaussian and Markovian processes, and it is described in terms of the stochastic Langevin equation [1, 2, 3]‡

$$dx + \lambda x dt = \sigma dB_t. \tag{1}$$

Here dB_t is the increment of the well-known Brownian motion (Wiener process) B_t, and λ and σ are positive constants. $1/\lambda$ defines a natural dynamic time scale, and σ is the intensity of the fluctuations. Under certain conditions discussed below the Ornstein-Uhlenbeck process is the only non-trivial process in the class of Gauss-Markov processes that has a stationary solution [5]. Physically, overdamped Brownian particles in an optical tweezers trap [6] or tethered to an anchor by a flexible polymer [7]

‡ In the original notation, the Langevin equation is formulated for the velocity co-ordinate. Having contemporary optical tweezers experiments in mind we use the overdamped formulation in terms of the position co-ordinate. We also note that in mathematical finance the Langevin equation (1) with an additional drift μ, $dx + \lambda(x-\mu)dt = \sigma dB_t$ is used [4].

are adequately described in terms of an Ornstein-Uhlenbeck process. The Ornstein-Uhlenbeck process is also used as a phenomenological model for the confinement observed in the tracer diffusion in critical random environments [8]. A wide field of applications of the Ornstein-Uhlenbeck process lies in finance. The Ornstein-Uhlenbeck process was adopted in 1970s by Vašíček to model the evolution of the interest rate of financial markets [4]. Extending this Vašíček model, Hull and White took into account explicitly time dependent μ and λ [9]. There are other variants of the Vašíček model, for instance, the jump-extended Vašíček model in which an exponential jump noise following a Poisson distribution is added to equation (1) [10]. There also exist extensions of the Ornstein-Uhlenbeck process to non-Gaussian processes with applications in finance [11], including such option pricing [12], commodity derivative pricing [13] and electricity pricing [14]. They have also been utilised to model neural activity [15] or to study the statistics of neuron spikes [16]. The Ornstein-Uhlenbeck process corresponds to the continuous-time analogue of a discrete-time autoregressive AR(1)-process [17, 18, 19].

In a direct extension of the Ornstein-Uhlenbeck process (1) one replaces the white Gaussian noise dB_t by power-law correlated fractional Gaussian noise [20]. In absence of the damping term this so-called fractional Brownian motion captures the motion of diffusive particles in viscoelastic environments, such as artificially crowded media [21, 22, 23], lipid bilayer membranes [24, 25, 26], or the cytoplasm of living biological cells [27, 28, 29]. The correlations in the noise effect anomalous diffusion of the form $\langle x^2(t)\rangle \simeq t^\alpha$ [30, 31]. Combined with a Hookean restoring force exerted by optical tweezers a tracer particle in a biological cell [28, 32] then follows the fractional Ornstein-Uhlenbeck process [33]. Formally, the fractional Ornstein-Uhlenbeck process is still Gaussian and stationary, yet it is strongly non-Markovian. As we will see this causes fundamental differences.

With modern microscopic technology it is possible to track single sub-micron tracer particles and even single molecules through complex media such as live biological cells [6, 34]. The time-series extracted from such single-particle trajectories are typically evaluated in terms of time-averaged physical observables [35, 36]. To address the motion of a Brownian or fractional Brownian particle under the action of an external potential by analysing a single trajectory of its movement, it is essential to understand whether the physical process governing the motion of the particle is ergodic, or not [31, 37, 38]. To infer the ergodic property of a given Gaussian process it is sufficient that the associated two-time covariance function solely depends on the difference of the two times [39]. This property rests on the fact that for Gaussian processes all properties can be deduced from the mean and covariance function [40, 41]. An indirect approach to deduce the ergodic property of the process is to compare the behaviour of the mean squared displacement (MSD) and the time averaged MSD [31, 42, 43, 44].

We here scrutinise the exact ergodic and stationary behaviour of the regular and fractional Ornstein-Uhlenbeck processes and show that they fundamentally differ in some of their behaviour, despite of the fact that both are ergodic. In particular, we elucidate the precise role of the initial condition and invalidate the general belief that the

assertion of an equilibrium initial condition necessarily recovers the stationary property of the process. We first analyse the detailed statistical properties from the covariance of the Ornstein-Uhlenbeck process in section 2, including the ensemble- and time-averaged MSDs and the effect of the initial condition. Section 3 provides an analogous analysis for the fractional Ornstein-Uhlenbeck process. In section 4 we discuss our results and conclude. Some mathematical details are deferred to the appendix.

2. Ornstein-Uhlenbeck Process

We define the Ornstein-Uhlenbeck process in terms of the stochastic differential equation (1), in which dB_t is the increment of Brownian motion B_t with the covariance function [45]

$$\mathrm{Cov}(B_t, B_s) = \left\langle \Big(B_t - \langle B_t \rangle\Big)\Big(B_s - \langle B_s \rangle\Big) \right\rangle = \min(t, s). \tag{2}$$

In this formulation, Gaussian white noise corresponds to the time derivative of the increment, dB_t/dt. After solving the stochastic differential equation (1), $x(t)$ is formally obtained as

$$x(t) = e^{-\lambda t}\left(x_0 + \sigma \int_0^t e^{\lambda s} dB_s\right), \tag{3}$$

where $x_0 = x(t = 0)$ defines the initial condition. Since B_t is a continuous process, via integration by parts the above equation is recast into

$$x(t) = e^{-\lambda t}\left(x_0 - \sigma\lambda \int_0^t B_s e^{\lambda s} ds\right) + \sigma B_t, \tag{4}$$

with $B_0 = 0$. The MSD for a random process $x(t)$ is defined as

$$\langle \Omega^2(t) \rangle = \langle [\delta x(t) - \delta x_0]^2 \rangle, \tag{5}$$

where $\delta x(t) = x(t) - \langle x(t) \rangle$. The MSD can also be written in terms of the covariance function,

$$\langle \Omega^2(t) \rangle = \mathrm{Cov}(x(t), x(t)) + \mathrm{Cov}(x_0, x_0) - 2\mathrm{Cov}(x(t), x_0). \tag{6}$$

For the Ornstein-Uhlenbeck process the MSD then assumes the following expression,

$$\langle \Omega^2(t) \rangle = \mathrm{Var}(x_0)\left(1 - e^{-\lambda t}\right)^2 + \frac{\sigma^2}{2\lambda}\left(1 - e^{-2\lambda t}\right), \tag{7}$$

where $\mathrm{Var}(X)$ stands on the variance of a random variable X. Note that in the limit $\lambda \to 0$ of free Brownian motion this notation leads to the MSD $\lim_{\lambda\to 0}\langle \Omega^2(t) \rangle = \sigma^2 t$. The time-averaged MSD (TAMSD) is defined as [31, 35, 42]§

$$\left\langle \overline{\delta^2(\Delta)} \right\rangle = \frac{1}{T - \Delta} \int_0^T \left\langle \Big(\delta x(t + \Delta) - \delta x(t)\Big)^2 \right\rangle dt, \tag{8}$$

§ Note that for simplicity we use the term TAMSD for expression (8). More precisely, the definition without the angular brackets is called TAMSD, and the angular brackets denote an additional average over an ensemble of individual trajectories [31, 35, 42].

where T is the total measurement time and Δ is called the lag time. For the Ornstein-Uhlenbeck process, the TAMSD yields in the form

$$\left\langle \overline{\delta^2(\Delta)} \right\rangle = \frac{\sigma^2}{\lambda}\left(1-e^{-\lambda\Delta}\right) + \left(\mathrm{Var}(x_0) - \frac{\sigma^2}{2\lambda}\right)\left(1-e^{-\lambda\Delta}\right)^2 \frac{1-e^{-2\lambda(T-\Delta)}}{2\lambda(T-\Delta)}. \tag{9}$$

2.1. Properties of the Ornstein-Uhlenbeck process

Since the Ornstein-Uhlenbeck process is a Gaussian process, it suffices to know the covariance function and mean to infer its properties. The mean of $x(t)$ according to equation (4) is $\langle x(t)\rangle = e^{-\lambda t}\langle x_0\rangle$. The covariance function of the process is

$$\mathrm{Cov}\Big(x(t_1), x(t_2)\Big) = \left(\mathrm{Var}(x_0) - \frac{\sigma^2}{2\lambda}\right) e^{-\lambda(t_1+t_2)} + \frac{\sigma^2}{2\lambda} e^{-\lambda|t_2-t_1|}. \tag{10}$$

Recall that a Gaussian process is stationary and ergodic if the covariance function at two times exclusively depends on the time difference, that is, $\mathrm{Cov}(x(t_1), x(t_2)) = G(|t_2-t_1|)$ in terms of the continuous function G. The covariance (10) satisfies the requirements of stationarity if (i) t_1 or t_2 are significantly larger than $1/\lambda$, or (ii) if $\mathrm{Var}(x_0) = \frac{\sigma^2}{2\lambda}$. The first condition is asymptotic with respect to $1/\lambda$: the process loses the memory of its initial condition after the correlation time $1/\lambda$. The second condition is valid for all times, it corresponds to starting the process with the equilibrium distribution.

The equilibrium stationary distribution can be deduced from Fokker-Planck equation of the Ornstein-Uhlenbeck process [46]

$$\frac{\partial P(x,t)}{\partial t} = \lambda \frac{\partial}{\partial x}\Big(xP(x,t)\Big) + \frac{\sigma^2}{2}\frac{\partial^2}{\partial^2 x} P(x,t), \tag{11}$$

where $P(x,t)$ is the probability density function of the process. The solution for $P(x,t)$ is [3, 46]

$$P(x,t) = \sqrt{\frac{\lambda}{\pi\sigma^2\left(1-e^{-2\lambda t}\right)}} \exp\left(-\frac{\lambda}{\sigma^2}\frac{(x-x_0e^{-\lambda t})^2}{1-e^{-2\lambda t}}\right). \tag{12}$$

In the stationary limit $t \gg 1/\lambda$ the stationary probability density function is given by $P(x) = [\lambda/(\pi\sigma^2)]^{-1/2}\exp(-\lambda x^2/\sigma^2)$, for which the variance becomes

$$\mathrm{Var}(x) = \int_{-\infty}^{\infty} P(x)x^2dx - \left(\int_{-\infty}^{\infty} P(x)xdx\right)^2 = \int_{-\infty}^{\infty}\sqrt{\frac{\lambda}{\pi\sigma^2}} e^{-\frac{\lambda x^2}{\sigma^2}} x^2 dx = \frac{\sigma^2}{2\lambda}. \tag{13}$$

Assume that the distribution of x_0 satisfies the stationary distribution, $\mathrm{Var}(x_0) = \sigma^2/(2\lambda)$, from equations (7) and (9) one arrives at

$$\langle \Omega^2(t)\rangle = \frac{\sigma^2}{\lambda}\left(1-e^{-\lambda t}\right) \tag{14}$$

$$\left\langle \overline{\delta^2(\Delta)} \right\rangle = \frac{\sigma^2}{\lambda}\left(1-e^{-\lambda\Delta}\right). \tag{15}$$

The fact that MSD and TAMSD are equivalent for an equilibrium stationary initial distribution is the direct consequence of the stationary property of the process, that can be directly inferred from the covariance (10). Thus, MSD and TAMSD indeed

coincide. Yet there exists an intrinsic problem regarding the way MSD and TAMSD are defined, and the equivalency between the two is only valid under the strict conditions that the equilibrium initial condition is met *and* that the process is both Gaussian and Markovian, see the next section for the non-Markovian fractional Ornstein-Uhlenbeck process.

Compare the pairs of equations (7) and (9) as well as (14) and (15). In the first pair, (7) and (9), we note the existence of two time scales in the TAMSD, Δ and T, the latter of which does not exist in the definition of the MSD. This effects a disparity in inferring the stationary state in a consistent way from MSD and TAMSD. From the MSD, the stationary state is reached when the expression ceases to depend on t, that is when $t \gg 1/\lambda$. In contrast, for the TAMSD the stationarity condition depends on the interplay between lag time Δ and measurement time T. The observation time T identifies the total time the process has been monitored to evolve, and one identifies the stationary state of the process when $T \gg 1/\lambda$. Yet Δ signifies the magnitude of the time window in the sliding average, comparing two instances of the process. Necessarily, $\Delta < T$, however, also the lag time Δ needs to be compared with the natural dynamical time scale imposed by $1/\lambda$. There exist two distinct regimes: (i) if Δ is much smaller than $1/\lambda$ the fluctuations present in the system during this time interval have not relaxed. Therefore any statistical inference cannot be justified although the overall process has reached stationarity for $T \gg 1/\lambda$. (ii) Stationarity is reached when $T \gg 1/\lambda$ and $\Delta \gg 1/\lambda$, as long as $\Delta \ll T$ is simultaneously fulfilled. Obviously, for the trivial case $T < 1/\lambda$ the process cannot be stationary. When the initial condition is chosen to be the equilibrium distribution, $\mathrm{Var}(x_0) = \sigma^2/2\lambda$, we see from equations (14) and (15) that the situation is different: here stationarity is reached once $t \gg 1/\lambda$ for the MSD and $\Delta \gg 1/\lambda$ for the TAMSD. Note that the signature of T disappears (an indication of stationarity). The caveat here is that, for the MSD, asserting the equilibrium initial condition, which implies the stationary property of the process, does not imply the independence of the MSD of t, in contrast to the case of the TAMSD, in which the dependency on T disappears.

This discrepancy also manifests itself in the asymptotes of MSD and TAMSD when the equilibrium initial condition is not asserted. The asymptotes of MSD and TAMSD in the stationary state read

$$\lim_{t\gg 1/\Delta} \langle \Omega^2(t) \rangle = \mathrm{Var}(x_0) + \frac{\sigma^2}{2\lambda}, \tag{16}$$

$$\lim_{T\gg\Delta\gg 1/\lambda} \left\langle \overline{\delta^2(\Delta)} \right\rangle = \frac{\sigma^2}{\lambda}. \tag{17}$$

Indeed, for the MSD the stationary value asymptote depends on the variance $\mathrm{Var}(x_0)$ of the chosen initial distribution. This contradicts the common intuition that, once the process reaches its stationary state, any trace of the initial condition must have vanished. In contrast, $\mathrm{Var}(x_0)$ is absent from the limiting value of the TAMSD. Knowing that the Ornstein-Uhlenbeck process is stationary and ergodic, these observables, suggesting non-ergodic behaviour, are thus unsuitable. In particular, the above difference could

potentially lead to wrong conclusions for the ratio of noise strength σ^2 and trap strength λ depending on which measure is chosen for the evaluation of an experiment.

This discussion elucidates the fundamental difference between the generic definitions of the MSD and the TAMSD, essentially quantifying different properties of a random process. Thus, while the MSD quantifies the dispersal of an ensemble of walkers at a given time instant t with respect to the initial condition, the TAMSD quantifies how increments of the process evolve as function of the lag time. We now embark for modified definitions of these most widely used physical observables for stochastic processes for the case of the Ornstein-Uhlenbeck process.

2.2. Generalised definitions of the ensemble-averaged MSD

We propose to recalibrate the definition of the MSD in the generalised form

$$\langle \Omega^2_\Delta(t) \rangle = \left\langle \Big(\delta x(t+\Delta) - \delta x(t) \Big)^2 \right\rangle, \tag{18}$$

where the subscript Δ indicates the generalisation. This modified MSD describes the *dispersal* of the process from time t to $t+\Delta$; in other words, the dispersal of increments in which the mean effect of the initial condition and the drift are removed. We can rewrite expression (18) in terms of the covariance function in the form

$$\begin{aligned} \langle \Omega^2_\Delta(t) \rangle &= \mathrm{Cov}\Big(x(t+\Delta), x(t+\Delta) \Big) + \mathrm{Cov}\Big(x(t), x(t) \Big) - 2\mathrm{Cov}\Big(x(t+\Delta), x(t) \Big) \\ &= \frac{\sigma^2}{\lambda} \left(1 - e^{-\lambda\Delta} \right) + \left(\mathrm{Var}(x_0) - \frac{\sigma^2}{2\lambda} \right) \left(1 - e^{-\lambda\Delta} \right)^2 e^{-2\lambda t}. \end{aligned} \tag{19}$$

In the limit $\lambda \to 0$ of free Brownian motion, this definition produces $\lim_{\lambda\to 0} \langle \Omega^2_\Delta(t) \rangle = \sigma^2 \Delta$, which is the same expression as obtained for the classical definition, albeit with t replaced by Δ. In this generalised formulation the integrand of the TAMSD (8) is exactly the generalised expression of the MSD given by equation (18), that is,

$$\left\langle \overline{\delta^2(\Delta)} \right\rangle = \frac{1}{T-\Delta} \int_0^{T-\Delta} \left\langle \Omega^2_\Delta(t) \right\rangle dt \tag{20}$$

which readily yields equation (9). We observe that for equilibrium initial conditions, $\mathrm{Var}(x_0) = \sigma^2/2\lambda$, the generalised expressions for MSD and TAMSD yield *exactly* the same result $(\sigma^2/\lambda)[1 - \exp(-\lambda\Delta)]$.

3. Fractional Ornstein-Uhlenbeck Processes

The fractional Ornstein-Uhlenbeck process is the extension of the normal Ornstein-Uhlenbeck process (1), in which the increments of Brownian motion are substituted by the increments of fractional Brownian motion, B^H_t. Here H is the Hurst exponent, which is allowed to vary in the interval $H \in (0, 1]$ [20]. The fractional Ornstein-Uhlenbeck

process is therefore given by the stochastic differential equation [33]‖

$$dx + \lambda x dt = \sigma d\widetilde{B_t^H}. \tag{21}$$

Here $d\widetilde{B_t^H}$ is the increment of fractional Brownian motion $\widetilde{B_t^H}$.¶ The tilde is introduced here to denote the extension of fractional Brownian motion to the negative time domain, such that

$$\widetilde{B_t^H} = \begin{cases} B_t^H, & \text{if } t \geq 0 \\ B_{-t}^H, & \text{otherwise} \end{cases}. \tag{22}$$

Fractional Brownian motion with Hurst parameter $H \in (0, 1]$, is a continuous centred Gaussian process defined by the covariance function [20]

$$\mathrm{Cov}\left(\widetilde{B_{t_1}^H}, \widetilde{B_{t_2}^H}\right) = \frac{1}{2}\left(|t_1|^{2H} + |t_2|^{2H} - |t_1 - t_2|^{2H}\right). \tag{23}$$

For $H = 1/2$, $\widetilde{B_t^{1/2}}$ reduces to conventional Brownian motion. From the definition above the following properties are deduced in one dimension, (i) $B_0^H = 0$ and $\left\langle \widetilde{B_t^H} \right\rangle = 0$ for all $t \in \mathbb{R}$. (ii) $\widetilde{B_t^H}$ has stationary increments and $\left\langle \left(\widetilde{B_t^H}\right)^2 \right\rangle = |t|^{2H}$. (iii) The trajectories of $\widetilde{B_t^H}$ are continuous.

For $t \in [0, \infty)$, the formal solution of the equation (21) is

$$x(t) = e^{-\lambda t}\left(x_0 + \sigma \int_0^t e^{\lambda t'} dB_{t'}^H\right). \tag{24}$$

Since fractional Brownian motion is a continuous process this integral exists [53]. Integrating by parts the equation above can be rewritten in terms of B_t^H in the form

$$x(t) = e^{-\lambda t}\left(x_0 - \sigma\lambda \int_0^t B_{t'}^H e^{\lambda t'} dt'\right) + \sigma B_t^H. \tag{25}$$

Then the covariance function becomes

$$\begin{aligned} \mathrm{Cov}\Big(x(t_1), x(s_2)\Big) = {} & e^{-\lambda(t_1+t_2)}\mathrm{Var}(x_0) + \sigma e^{-\lambda t_1}\left\langle x_0 B_{t_2}^H \right\rangle + \sigma e^{-\lambda t_2}\left\langle x_0 B_{t_1}^H \right\rangle \\ & -\sigma\lambda e^{-\lambda(t_1+t_2)}\left(\int_0^{t_1} e^{\lambda t_1'}\left\langle x_0 B_{t_1'}^H \right\rangle dt_1' + \int_0^{t_2} e^{\lambda t_2'}\left\langle x_0 B_{t_2'}^H \right\rangle dt_2'\right) \\ & -\sigma^2\lambda e^{-\lambda t_1}\int_0^{t_1} e^{\lambda t_1'}\left\langle B_{t_1'}^H B_{t_2}^H \right\rangle dt_1' - \sigma^2\lambda e^{-\lambda t_2}\int_0^{t_2} e^{\lambda t_2'}\left\langle B_{t_2'}^H B_{t_1}^H \right\rangle dt_2' \\ & +\sigma^2\lambda^2 e^{-\lambda(t_1+t_2)}\int_0^{t_1}\int_0^{t_2} e^{\lambda(t_2'+t_1')}\left\langle B_{t_1'}^H B_{t_2'}^H \right\rangle dt_2' dt_1' + \sigma^2\left\langle B_{t_1}^H B_{t_2}^H \right\rangle. \end{aligned} \tag{26}$$

‖ This is sometimes called fractional Ornstein-Uhlenbeck process of "the first kind". The fractional Ornstein-Uhlenbeck process of "the second kind" is a Gaussian process that is the integral of Doob's transformation of fractional Brownian motion [47].

¶ Note that this process should not be confused with the "fractional Ornstein-Uhlenbeck" process based on continuous time random walks with scale-free, power-law distributed waiting times or jump lengths. In these cases, in the Fokker-Planck equation (11) the time derivative or the second-order spatial derivative, respectively, are replaced by a fractional differential operator [30, 31, 48, 49, 50, 51, 52].

We note that while free fractional Brownian motion, corresponding to the limit $\lambda \to 0$, is ergodic [43, 54, 55], transient non-ergodicity occurs when the process is confined. Namely, for an harmonic external confinement (the Ornstein-Uhlenbeck process, that is) it was shown analytically and experimentally that the relaxation of the MSD is exponential while a slower power-law relaxation is observed for the TAMSD [23, 56]

When x_0 is fixed or the distribution of x_0 is independent of the fractional Brownian motion all terms involving $\left\langle x_0 B_t^H \right\rangle$ vanish. Therefore the covariance function simplifies to

$$\begin{aligned}\mathrm{Cov}\Big(x(t_1), x(t_2)\Big) &= e^{-\lambda(t_1+t_2)}\mathrm{Var}(x_0) \\ &-\sigma^2\lambda e^{-\lambda t_1}\int_0^{t_1} e^{\lambda t_1'}\left\langle B_{t_1'}^H B_{t_2}^H\right\rangle dt_1' - \sigma^2\lambda e^{-\lambda t_2}\int_0^{t_2} e^{\lambda t_2'}\left\langle B_{t_2'}^H B_{t_1}^H\right\rangle dt_2' \\ &+\sigma^2\lambda^2 e^{-\lambda(t_1+t_2)}\int_0^{t_1}\int_0^{t_2} e^{\lambda(t_2'+t_1')}\left\langle B_{t_1'}^H B_{t_2'}^H\right\rangle dt_2' dt_1' + \sigma^2\left\langle B_{t_1}^H B_{t_2}^H\right\rangle . \end{aligned} \tag{27}$$

After calculating the integrals (see Appendix A for details) the covariance of the fractional Ornstein-Uhlenbeck process reads

$$\begin{aligned}\mathrm{Cov}\Big(x(t_1), x(t_2)\Big) &= \Bigg[\mathrm{Var}(x_0) + \frac{\sigma^2}{2}e^{\lambda t_1}t_1^{2H}\left(1 + \frac{\lambda t_1 e^{\lambda t_1}}{2(2H+1)}\mathcal{M}(2H+1, 2H+2, -\lambda t_1)\right. \\ &\left. -\frac{\lambda t_1 e^{-\lambda t_1}}{2(2H+1)}\mathcal{M}(2H+1, 2H+2, \lambda t_1)\right) \\ &+\frac{\sigma^2}{2}e^{\lambda t_2}t_2^{2H}\left(1 + \frac{\lambda t_2 e^{\lambda t_2}}{2(2H+1)}\mathcal{M}(2H+1, 2H+2, -\lambda t_2)\right. \\ &\left. -\frac{\lambda t_2 e^{-\lambda t_2}}{2(2H+1)}\mathcal{M}(2H+1, 2H+2, \lambda t_2)\right)\Bigg] e^{-\lambda(t_1+t_2)} \\ &-\frac{\sigma^2}{2}|t_2 - t_1|^{2H}\left(1 - \frac{\lambda|t_2-t_1|e^{-\lambda|t_2-t_1|}}{2(2H+1)}\mathcal{M}\left(2H+1, 2H+2, \lambda|t_2-t_1|\right)\right. \\ &\left. +\frac{\lambda|t_2-t_1|e^{\lambda|t_2-t_1|}}{2(2H+1)}\mathcal{M}\left(2H+1, 2H+2, -\lambda|t_2-t_1|\right)\right), \end{aligned} \tag{28}$$

where $\mathcal{M}(a, b, z)$ is Kummer's function of the first kind (the confluent hypergeometric function of the first kind [57]). The integral representation of this function is given by

$$\mathcal{M}(a, b, z) = \frac{\Gamma(b)}{\Gamma(b-a)\Gamma(a)}\int_0^1 e^{zt}t^{a-1}(1-t)^{b-a-1}dt. \tag{29}$$

For $H = 1/2$ the covariance function (28) consistently reduces to expression (10) of the regular Ornstein-Uhlenbeck process (note that $\mathcal{M}(2, 3, x) = 2(1 - e^x + xe^x)/x^2$).

On closer inspection of the covariance function, unlike for the case of the regular Ornstein-Uhlenbeck process above, in which the equilibrium distribution of the initial condition yields a stationary covariance function (see equation (10)), we notice that there is no possible form for $\mathrm{Var}(x_0)$ such that the covariance function (28) would exclusively depend only on the time difference between the two time points of the process. In other words, there is no initial condition, such that $\mathrm{Cov}(x(t_1), x(t_2)) = G(|t_2 - t_1|)$ for any given t_1 and t_2. Asserting equilibrium initial condition does not fulfil the requirement

of an ergodic and stationary process for any $t \geq 0$. Indeed, let us assume that the x_0 have an equilibrium distribution corresponding to the normal distribution $\mathcal{N}(0, \xi^2)$ with variance [33, 47, 53],

$$\xi^2 = \frac{\sigma^2 \Gamma(2H+1)\sin(\pi H)}{\pi \lambda^{2H}} \int_0^\infty \frac{|x|^{1-2H}}{1+x^2} = \frac{\sigma^2}{2\lambda^{2H}} \Gamma(2H+1). \tag{30}$$

Here the integral is calculated in Appendix D. This result can also be obtained by recalling that

$$x_0 = \sigma e^{-\lambda t} \int_{-\infty}^0 e^{\lambda t'} d\widetilde{B_{t'}^H}. \tag{31}$$

Integration by part leads to the expression

$$\left\langle x_0^2 \right\rangle = \frac{\sigma^2 \lambda^2}{2} \int_{-\infty}^0 \int_{-\infty}^0 \left\langle \widetilde{B_{t_1}^H} \widetilde{B_{t_2}^H} \right\rangle dt_1 dt_2, \tag{32}$$

which yields the results (30). Observe that by substituting the variance of x_0 in equation (28) the covariance function would still depend on the absolute times t_1 and t_2. To provide a hint why this is the case, recall our earlier assumption on x_0. Our assumption that x_0 and B_t^H are not correlated yielded a covariance function which is not stationary for finite t_1 and t_2. It asymptotically approaches the stationary covariance function when t_1 and t_2 tend to infinity. Furthermore, observe that x_0 and $\widetilde{B_t^H}$ are correlated in the case of fractional Ornstein-Uhlenbeck process, since the driving noise has a long-range memory.

This is also reflected in the generalised MSD and TAMSD. Since the closed analytical expressions for the generalised MSD and TAMSD are too cumbersome to be presented here, we refer to Appendix B and observe that indeed the generalised expressions for MSD and TAMSD differ from one another. As we show now, in the stationary state ergodicity is indeed fulfilled.

To proceed, we note that the fractional Ornstein-Uhlenbeck process has the stationary solution [47]

$$x_s(t) = e^{-\lambda t} \sigma \int_{-\infty}^t e^{\lambda t'} d\widetilde{B_{t'}^H}, \tag{33}$$

indicated by the subscript s. Note that to achieve this stationary solution the domain of t has been changed to $t \in (-\infty, \infty)$. For this case

$$\lim_{t\to\infty} \left[x_s(t) - x(t)\right] = \lim_{t\to\infty} \left[e^{-\lambda t} \left(x_s(0) - x(0)\right)\right] = 0, \tag{34}$$

from which it is inferred that every stationary solution $x_s(t)$ of the Langevin equation (21) has the same distribution as $x(t)$ in the long-time limit. Consequently, we deduce that the covariance function for the stationary solution is given by (see Appendix C for details)

$$\mathrm{Cov}\Big(x_s(t_1), x_s(t_2)\Big) = -\frac{\sigma^2}{2}|t_2 - t_1|^{2H}$$
$$+\frac{\sigma^2}{4\lambda^{2H}} e^{-\lambda|t_2-t_1|} \left(\Gamma(2H+1) + \frac{(\lambda|t_2-t_1|)^{2H+1}}{2H+1} \mathcal{M}(2H+1, 2H+2, \lambda|t_2-t_1|)\right)$$

$$+\frac{\sigma^2}{4\lambda^{2H}}e^{\lambda|t_2-t_1|}\left(\Gamma(2H+1)-\frac{(\lambda|t_2-t_1|)^{2H+1}}{2H+1}\mathcal{M}(2H+1,2H+2,-\lambda|t_2-t_1|)\right). \quad (35)$$

Obviously, the covariance function for the stationary solution depends only on the time difference between the two time points. With the use of equations (19) and (35) the generalised MSD and TAMSD are given by

$$\langle\Omega^2_\Delta(t)\rangle = \left\langle\overline{\delta^2(\Delta)}\right\rangle = \frac{\sigma^2}{\lambda^{2H}}\Gamma(2H+1)\Big(1-\cosh(\lambda\Delta)\Big)+\sigma^2\Delta^{2H}$$
$$-\frac{\sigma^2\lambda\Delta^{2H+1}}{2(2H+1)}\Big(e^{-\lambda\Delta}\mathcal{M}(2H+1,2H+2,\lambda\Delta)-e^{\lambda\Delta}\mathcal{M}(2H+1,2H+2,-\lambda\Delta)\Big). \quad (36)$$

From this equivalency we conclude that the fractional Ornstein-Uhlenbeck process is ergodic in the sense of the generalised MSD.

Figure 1 details the functional behaviour of the different MSDs. In the left panels for the non-stationary case, as expected the disparity between the generic MSD (5) and the TAMSD (8) is distinct. In contrast, using the generalised MSD (18) for the stationary solution the expected ergodic behaviour is restored.

For completeness, figure 2 shows how the two different versions of the MSD and the TAMSD approach the plateau value for different values of H. As can be seen for normal diffusion with $H = 1/2$ the relaxation is always exponential. In contrast, we recover a power-law relaxation for the TAMSD and for the generalised definition of the MSD. While this power-law form for the TAMSD was discussed earlier [56] and verified experimentally [23], the full agreement between the TAMSD and the generalised MSD is a distinct behaviour following from our definition (18) here.

4. Conclusions

It is commonly assumed that asserting equilibrium initial condition is sufficient and necessary for a confined stochastic process to remain stationary at all times $t \geq 0$. We here demonstrated that for the case of the fractional Ornstein-Uhlenbeck process this is in fact not true. Generally, for any process which is not a Markov process one should bear in mind that due to long range correlations the assumption that the process is stationary requires one to take into account the entire history of the system. Therefore, asserting any assumption on the initial condition of the process would perturb the stationary state of the process, even in the case when this initial condition is the equilibrium distribution.

Moreover, we revealed another subtle point on how to define the stationary state of the process based on generalised definitions of the MSD and the TAMSD. While it is often believed that the sufficient condition to infer that the process has reached its stationary state when in the TAMSD the observation time tends to infinity. In this statement, though, it is neglected that Δ needs to be considered, as well. Indeed, while the lag time should remain significantly below the observation time, $\Delta \ll T$, the lag time needs to be much larger than the natural dynamic time scale of the process, $\Delta \gg 1/\lambda$.

The Ornstein-Uhlenbeck process and its fractional extension are essential in modelling physical systems in the presence of an external potential. They are Gaussian

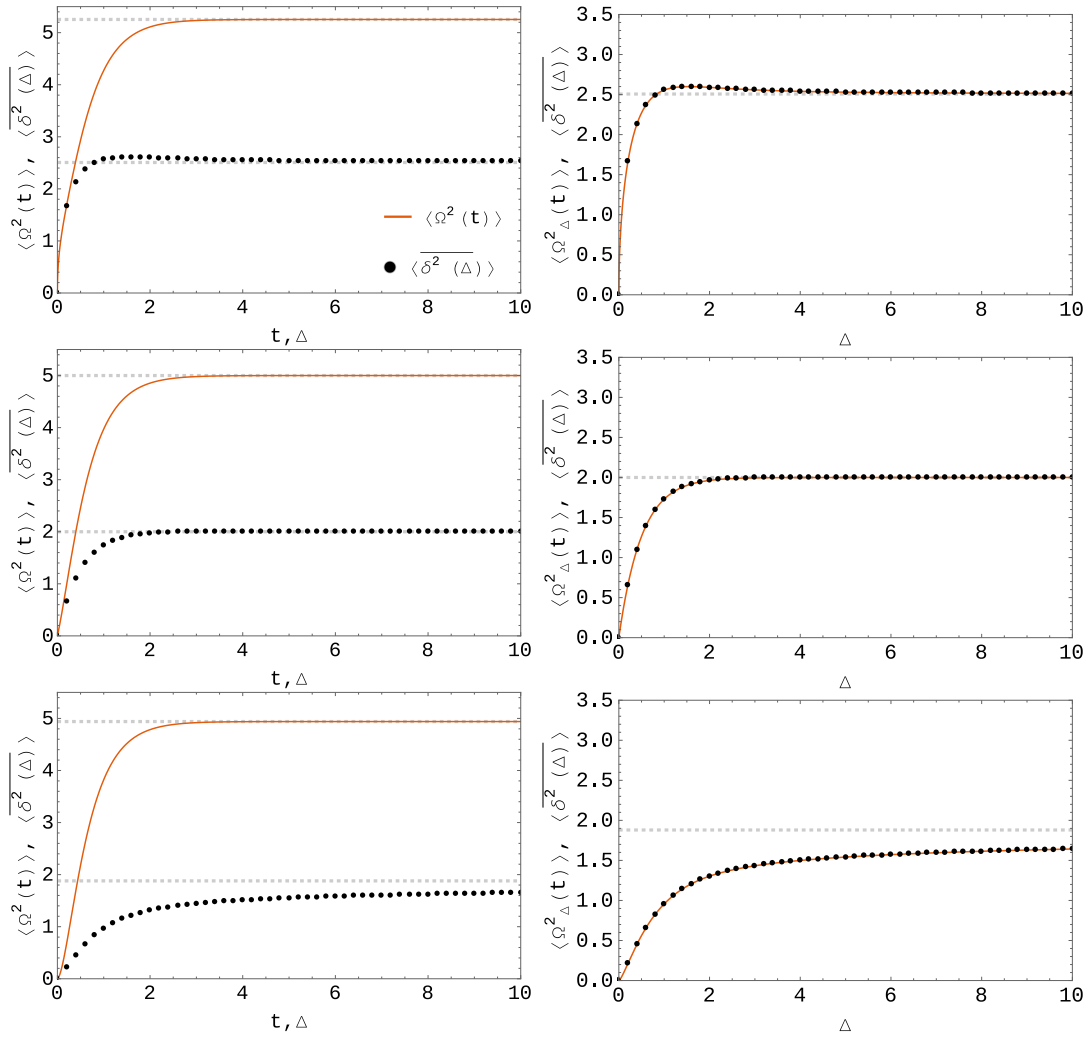

Figure 1. Left panels: Generic MSD and TAMSD (5) and (8) for the non-stationary solution of the fractional Ornstein-Uhlenbeck process (24) as function of time. In all three cases, $T = 100$. Right panels: Generalised MSD and TAMSD (18) and (8) for the stationary solution of the same process. From top to bottom the rows correspond to subdiffusion with $H = 1/4$, Brownian motion with $H = 1/2$, and superdiffusion with $H = 3/4$. The parameters are $\sigma = \lambda = 2 = \mathrm{Var}(x_0) = 2$. Note the discrepancy between the generic definitions of MSD and TAMSD, despite the fact that the process has reached the stationary state.

processes with the difference that in the former case, the correlations are short-lived (Markov process) while in the latter case the correlations are long-ranged. It was further demonstrated that the Ornstein-Uhlenbeck process is stationary for all $t \geq 0$ if the equilibrium initial condition is asserted. In contrast, this does not hold true for the fractional Ornstein-Uhlenbeck process due to the fact that the process is not Markovian.

These results will also be important for the correct analysis of measured trajectories of generic processes driven by fractional Gaussian noise in terms of the TAMSD, for instance, under confinement [58]. Moreover, the finite-time ergodic properties of the normal Ornstein-Uhlenbeck process as studied in [59, 60] should be considered in view

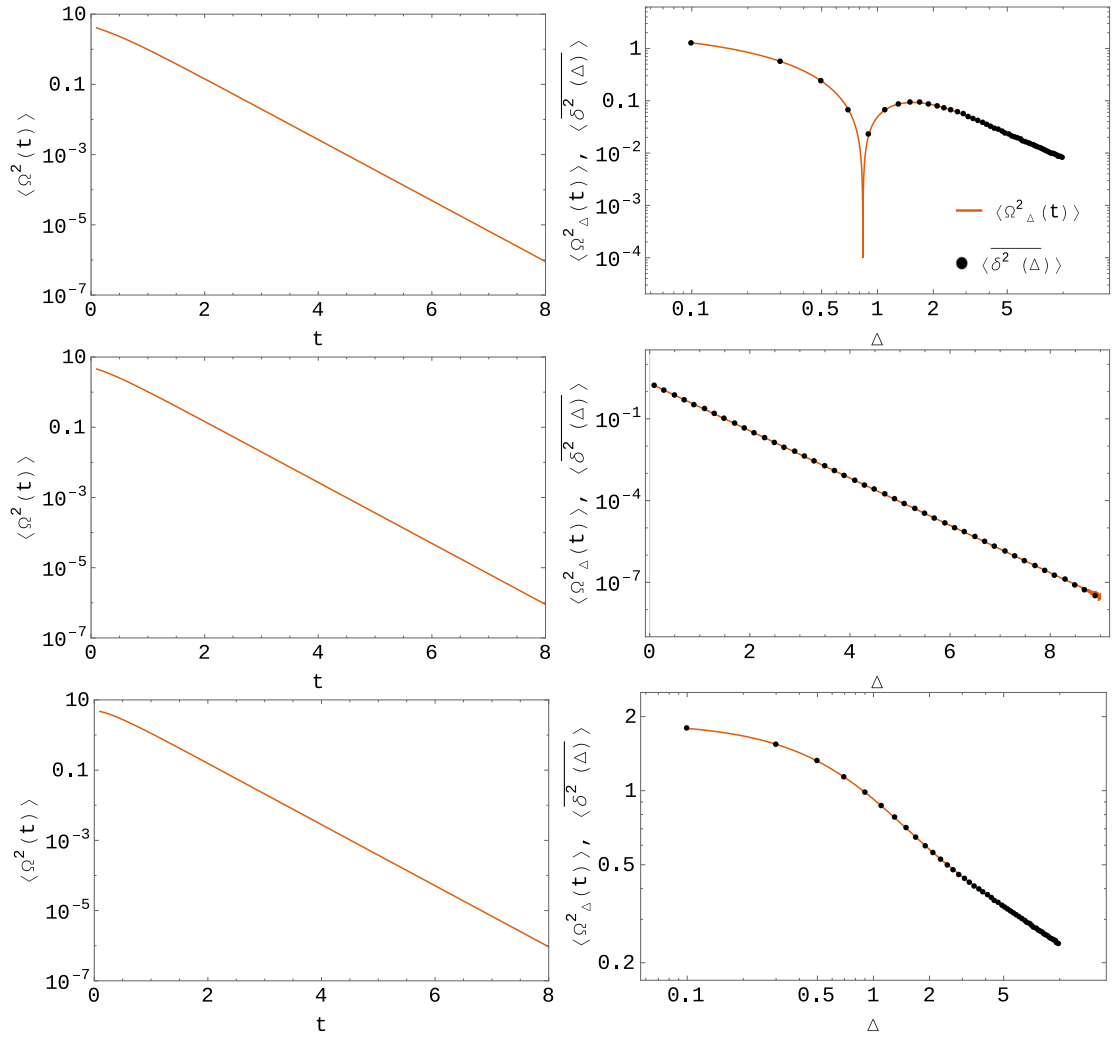

Figure 2. Relaxation dynamics of the normal and fractional Ornstein-Uhlenbeck process as described by the standard MSD (Left panels), compared to the cases of the generalised MSD and the TAMSD (Right panels). In all panels we plot the absolute value of the difference of the plateau value and the respective MSD or TAMSD. From top to bottom the corresponding Hurst coefficients are $H = 1/4$, $H = 1/2$, and $H = 3/4$. For the anomalous cases in the top and bottom rows, the generalised MSD and the TAMSD show a distinct power-law relaxation. The γ-shape for the case $H = 1/4$ is due to the fact that the functions slightly overshoot the plateau value at intermediate time scales (compare figure 1). Note the different scales (linear versus logarithmic) of the time axis.

of the generalised definitions of the MSD and TAMSD provided here.

Acknowledgments

We acknowledge funding from the Deutsche Forschungsgemeinschaft (DFG), grant number ME 1535/7-1. RM acknowledges the Foundation for Polish Science (Fundacja na rzecz Nauki Polskiej, FNP) for support within an Alexander von Humboldt Honorary

Polish Research Scholarship.

Appendix A. Covariance function of the non-stationary fractional Ornstein-Uhlenbeck process

To calculate the covariance function given by equation (27) two types of integrals need to be calculated. One are the single integrals with respect to either t_1' or t_2'. The other is the double integral with respect to the t_1' and t_2'. Throughout the integrations, it is always assumed that $t_2 > t_1$ for simplicity. Whenever the difference between the two times is relevant, the result is written in terms of the modulus.

The single integral with respect to t_1' is given by

$$\begin{aligned}
&\int_0^{t_1} e^{\lambda t_1'}\Big(t_1'^{2H} + t_2^{2H} - |t_1' - t_2|^{2H}\Big)dt_1' \\
&= \int_0^{t_1} e^{\lambda t_1'} t_1'^{2H} dt_1' + \frac{\left(e^{\lambda t_1} - 1\right) t_2^{2H}}{\lambda} - \int_0^{t_1} e^{\lambda t_1'}(t_2 - t_1')^{2H} dt_1' \\
&= t_1^{2H+1}\int_0^1 e^{\lambda t_1 q} q^{2H} dq + \frac{\left(e^{\lambda t_1} - 1\right) t_2^{2H}}{\lambda} + \int_{t_2}^{t_2 - t_1} e^{\lambda(t_2 - q)} q^{2H} dq \\
&= \frac{\left(e^{\lambda t_1} - 1\right) t_2^{2H}}{\lambda} + \frac{t_1^{2H+1}}{2H+1}\mathcal{M}(2H+1, 2H+2, \lambda t_1) \\
&- \frac{e^{\lambda t_2} t_2^{2H+1}}{2H+1}\mathcal{M}(2H+1, 2H+2, -\lambda t_2) \\
&+ \frac{e^{\lambda t_2}|t_2 - t_1|^{2H+1}}{2H+1}\mathcal{M}(2H+1, 2H+2, -\lambda|t_2 - t_1|).
\end{aligned} \tag{A.1}$$

Following the same procedure one arrives at a similar expression for the integral with respect to t_2'

$$\begin{aligned}
&\int_0^{t_2} e^{\lambda t_2'}\Big(t_1^{2H} + t_2'^{2H} - |t_1 - t_2'|^{2H}\Big)dt_2' \\
&= \frac{\left(e^{\lambda t_2} - 1\right) t_1^{2H}}{\lambda} + \frac{t_2^{2H+1}}{2H+1}\mathcal{M}(2H+1, 2H+2, \lambda t_2) \\
&- \frac{e^{\lambda t_1} t_1^{2H+1}}{2H+1}\mathcal{M}(2H+1, 2H+2, -\lambda t_1) \\
&- \frac{e^{\lambda t_1}|t_2 - t_1|^{2H+1}}{2H+1}\mathcal{M}(2H+1, 2H+2, \lambda|t_2 - t_1|).
\end{aligned} \tag{A.2}$$

The second type of the integrals appearing in the covariance of fractional Ornstein-Uhlenbeck process is given by

$$\begin{aligned}
&\int_0^{t_1}\int_0^{t_2} e^{\lambda(t_1' + t_2')}\left(t_1'^{2H} + t_2'^{2H} - |t_1' - t_2'|^{2H}\right) dt_1' dt_2' \\
&= \int_0^{t_1}\int_0^{t_2} e^{\lambda(t_1' + t_2')} t_1'^{2H} dt_1' dt_2' + \int_0^{t_1}\int_0^{t_2} e^{\lambda(t_1' + t_2')} t_2'^{2H} dt_1' dt_2' \\
&- \int_0^{t_1}\int_0^{t_2} e^{\lambda(t_1' + t_2')}|t_1' - t_2'|^{2H} dt_1' dt_2'
\end{aligned}$$

$$
\begin{aligned}
&= \frac{\left(e^{\lambda t_2}-1\right) t_1^{2H+1}}{\lambda(2H+1)} \mathcal{M}(2H+1,2H+2,\lambda t_1) \\
&+ \frac{\left(e^{\lambda t_1}-1\right) t_2^{2H+1}}{\lambda(2H+1)} \mathcal{M}(2H+1,2H+2,\lambda t_2) \\
&- \int_0^{t_1} \left(\int_0^{t_1'} e^{\lambda(t_1'+t_2')} (t_1'-t_2')^{2H} dt_2' + \int_{t_1'}^{t_2} e^{\lambda(t_1'+t_2')} (t_2'-t_1')^{2H} dt_2' \right) dt_1'.
\end{aligned}
$$

Take the last two double integrals,

$$
\begin{aligned}
&- \int_0^{t_1} \left(\int_0^{t_1'} e^{\lambda(t_1'+t_2')} (t_1'-t_2')^{2H} dt_2' + \int_{t_1'}^{t_2} e^{\lambda(t_1'+t_2')} (t_2'-t_1')^{2H} dt_2' \right) dt_1' \\
&= - \int_0^{t_1} e^{\lambda t_1'} dt_1' \int_0^{t_1'} e^{\lambda(t_1'-q)} q^{2H} dq - \int_0^{t_1} e^{\lambda t_1'} dt_1' \int_0^{t_2-t_1'} e^{\lambda(t_1'+q)} q^{2H} dq \\
&= - \int_0^{t_1} e^{2\lambda t_1'} dt_1' \int_0^{t_1'} e^{-\lambda q} q^{2H} dq - \int_0^{t_1} e^{2\lambda t_1'} dt_1' \int_0^{t_2-t_1'} e^{\lambda q} q^{2H} dq \\
&= - \int_q^{t_1} e^{2\lambda t_1'} dt_1' \int_0^{t_1} e^{-\lambda q} q^{2H} dq - \int_0^{t_2-q} e^{2\lambda t_1'} dt_1' \int_0^{t_2} e^{\lambda q} q^{2H} dq \\
&+ \int_{t_1}^{t_2-q} e^{2\lambda t_1'} dt_1' \int_0^{t_2-t_1} e^{\lambda q} q^{2H} dq \\
&= \frac{t_1^{2H+1}}{2\lambda(2H+1)} \mathcal{M}(2H+1,2H+2,\lambda t_1) - \frac{e^{2\lambda t_1} t_1^{2H+1}}{2\lambda(2H+1)} \mathcal{M}(2H+1,2H+2,-\lambda t_1) \\
&+ \frac{t_2^{2H+1}}{2\lambda(2H+1)} \mathcal{M}(2H+1,2H+2,\lambda t_2) - \frac{e^{2\lambda t_2} t_2^{2H+1}}{2\lambda(2H+1)} \mathcal{M}(2H+1,2H+2,-\lambda t_2) \\
&+ \frac{e^{2\lambda t_2} |t_2-t_1|^{2H+1}}{2\lambda(2H+1)} \mathcal{M}(2H+1,2H+2,-\lambda|t_2-t_1|) \\
&- \frac{e^{2\lambda t_1} |t_2-t_1|^{2H+1}}{2\lambda(2H+1)} \mathcal{M}(2H+1,2H+2,\lambda|t_2-t_1|).
\end{aligned}
$$

Hence we arrive at the following expression for the double integral,

$$
\begin{aligned}
&\int_0^{t_1} \int_0^{t_2} e^{\lambda(t_1'+t_2')} \left(t_1'^{2H} + t_2'^{2H} - |t_1'-t_2'|^{2H} \right) dt_1' dt_2' \\
&= \frac{e^{\lambda t_2} t_1^{2H+1}}{\lambda(2H+1)} \mathcal{M}(2H+1,2H+2,\lambda t_1) - \frac{t_1^{2H+1}}{2\lambda(2H+1)} \mathcal{M}(2H+1,2H+2,\lambda t_1) \\
&+ \frac{e^{\lambda t_1} t_2^{2H+1}}{\lambda(2H+1)} \mathcal{M}(2H+1,2H+2,\lambda t_2) - \frac{t_2^{2H+1}}{2\lambda(2H+1)} \mathcal{M}(2H+1,2H+2,\lambda t_2) \\
&- \frac{e^{2\lambda t_1} t_1^{2H+1}}{2\lambda(2H+1)} \mathcal{M}(2H+1,2H+2,-\lambda t_1) - \frac{e^{2\lambda t_2} t_2^{2H+1}}{2\lambda(2H+1)} \mathcal{M}(2H+1,2H+2,-\lambda t_2) \\
&+ \frac{e^{2\lambda t_2} |t_2-t_1|^{2H+1}}{2\lambda(2H+1)} \mathcal{M}(2H+1,2H+2,-\lambda|t_2-t_1|) \\
&- \frac{e^{2\lambda t_1} |t_2-t_1|^{2H+1}}{2\lambda(2H+1)} \mathcal{M}(2H+1,2H+2,\lambda|t_2-t_1|).
\end{aligned} \tag{A.3}
$$

Appendix B. MSD and TAMSD of the non-stationary fractional Ornstein-Uhlenbeck process

After arriving at the covariance function for the non-stationary solution (28) the MSD of the fractional Ornstein-Uhlenbeck processes is deduced from

$$\langle\Omega^2_\Delta(t)\rangle = \mathrm{Cov}\Big(x(t+\Delta),x(t+\Delta)\Big) + \mathrm{Cov}\Big(x(t),x(t)\Big) - 2\mathrm{Cov}(x(t+\Delta),x(t)),$$

such that

$$\begin{aligned}
\langle\Omega^2(t)\rangle &= \mathrm{Var}(x_0)\left(1-e^{-\lambda\Delta}\right)^2 e^{-2\lambda t}\\
&+\sigma^2(t+\Delta)^{2H}e^{-\lambda(t+\Delta)}\Big[1+\frac{\lambda(t+\Delta)e^{\lambda(t+\Delta)}}{2(2H+1)}\mathcal{M}(2H+1,2H+2,-\lambda(t+\Delta)\\
&\qquad -\frac{\lambda(t+\Delta)e^{-\lambda(t+\Delta)}}{2(2H+1)}\mathcal{M}(2H+1,2H+2,\lambda(t+\Delta)\Big]\left(1-e^{\lambda\Delta}\right)\\
&+\sigma^2t^{2H}e^{-\lambda t}\Big[1+\frac{\lambda te^{\lambda t}}{2(2H+1)}\mathcal{M}(2H+1,2H+2,-\lambda t)\\
&\qquad -\frac{\lambda te^{-\lambda t}}{2(2H+1)}\mathcal{M}(2H+1,2H+2,\lambda t)\Big]\left(1-e^{-\lambda\Delta}\right)\\
&+\sigma^2\Delta^{2H}\Big[1-\frac{\lambda\Delta e^{-\lambda\Delta}}{2(2H+1)}\mathcal{M}(2H+1,2H+2,\lambda\Delta)\\
&\qquad +\frac{\lambda\Delta e^{\lambda\Delta}}{2(2H+1)}\mathcal{M}(2H+1,2H+2,-\lambda\Delta)\Big].
\end{aligned}\tag{B.1}$$

Before calculating the TAMSD it is worthwhile checking that in the long time limit the expression above coincides with the earlier equation (36). In the limit $t\to\infty$ the expression in the last square brackets remains unchanged while for the first and second square brackets it is only the second term which contributes to a non-zero value, namely, $(t+\Delta)^{2H+1}\mathcal{M}(2H+1,2H+2,-\lambda(t+\Delta))$ and $t^{2H+1}\mathcal{M}(2H+1,2H+2,-\lambda t)$. Considering the latter in the aforementioned long-time limit,

$$\begin{aligned}
&\lim_{t\to\infty} t^{2H+1}\mathcal{M}(2H+1,2H+2,-\lambda t)\\
&=\lim_{t\to\infty}(2H+1)\int_0^1 t^{2H+1}e^{-\lambda tz}z^{2H}dz\\
&=\lim_{t\to\infty}(2H+1)\int_0^1 e^{-\lambda tz}(tz)^{2H}d(tz)=\lim_{t\to\infty}\frac{2H+1}{\lambda^{2H+1}}\int_0^{\lambda t}e^{-q}q^{2H}dq\\
&=\lim_{t\to\infty}\frac{2H+1}{\lambda^{2H+1}}\gamma(2H+1,\lambda t)=\frac{2H+1}{\lambda^{2H+1}}\Gamma(2H+1),
\end{aligned}$$

where $\gamma(s,x)$ is the lower incomplete Gamma function. Therefore, in the limit $t\to\infty$ one indeed consistently recovers the expression of the generalised MSD for the stationary solution of the fractional Ornstein-Uhlenbeck process, equation (36).

The complexity in the integration of the generalised MSD for the TAMSD is due to terms of the kind $t^{2H+1}\mathcal{M}(2H+1,2H+2,-\lambda t)$ and $t^{2H+1}e^{-2\lambda t}\mathcal{M}(2H+1,2H+2,\lambda t)$.

The integration of such terms can be achieved as follows,

$$\begin{aligned}
&\int_0^{T-\Delta} t^{2H+1}\mathcal{M}(2H+1,2H+2,-\lambda t)dt \\
&\qquad = (2H+1)\int_0^{T-\Delta} t^{2H+1}\left(\int_0^1 e^{-\lambda t q}q^{2H}dq\right)dt \\
&\qquad = (2H+1)\int_0^{T-\Delta} t^{2H+1}\left(\int_0^{\lambda t} e^{-z}\left(\frac{z}{\lambda t}\right)^{2H}\frac{dz}{\lambda t}\right)dt \\
&\qquad = \frac{2H+1}{\lambda^{2H+1}}\int_0^{T-\Delta}\left(\int_0^{\lambda t} e^{-z}z^{2H}dz\right)dt.
\end{aligned}$$

After changing the order of the integration,

$$\begin{aligned}
&\frac{2H+1}{\lambda^{2H+1}}\int_0^{T-\Delta}\left(\int_0^{\lambda t} e^{-z}z^{2H}dz\right)dt \\
&\qquad = \frac{2H+1}{\lambda^{2H+1}}\int_0^{\lambda(T-\Delta)} e^{-z}z^{2H}dz\int_{z/\lambda}^{T-\Delta}dt \\
&\qquad = \frac{2H+1}{\lambda^{2H+1}}\int_0^{\lambda(T-\Delta)} e^{-z}z^{2H}\left(T-\Delta-\frac{z}{\lambda}\right)dz \\
&\qquad = (2H+1)(T-\Delta)^{2H+2}\int_0^1 e^{-\lambda(T-\Delta)q}q^{2H}(1-q)dq \\
&\qquad = \frac{(T-\Delta)^{2H+2}}{2H+2}\mathcal{M}(2H+1,2H+3,-\lambda(T-\Delta)).
\end{aligned}$$

Similarly, the second type of integration can be performed along the following steps,

$$\begin{aligned}
&\int_0^{T-\Delta} e^{-2\lambda t}t^{2H+1}\mathcal{M}(2H+1,2H+2,\lambda t)dt \\
&\qquad = (2H+1)\int_0^{T-\Delta} e^{-2\lambda t}t^{2H+1}\left(\int_0^1 e^{\lambda t q}q^{2H}dq\right)dt \\
&\qquad = (2H+1)\int_0^{T-\Delta} e^{-2\lambda t}t^{2H+1}\left(\int_0^{\lambda t} e^{z}\left(\frac{z}{\lambda t}\right)^{2H}\frac{dz}{\lambda t}\right)dt \\
&\qquad = \frac{2H+1}{\lambda^{2H+1}}\int_0^{T-\Delta} e^{-2\lambda t}\left(\int_0^{\lambda t} e^{z}z^{2H}dz\right)dt \\
&\qquad = \frac{2H+1}{\lambda^{2H+1}}\int_{z/\lambda}^{T-\Delta} e^{-2\lambda t}\left(\int_0^{\lambda(T-\Delta)} e^{z}z^{2H}dz\right)dt \\
&\qquad = -\frac{2H+1}{2\lambda^{2H+2}}\int_0^{\lambda(T-\Delta)} e^{z}z^{2H}\left(e^{-2\lambda(T-\Delta)}-e^{-2z}\right)dz \\
&\qquad = \frac{(T-\Delta)^{2H+1}}{2\lambda}\Big[\mathcal{M}(2H+1,2H+2,-\lambda(T-\Delta)) \\
&\qquad - e^{-2\lambda(T-\Delta)}\mathcal{M}(2H+1,2H+2,\lambda(T-\Delta))\Big]
\end{aligned}$$

Analogously,

$$\int_0^{T-\Delta}(t+\Delta)^{2H+1}\mathcal{M}(2H+1,2H+2,-\lambda(t+\Delta))dt$$

$$
\begin{aligned}
&= (2H+1)\int_0^{T-\Delta}(t+\Delta)^{2H+1}\left(\int_0^1 e^{-\lambda(t+\Delta)}x^{2H}dx\right)dt\\
&= (2H+1)\int_\Delta^{T} y^{2H+1}\left(\int_0^1 e^{-\lambda yx}x^{2H}dx\right)dy\\
&= \frac{2H+1}{\lambda^{2H+1}}\int_\Delta^{T}\left(\int_0^{\lambda y} e^{-z}z^{2H}dz\right)dy\\
&= \frac{2H+1}{\lambda^{2H+1}}\left(\int_{z/\lambda}^{T}\left(\int_0^{\lambda T} e^{-z}z^{2H}dz\right)dy - \int_{z/\lambda}^{\Delta}\left(\int_0^{\lambda\Delta} e^{-z}z^{2H}dz\right)dy\right)\\
&= \frac{2H+1}{\lambda^{2H+1}}\left(\int_0^{\lambda T} e^{-z}z^{2H}\left(T-\frac{z}{\lambda}\right)dz - \int_0^{\lambda\Delta} e^{-z}z^{2H}\left(\Delta-\frac{z}{\lambda}\right)dz\right)\\
&= (2H+1)T^{2H+2}\left(\int_0^1 e^{-\lambda Tq}q^{2H}(1-q)dq\right)\\
&-(2H+1)\Delta^{2H+2}\left(\int_0^1 e^{-\lambda\Delta q}q^{2H}(1-q)dq\right)\\
&= \frac{T^{2H+2}}{2H+2}(2H+1,2H+3,-\lambda T) - \frac{\Delta^{2H+2}}{2H+2}(2H+1,2H+3,-\lambda\Delta).
\end{aligned}
$$

And lastly,

$$
\begin{aligned}
&\int_0^{T-\Delta} e^{-2\lambda(t+\Delta)}(t+\Delta)^{2H+1}\mathcal{M}(2H+1,2H+2,\lambda(t+\Delta))dt\\
&= (2H+1)\int_0^{T-\Delta} e^{-2\lambda(t+\Delta)}(t+\Delta)^{2H+1}\left(\int_0^1 e^{\lambda(t+\Delta)x}x^{2H}dx\right)dt\\
&= \frac{2H+1}{\lambda^{2H+1}}\int_0^{T-\Delta} e^{-2\lambda(t+\Delta)}\left(\int_0^{\lambda(t+\Delta)} e^{z}z^{2H}dz\right)dt\\
&= \frac{2H+1}{\lambda^{2H+1}}\int_\Delta^{T} e^{-2\lambda y}\left(\int_0^{\lambda y} e^{z}z^{2H}dz\right)dy\\
&= \frac{2H+1}{\lambda^{2H+1}}\left(\int_{z/\lambda}^{T} e^{-2\lambda y}\left(\int_0^{\lambda T} e^{z}z^{2H}dz\right)dy - \int_{z/\lambda}^{\Delta} e^{-2\lambda y}\left(\int_0^{\lambda\Delta} e^{z}z^{2H}dzdz\right)dy\right)\\
&= -\frac{2H+1}{2\lambda^{2H+2}}\left(\int_0^{\lambda T} e^{z}z^{2H}\left(e^{-2\lambda T}-e^{-2z}\right)dz - \int_0^{\lambda\Delta}\left(e^{-2\lambda\Delta}-e^{-2z}\right)dz\right)\\
&= -\frac{2H+1}{2\lambda^{2H+2}}\Big(\int_0^1 (\lambda T)^{2H+1}e^{\lambda Tq}q^{2H}\left(e^{-2\lambda T}-e^{-2\lambda Tq}\right)dq\\
&-\int_0^1 (\lambda\Delta)^{2H+1}e^{\lambda\Delta q}q^{2H}\left(e^{-2\lambda\Delta}-e^{-2\lambda\Delta q}\right)dq\Big)\\
&= -\frac{T^{2H+1}}{2\lambda}\Big(e^{-2\lambda T}\mathcal{M}(2H+1,2H+2,\lambda T) - \mathcal{M}(2H+1,2H+2,-\lambda T)\Big)\\
&+\frac{\Delta^{2H+1}}{2\lambda}\Big(e^{-2\lambda\Delta}\mathcal{M}(2H+1,2H+2,\lambda\Delta) - \mathcal{M}(2H+1,2H+2,-\lambda\Delta)\Big).
\end{aligned}
$$

The final result for the TAMSD is then given by

$$
\left\langle\overline{\delta^2(T,\Delta)}\right\rangle = \int_0^{T-\Delta}\langle\Omega^2(t)\rangle dt = \mathrm{Var}(x_0)\left(1-e^{-\lambda\Delta}\right)^2\frac{1-e^{-2\lambda(T-\Delta)}}{2\lambda(T-\Delta)}
$$

$$
\begin{aligned}
&+\frac{\sigma^2(1-e^{\lambda\Delta})}{T-\Delta}\Bigg[\frac{T^{2H+1}}{2H+1}\mathcal{M}(2H+1,2H+2,-\lambda T)\\
&\quad-\frac{\Delta^{2H+1}}{2H+1}\mathcal{M}(2H+1,2H+2,-\lambda\Delta)\\
&\quad+\frac{\lambda\Gamma(2H+1)}{2\Gamma(2H+3)}\Big(T^{2H+2}\mathcal{M}(2H+1,2H+3,-\lambda T)\\
&\qquad-\Delta^{2H+2}\mathcal{M}(2H+1,2H+3,-\lambda\Delta)\Big)\\
&\quad-\frac{1}{4(2H+1)}\Big(e^{-2\lambda\Delta}\Delta^{2H+1}\mathcal{M}(2H+1,2H+2,\lambda\Delta)\\
&\qquad-\Delta^{2H+1}\mathcal{M}(2H+1,2H+2,-\lambda\Delta)\\
&\qquad-e^{-2\lambda T}T^{2H+1}\mathcal{M}(2H+1,2H+2,\lambda T)\\
&\qquad+T^{2H+1}\mathcal{M}(2H+1,2H+2,-\lambda T)\Big)\Bigg]\\
&+\frac{\sigma^2(1-e^{-\lambda\Delta})}{T-\Delta}\Bigg[\frac{(T-\Delta)^{2H+1}}{2H+1}\mathcal{M}(2H+1,2H+2,-\lambda(T-\Delta))\\
&\quad+\frac{\lambda\Gamma(2H+1)}{2\Gamma(2H+3)}(T-\Delta)^{2H+2}\mathcal{M}(2H+1,2H+3,-\lambda(T-\Delta))\\
&\quad-\frac{(T-\Delta)^{2H+1}}{4(2H+1)}\Big(\mathcal{M}(2H+1,2H+2,-\lambda(T-\Delta))\\
&\qquad-e^{-2\lambda(T-\Delta)}\mathcal{M}(2H+1,2H+2,\lambda(T-\Delta))\Big)\Bigg]\\
&+\sigma^2\Delta^{2H}\left(1-\frac{\lambda\Delta e^{-\lambda\Delta}}{2(2H+1)}\mathcal{M}(2H+1,2H+2,\lambda\Delta)\right.\\
&\quad\left.+\frac{\lambda\Delta e^{\lambda\Delta}}{2(2H+1)}\mathcal{M}(2H+1,2H+2,-\lambda\Delta)\right).
\end{aligned}
\tag{B.2}
$$

While the expressions for the TAMSD and the generalised MSD differ, both share the same asymptote in the long-time limit $t, T \to \infty$. Moreover, the disparity between both is expected when the system has not yet reached the stationarity.

Appendix C. Covariance of the stationary fractional Ornstein-Uhlenbeck process

For the derivation of the covariance (35) we calculate the following integrals

$$
\begin{aligned}
&\int_{-\infty}^{t_2} e^{\lambda t_2'}\Big(|t_1|^{2H}+|t_2'|^{2H}-|t_1-t_2'|^{2H}\Big)dt_2\\
&=\frac{e^{\lambda t_2}|t_1|^{2H}}{\lambda}+\int_{-\infty}^{0} e^{\lambda t_2'}|t_2'|^{2H}dt_2'+\int_{0}^{t_2} e^{\lambda t_2'}|t_2'|^{2H}dt_2'\\
&\qquad-\int_{-\infty}^{t_1} e^{\lambda t_2'}(t_1-t_2')^{2H}dt_2'-\int_{t_1}^{t_2} e^{\lambda t_2'}(t_2'-t_1)^{2H}dt_2'\\
&=\frac{e^{\lambda t_2}|t_1|^{2H}}{\lambda}+\int_{0}^{\infty} e^{-\lambda t_2'}|t_2'|^{2H}dt_2'+t_2^{2H+1}\int_{0}^{1} e^{\lambda t_2 q}q^{2H}dq
\end{aligned}
$$

$$
\begin{aligned}
&- \int_0^{\infty} e^{\lambda(t_1-q)} q^{2H} dq - \int_0^{t_2-t_1} e^{\lambda(t_1+q)} q^{2H} dq \\
&= \frac{e^{\lambda t_2}|t_1|^{2H}}{\lambda} + \frac{\Gamma(2H+1)}{\lambda^{2H+1}} + \frac{|t_2|^{2H+1}}{2H+1}\mathcal{M}(2H+1,2H+2,\lambda t_2) \\
&- \frac{e^{\lambda t_1}\Gamma(2H+1)}{\lambda^{2H+1}} - e^{\lambda t_1}(t_2-t_1)^{2H+1}\int_0^1 e^{(t_2-t_1)x} x^{2H} dx \\
&= \frac{e^{\lambda t_2}|t_1|^{2H}}{\lambda} + \frac{\Gamma(2H+1)}{\lambda^{2H+1}} + \frac{|t_2|^{2H+1}}{2H+1}\mathcal{M}(2H+1,2H+2,\lambda t_2) \\
&- \frac{e^{\lambda t_1}\Gamma(2H+1)}{\lambda^{2H+1}} - \frac{e^{\lambda t_1}|t_2-t_1|^{2H+1}}{2H+1}\mathcal{M}(2H+1,2H+2,\lambda|t_2-t_1|).
\end{aligned}
$$

Subsequently, one arrives at the following expression

$$
\begin{aligned}
&\int_{-\infty}^{t_2} e^{\lambda t_2'}\Big(|t_1|^{2H} + |t_2'|^{2H} - |t_1 - t_2'|^{2H}\Big) dt_2' \\
&= \frac{e^{\lambda t_2}|t_1|^{2H}}{\lambda} + \frac{\Gamma(2H+1)}{\lambda^{2H+1}}\left(1 - e^{\lambda t_1}\right) + \frac{|t_2|^{2H+1}}{2H+1}\mathcal{M}(2H+1,2H+2,\lambda t_2) \\
&- \frac{e^{\lambda t_1}|t_2-t_1|^{2H+1}}{2H+1}\mathcal{M}(2H+1,2H+2,\lambda|t_2-t_1|). \qquad \text{(C.1)}
\end{aligned}
$$

Following the same procedure one obtains the expression below for the integral with the differential dt_1',

$$
\begin{aligned}
&\int_{-\infty}^{t_1} e^{\lambda t_2'}\Big(|t_1'|^{2H} + |t_2|^{2H} - |t_1' - t_2|^{2H}\Big) dt_1' \\
&= \frac{e^{\lambda t_1}|t_2|^{2H}}{\lambda} + \frac{\Gamma(2H+1)}{\lambda^{2H+1}}\left(1 - e^{\lambda t_2}\right) + \frac{|t_1|^{2H+1}}{2H+1}\mathcal{M}(2H+1,2H+2,\lambda t_1) \\
&+ \frac{e^{\lambda t_2}|t_2-t_1|^{2H+1}}{2H+1}\mathcal{M}(2H+1,2H+2,-\lambda|t_2-t_1|).
\end{aligned}
$$

The second type of integrals appearing in the covariance function is given by

$$
\begin{aligned}
&\int_{-\infty}^{t_1}\int_{-\infty}^{t_2} e^{\lambda(t_1'+t_2')}\Big(|t_1'|^{2H} + |t_2'|^{2H} - |t_1' - t_2'|^{2H}\Big) dt_1' dt_2' \\
&= \int_{-\infty}^{t_1} e^{\lambda t_1'}|t_1'|^{2H} dt_1' \int_{-\infty}^{t_2} e^{\lambda t_2'} dt_2' + \int_{-\infty}^{t_1} e^{\lambda t_1'} dt_1' \int_{-\infty}^{t_2} e^{\lambda t_2'}|t_2'|^{2H} dt_2' \\
&\qquad - \int_{-\infty}^{t_1}\int_{-\infty}^{t_2} e^{\lambda(t_1'+t_2')}|t_1' - t_2'|^{2H} dt_1' dt_2' \\
&= \frac{e^{\lambda t_2}}{\lambda}\Big(\int_{-\infty}^{0}(-t_1')^{2H} e^{\lambda t_1'} dt_1' + \int_0^{t_1} t_1'^{2H} e^{\lambda t_1'} dt_1'\Big) \\
&+ \frac{e^{\lambda t_1}}{\lambda}\Big(\int_{-\infty}^{0}(-t_2')^{2H} e^{\lambda t_2'} dt_2' + \int_0^{t_2} t_2'^{2H} e^{\lambda t_2'} dt_2'\Big) \\
&- \int_{-\infty}^{t_1}\int_{-\infty}^{t_1'} e^{\lambda(t_1'+t_2')}(t_1' - t_2')^{2H} dt_1' dt_2' - \int_{-\infty}^{t_1}\int_{t_1'}^{t_2} e^{\lambda(t_1'+t_2')}(t_2' - t_1')^{2H} dt_1' dt_2'.
\end{aligned}
$$

The first two integrals are easily evaluated. In the last two integrals, by changing of variable $t_1' - t_2' = q$ one arrives at

$$
\begin{aligned}
&= \frac{e^{\lambda t_2}}{\lambda}\left(\frac{\Gamma(2H+1)}{\lambda^{2H+1}} + \frac{|t_1|^{2H+1}}{2H+1}\mathcal{M}(2H+1,2H+2,\lambda t_1)\right)\\
&+\frac{e^{\lambda t_1}}{\lambda}\left(\frac{\Gamma(2H+1)}{\lambda^{2H+1}} + \frac{|t_2|^{2H+1}}{2H+1}\mathcal{M}(2H+1,2H+2,\lambda t_2)\right)\\
&-\int_{-\infty}^{t_1} e^{\lambda t_1'}dt_1'\int_0^{\infty} e^{\lambda(t_1'-q)}q^{2H}dq - \int_{-\infty}^{t_1} e^{\lambda t_1'}dt_1'\int_0^{t_2-t_1'} e^{\lambda(t_1'+q)}q^{2H}dq.
\end{aligned}
$$

The evaluation of the first double integral is straightforward and it yields $\frac{e^{2\lambda t_1}}{2\lambda^{2H+2}}\Gamma(2H+1)$. Evaluating the second double-integral requires changing the order of integration. For the last integral one arrives at the following,

$$
\begin{aligned}
&-\int_{-\infty}^{t_1} e^{\lambda t_1'}dt_1'\int_0^{t_2-t_1'} e^{\lambda(t_1'+q)}q^{2H}dq =\\
&-\int_0^{\infty} e^{\lambda q}q^{2H}dq\int_{-\infty}^{t_2-q} e^{2\lambda t_1'}dt_1' + \int_0^{t_2-t_1} e^{\lambda q}q^{2H}dq\int_{t_1}^{t_2-q} e^{2\lambda t_1'}dt_1'\\
&-\frac{e^{2\lambda t_2}}{2\lambda}\int_0^{\infty} e^{-\lambda q}q^{2H}dq + \frac{e^{2\lambda t_2}}{2\lambda}\int_0^{t_2-t_1} e^{-\lambda q}q^{2H}dq - \frac{e^{2\lambda t_1}}{2\lambda}\int_0^{t_2-t_1} e^{\lambda q}q^{2H}dq.
\end{aligned}
$$

Subsequently,

$$
\begin{aligned}
&-\frac{e^{2\lambda t_2}}{2\lambda^{2H+2}}\Gamma(2H+1)\\
&-\frac{e^{2\lambda t_2}}{2\lambda(2H+1)}(t_2-t_1)^{2H+1}\mathcal{M}(2H+1,2H+2,\lambda(t_1-t_2))\\
&+\frac{e^{2\lambda t_1}}{2\lambda(2H+1)}(t_2-t_1)^{2H+1}\mathcal{M}(2H+1,2H+2,\lambda(t_2-t_1)).
\end{aligned}
$$

Summing up all the calculations, we obtain

$$
\begin{aligned}
&\int_{-\infty}^{t_1}\int_{-\infty}^{t_2} e^{\lambda(t_1'+t_2')}\Big(|t_1'|^{2H}+|t_2'|^{2H}-|t_1'-t_2'|^{2H}\Big)dt_1'dt_2'\\
&\quad= \frac{e^{\lambda t_2}}{\lambda}\left(\frac{\Gamma(2H+1)}{\lambda^{2H+1}} + \frac{|t_1|^{2H+1}}{2H+1}\mathcal{M}(2H+1,2H+2,\lambda t_1)\right)\\
&\quad+ \frac{e^{\lambda t_1}}{\lambda}\left(\frac{\Gamma(2H+1)}{\lambda^{2H+1}} + \frac{|t_2|^{2H+1}}{2H+1}\mathcal{M}(2H+1,2H+2,\lambda t_2)\right)\\
&\quad- \frac{e^{2\lambda t_1}}{2\lambda^{2H+2}}\Gamma(2H+1) - \frac{e^{2\lambda t_2}}{2\lambda^{2H+2}}\Gamma(2H+1)\\
&\quad- \frac{e^{2\lambda t_2}}{2\lambda(2H+1)}|t_2-t_1|^{2H+1}\mathcal{M}(2H+1,2H+2,-\lambda|t_2-t_1|)\\
&\quad+ \frac{e^{2\lambda t_1}}{2\lambda(2H+1)}|t_2-t_1|^{2H+1}\mathcal{M}(2H+1,2H+2,\lambda|t_2-t_1|). \qquad \text{(C.2)}
\end{aligned}
$$

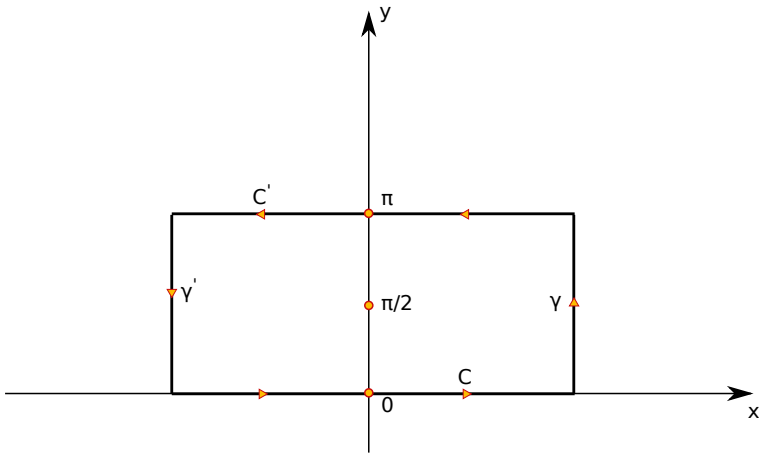

Figure D1. Contour of integration in equation (30.)

Appendix D. Variance of the normally distributed initial condition

We now perform the integration for the variance of the initial condition for the fractional Ornstein-Uhlenbeck processes. The integral given by (30) reads

$$\xi^2 = \frac{\sigma^2 \Gamma(2H+1)\sin(\pi H)}{\pi \lambda^{2H}} \int_0^\infty \frac{|x|^{1-2H}}{1+x^2} dx.$$

The integral can be calculated by the means of the theorem of residues. We substitute x by e^t and arrive

$$\int_0^\infty \frac{|x|^{1-2H}}{1+x^2} dx = \frac{1}{2}\int_{-\infty}^\infty \frac{|x|^{1-2H}}{1+x^2} dx = \frac{1}{2}\int_{-\infty}^\infty \frac{e^{(2-2H)t}}{1+e^{2t}} dx.$$

Now consider the complex function $f(z) = \exp([2-2H]z)/(1+\exp(2z))$ and the contour $C \cup C' \cup \gamma \cup \gamma'$ depicted in following figure D1.

The complex function $f(z)$ has a simple pole at $z = i\pi/2$ within the contour. depicted in the figure. As the theorem of residues indicates, the evaluation of the integral in equation (30) is then

$$\begin{aligned}\oint \frac{e^{(2-2H)z}}{1+e^{2z}} dz &= \int_C f(z)dz + \int_\gamma f(z)dz + \int_{C'} f(z)dz + \int_{\gamma'} f(z)dz \\ &= \operatorname{Res}\left(f(z), \frac{\pi i}{2}\right),\end{aligned}$$

which is equivalent to the evaluation of the following integrals according to the geometry of the contour in figure D1,

$$\begin{aligned}\lim_{R\to\infty} \Bigg(&\int_{-R}^{R} \frac{e^{(2-2H)x}}{1+e^{2x}} dx + \int_0^\pi \frac{e^{(2-2H)(R+iy)}}{1+e^{2(R+iy)}} i dy \\ &+ \int_R^{-R} \frac{e^{(2-2H)(x+i\pi)}}{1+e^{2(x+i\pi)}} + \int_\pi^0 \frac{e^{(2-2H)(-R+iy)}}{1+e^{2(-R+iy)}} i dy \Bigg) \\ &= 2\pi i \lim_{z\to\pi i/2} \left(z - \frac{\pi i}{2}\right) \frac{e^{(2-2H)z}}{1+e^{2z}}.\end{aligned}$$

The second and fourth integrals are identically zero when $R \to \infty$ (note that $H \in (0, 1)$). Hence, the equation above is simplified to

$$\lim_{R\to\infty} \left(\left(1 - e^{-2\pi i H}\right) \int_{-R}^{R} \frac{e^{(2-2H)x}}{1 + e^{2x}} dx \right) = 2\pi i e^{-\pi i H},$$

and consequently,

$$\int_{-\infty}^{\infty} \frac{e^{(2-2H)x}}{1 + e^{2x}} dx = \frac{2\pi i e^{-\pi i H}}{1 - e^{-2\pi i H}} = \frac{\pi}{\sin(\pi H)}.$$

Readily, by substituting the result above into equation (30) we deduce that

$$\xi^2 = \frac{\sigma^2}{2\lambda^{2H}} \Gamma(2H + 1).$$

References

[1] Uhlenbeck GE and Ornstein LS 1930 On the Theory of the Brownian Motion *Phys. Rev.* **36**, 823
[2] Gardiner CW 2004 Handbook of Stochastic Methods for Physics, Chemistry, and the Natural Sciences (Springer, Berlin)
[3] van Kampen NG 1992 Stochastic Processes in Physics and Chemistry (North-Holland, Amsterdam)
[4] Vasicek O 1977 An Equilibrium Characterization of the Term Structure *J. Financ. Econ.* **5**, 177
[5] Doob JL 1942 The Brownian Movement and Stochastic Equations *Ann. Math.* 351
[6] Nørregaard K, Metzler R, Ritter CM, Berg-Sørensen K and Oddershede LB 2017 Manipulation and Motion of Organelles and Single Molecules in Living Cells *Chem. Rev.* **117**, 4342
[7] Tolić-Nørrelykke SF, Rasmussen MB, Pavone FS, Berg-Sørensen K and Oddershede LB 2006 Stepwise bending of DNA by a single TATA-box binding protein *Biophys. J.* **90**, 3694
[8] Mardoukhi Y, Jeon JH, Chechkin AV and Metzler R 2018 Fluctuations of random walks in critical random environments *Phys. Chem. Chem. Phys.* **20**, 20427
[9] Hull J and White A 1990 Pricing Interest-Rate-Derivative Securities *Rev. Financ. Stud.* **3**, 573
[10] Beliaeva AN, Nawalkha SK and Soto GM 2008 Pricing American Interest Rate Options under the Jump-Extended Vasicek Model *J. Deriv.* **16**, 29
[11] Barndorff-Nielsen OE and Shephard N 2001 Non-Gaussian Ornstein-Uhlenbeck-Based Models and Some of Their Uses in Financial Economics *J. Roy. Stat. Soc. B* **63**, 167
[12] Nicolato E and Venardos E Option Pricing in Stochastic Volatility Models of the Ornstein-Uhlenbeck Type *Math. Financ.* **13**, 445
[13] Li L and Linetsky V 2014 Time-Changed Ornstein-Uhlenbeck Processes and Their Applications in Commodity Derivative Models *Math. Financ.* **24**, 289
[14] Benth FE, Kallsen J and Meyer-Brandis T 2007 A Non-Gaussian Ornstein-Uhlenbeck Process for Electricity Spot Price Modeling and Derivatives Pricing *Appl. Math. Financ.* **14**, 153
[15] Ricciardi LM and Sacerdote L 1979 The Ornstein-Uhlenbeck Process as a Model for Neuronal Activity *Biol. Cybern.* **35**, 1
[16] Shinomoto S, Sakai Y and Funahashi S 1999 The Ornstein-Uhlenbeck Process Does not Reproduce Spiking Statistics of Neurons in Prefrontal Cortex *Neural. Comput.* **11**, 935
[17] Mills TC 1990 Time Series Techniques for Economists (Cambridge University Press, Cambridge, UK)
[18] Tsay RS 2000 Time series and forecasting: brief history and future research *J. Am. Stat. Assoc.* **95**, 638
[19] Ślęzak J, Burnecki K and Metzler R 2019 Random coefficient autoregressive processes describe non-Gaussian diffusion in heterogeneous systems *New J. Phys.* **21**, 073056
[20] Mandelbrot BB and van Ness JW 1968 Fractional Brownian Motions, Fractional Noises and Applications *SIAM Rev.* **10**, 422

[21] Weiss M 2013 Single-particle tracking reveals anticorrelated fractional Brownian motion in crowded fuilds *Phys. Rev. E* **88**, 010101(R)

[22] Szymanski J and Weiss M 2009 Elucidating the Origin of Anomalous Diffusion in Crowded Fluids *Phys. Rev. Lett.* **103**, 038102

[23] Jeon JH, Leijnse N, Oddershede L and Metzler R 2013 Anomalous diffusion and power-law relaxation in wormlike micellar solution *New J. Phys.* **15**, 045011

[24] Kneller GR, Baczynski K and Pasenkiewicz-Gierula M 2011 Consistent picture of lateral subdiffusion in lipid bilayers: Molecular dynamics simulation and exact results *J. Chem. Phys.* **135**, 141105

[25] Jeon JH, Martinez-Seara H, Javanainen M and Metzler R 2012 Lateral motion of phospholipids and cholesterols in a lipid bilayer: anomalous diffusion and its origins *Phys. Rev. Lett.* **109**, 188103

[26] Jeon JH, Javanainen M, Martinez-Seara H, Metzler R and Vattulainen I 2016 Protein crowding in lipid bilayers gives rise to non-Gaussian anomalous lateral diffusion of phospholipids and proteins *Phys. Rev. X* **6**, 021006

[27] Weber SC, Spakowitz AJ and Theriot JA 2010 Bacterial chromosomal loci move subdiffusively through a viscoelastic cytoplasm *Phys. Rev. Lett.* **104**, 238102

[28] Jeon JH, Tejedor V, Burov S, Barkai E, Selhuber-Unkel S, Berg-Sørensen K, Oddershede LB and Metzler R 2011 In Vivo Anomalous Diffusion and Weak Ergodicity Breaking of Lipid Granules *Phys. Rev. Lett.* **106**, 048103

[29] Lampo TJ, Stylianidou S, Backlund MP, Wiggins PA and Spakowitz AJ Cytoplasmic RNA-protein particles exhibit non-Gaussian subdiffusive behavior *Biophys. J.* **112**, 532

[30] Metzler R and Klafter J 2000 The random walk's guide to anomalous diffusion: A fractional dynamics approach *Phys. Rep.* **339**, 1

[31] Metzler R, Jeon JH, Cherstvy AG and Barkai E 2014 Anomalous diffusion models and their properties: non-stationarity, non-ergodicity, and ageing at the centenary of single particle tracking *Phys. Chem. Chem. Phys.* **16**, 24128

[32] Selhuber-Unkel C, Yde P, Berg-Sørensen K and Oddershede LB 2009 Variety in intracellular diffusion during the cell cycle *Phys. Biol.* **6**, 025015

[33] Cheridito P, Kawaguchi H and Maejima M 2003 Fractional Ornstein-Uhlenbeck Processes *Electron. J. Probab.* **8**, 3

[34] Höfling F and Franosch T 2013 Anomalous transport in the crowded world of biological cells *Rep. Prog. Phys.* **76**, 046602

[35] Barkai E, Garini Y and Metzler R 2012 Strange Kinetics of Single Molecules in Living Cells *Phys. Today* **65**(8), 29

[36] Krapf D and Metzler R 2019 Strange interfacial molecular dynamics *Phys. Today* **72(9)**, 48

[37] Khinchin AI 1949 Mathematical Foundations of Statistical Mechanics (Dover, New York, NY).

[38] Burov S, Metzler R and Barkai E 2010 Aging and non-ergodicity beyond the Khinchin theorem *Proc. Natl. Acad. Sci. USA* **107**, 13228

[39] Driggers RG 2003 Encyclopedia of Optical Engineering, Dekker Encyclopedias Series (Marcel Dekker, New York, NY)

[40] Hida T and Hitsuda M 1993 Gaussian Processes (American Mathematical Society, Providence, RI)

[41] Rasmussen CE and Williams CKI 2006 Gaussian Processes for Machine Learning (MIT Press, Cambridge, MA)

[42] He Y, Burov S, Metzler R and Barkai E 2008 Random Time-Scale Invariant Diffusion and Transport Coefficients *Phys. Rev. Lett.* **101**, 058101

[43] Deng W and Barkai E 2009 Ergodic properties of fractional Brownian-Langevin motion *Phys. Rev. E* **79**, 011112

[44] Ślęzak J, Metzler R and Magdziarz M 2019 Codifference can detect ergodicity breaking and non-Gaussianity *New J. Phys.* **21**, 053008

[45] Takeyuki H 2005 Stochastic Analysis: Classical And Quantum: Perspectives Of White Noise

Theory (World Scientific, Singapore)
[46] Risken H 1989 The Fokker-Planck equation (Springer, Heidelberg)
[47] Kaarakka T and Salminen P 2011 On Fractional Ornstein-Uhlenbeck Processes *Comm. Stoch. Anal.* **5**, 8
[48] Metzler R, Barkai E and Klafter J 1999 Anomalous diffusion and relaxation close to thermal equilibrium: A fractional Fokker-Planck equation approach *Phys. Rev. Lett.* **82**, 3563
[49] Fogedby HC 1994 Langevin Equations for Continuous Time Lévy Flights *Phys. Rev. E* **50**, 1657
[50] Jespersen S, Metzler R and Fogedby HC 1999 Lévy flights in external force fields: Langevin and fractional Fokker-Planck equations and their solutions *Phys. Rev. E* **59**, 2736
[51] Chechkin AV and Gonchar VYu 2000 Linear relaxation processes governed by fractional symmetric kinetic equations *J. Exp. Theoret. Phys.* **91**, 635
[52] Baule A and Friedrich R 2007 Two-Point Correlation Function of the Fractional Ornstein-Uhlenbeck Process *Europhys. Lett.* **79**, 60004
[53] Pipiras V and Taqqu MS 2000 Integration Questions Related to Fractional Brownian Motion *Prob. Theory Rel.* **118**, 251
[54] Schwarzl M, Godec A and Metzler R 2017 Quantifying non-ergodicity of anomalous diffusion with higher order moments *Sci. Rep.* **7**, 3878
[55] Wang W, Cherstvy AG, Chechkin AV, Thapa S, Seno F, Liu X and Metzler R 2020 Fractional Brownian motion with random diffusivity: emerging residual nonergodicity below the correlation time *E-print*
[56] Jeon JH and Metzler R 2012 Inequivalence of time and ensemble averages in ergodic systems: exponential versus power-law relaxation in confinement *Phys. Rev. E* **85**, 021147
[57] Buchholz H, Lichtblau H and Wetzel K 2013 The Confluent Hypergeometric Function: with Special Emphasis on its Applications (Springer, Berlin)
[58] Guggenberger T, Pagnini G, Vojta T and Metzler R 2019 Fractional Brownian motion in a finite interval: correlations effect depletion or accretion zones of particles near boundaries *New J. Phys* **21**, 022002
[59] Grebenkov DS 2011 Time-average quadratic functionals of a Gaussian process *Phys. Rev. E* **83**, 061117
[60] Cherstvy AG, Thapa S, Mardoukhi Y, Chechkin AV and Metzler R 2018 Time averages and their statistical variation for the Ornstein-Uhlenbeck process: role of initial particle conditions and relaxation to stationarity *Phys. Rev. E* **98**, 022134

Errata

- Typo, English Abstract, Line 22: $t^{(d+d_f(\tau-2))/d_w} \rightarrow t^{(d+d_f(2-\tau))/d_w}$
- Typo, German Abstract, Line 24: $t^{(d+d_f(\tau-2))/d_w} \rightarrow t^{(d+d_f(2-\tau))/d_w}$
- Typo, Page 17, Line 4, after Eq. (2.14): $\chi = \mathcal{D}||\mathcal{C}||^{2/d_f} \rightarrow \chi = ||\mathcal{C}||^{2/d_f}/\mathcal{D}$
- References missing, Page 29, Line 9, after *"identified to be* $\frac{2+d_f(2-\tau)}{d_w}$ *"*

  Gefen, Y., Aharony, A. and Alexander, S., 1983. *Anomalous diffusion on percolating clusters*. Physical Review Letters, 50(1), pp.77-80.

  Kertész, J. and Metzger, J., 1983. *Properties of the density relaxation function in classical diffusion models with percolation transition*. Journal of Physics A: Mathematical and General, 16(18), pp.L735-L739.

  Kammerer, A., Höfling, F. and Franosch, T., 2008. *Cluster-resolved dynamic scaling theory and universal corrections for transport on percolating systems*. Europhysics Letters, 84(6), p.66002.